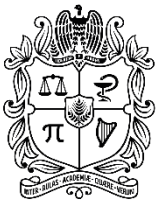

UNIVERSIDAD
NACIONAL
DE COLOMBIA

Implementation and performance assessment of a real-time optimization system on a virtual fluidized-bed catalytic-cracking plant

Adriana Lisbeth Rodríguez Dionicio

Universidad Nacional de Colombia

Facultad de Ingeniería

Departamento de Ingeniería Química y Ambiental

Bogotá D.C., Colombia

2019

UNIVERSIDAD
NACIONAL
DE COLOMBIA

Implementación y evaluación del desempeño de un sistema de optimización en tiempo real sobre una planta virtual de craqueo catalítico en lecho fluidizado

Adriana Lisbeth Rodríguez Dionicio

Universidad Nacional de Colombia

Facultad de Ingeniería

Departamento de Ingeniería Química y Ambiental

Bogotá D.C., Colombia

2019

Implementación y evaluación del desempeño de un sistema de optimización en tiempo real sobre una planta virtual de craqueo catalítico en lecho fluidizado

Adriana Lisbeth Rodríguez Dionicio

Tesis presentada como requisito parcial para optar al título de:

Magíster en Ingeniería Química

Director:

Ph.D. Carlos Arturo Martínez Riascos

Línea de Investigación:

Optimización y control

Grupo de Investigación:

Ingeniería de Sistemas de Proceso

Universidad Nacional de Colombia

Facultad de Ingeniería

Departamento de Ingeniería Química y Ambiental

Bogotá D.C, Colombia

2019

Acknowledgements

I am deeply greatful to my advisor Carlos Arturo Martinez for his accompaniment, advice and patience; to Mario Noriega for his unconditional support, encouragement and guidance, to Juan David Reyes as an incredible project partner, to Lorenz Biegler for his advice and opportunities, and to Bethany Nicholson for her time and knowledgement.

I wish to express my sincere gratitude to my lovely family, my parents and my sister, without their support this would not have been possible. Thanks to my friends and all the people who in one way or another were part of this process.

Finally, I want to thank my alma mater, the Universidad Nacional de Colombia, where I have spent the best years of my life and which I will always consider my second home.

Resumen

La optimización en tiempo real (RTO) es una herramienta que mejora la rentabilidad y la eficiencia de las plantas. Cuando el proceso sufre una perturbación, debido a factores internos o externos, la RTO actúa en tiempo real, re-estimando el punto de ajuste óptimo del proceso. Esta acción implica la maximización de una función de rentabilidad, mientras se cumple con las restricciones del proceso. A pesar de los grandes beneficios generados por la RTO, su aceptación en la industria se ha visto limitada por el escaso conocimiento de su funcionamiento y su falta de madurez tecnológica.

La unidad de craqueo catalítico (FCCU) es uno de los procesos más importantes en el refinado del petróleo, en donde grandes moléculas de hidrocarburos son transformadas en productos más valiosos, como la gasolina. Por lo tanto, la búsqueda continua de condiciones de funcionamiento óptimas hace que la FCCU sea un candidato ideal para una aplicación de RTO.

Esta tesis desarrolla y evalúa la implementación de la RTO en una planta virtual de FCCU, teniendo en cuenta cada etapa de una RTO (eliminación de ruido, detección de estado estable, validación de datos, estimación de parámetros y optimización). Los datos dinámicos para llevar a cabo este análisis se obtuvieron de una planta virtual de FCCU basada en un modelo determinista dinámico desarrollado en Matlab®. Los datos de salida del modelo se contaminaron con error de Gauss y error grueso para simular mediciones de una planta real. Para la eliminación de ruido, la detección de estado estable, la reconciliación de datos, la estimación de parámetros y la optimización, se estudiaron y evaluaron diferentes estrategias y algoritmos, mientras que para el sistema de control se propuso un PID descentralizado. Finalmente, se implementaron las estrategias más apropiadas para el estudio de caso y se evaluó su desempeño en conjunto.

Simultáneamente con la ejecución de la planta virtual, el sistema RTO pudo responder a las perturbaciones aplicadas, mejorando las ganancias. Esta respuesta implica limpiar los datos ruidosos, identificar el comienzo del estado estable, calcular los nuevos puntos de ajuste utilizando un algoritmo de optimización, e implementar los nuevos puntos de ajuste a través del sistema de control. En este trabajo, se evaluó el desempeño de una RTO bajo

perturbaciones típicas del proceso y se observó que, en todas las situaciones, la RTO lleva el proceso a una mejor condición operativa. La integración de la RTO con el control PID mejoró la rentabilidad de la FCCU en un 35% respecto a un escenario sin RTO, y se observó una variación en la rentabilidad no mayor al 7% luego de la ejecución de cada ciclo de la RTO.

Puntos Clave

- La RTO es una técnica promisoria en la optimización de la rentabilidad de una FCCU.
- El estudio de las etapas RTO por separado no garantiza su implementación exitosa.
- Las acciones RTO mejoraron la rentabilidad de la FCCU en todos los casos de estudio analizados.
- Se implementaron y evaluaron diferentes estrategias para cada etapa de RTO.
- Se simuló una planta virtual de FCCU sobre un modelo determinista dinámico.
- Para simular datos de una planta real, se agregó el ruido típico de datos reales al modelo de la FCCU.

Abstract

Real-time optimization (RTO) is a tool that improves plants profitability and efficiency. When a process suffers a disturbance, due to internal or external factors, RTO acts in real time, re-estimating the optimal process setpoint. This action involves maximizing a profitability function while meeting the process constraints. Despite the great benefits that are generated, its acceptance in the industry has been limited by the little knowledge about the operation and the lack of technological maturity.

The fluid catalytic cracking unit (FCCU) is one of the most important processes in oil refining, where large hydrocarbon molecules are transformed into more valuable products such as gasoline. Therefore, the continuous searching for optimal operating conditions makes the FCCU an ideal candidate for an RTO application.

This thesis develops and evaluates RTO implementation in a FCCU virtual plant, taking into account each RTO stage (noise elimination, steady-state detection, data validation, parameter estimation, and optimization). The dynamic data to carry out this analysis were obtained from an FCCU virtual plant based on a dynamic deterministic model developed in Matlab ®. The model output data were contaminated with Gaussian and gross errors to simulate measurements from a real plant. For denoising, steady-state detection, data reconciliation, parameter estimation, and optimization, different strategies and algorithms were studied and assessed, while a decentralized PID was proposed for the control system. Finally, the most appropriate strategies for the case study were implemented and their performance was fully evaluated.

Simultaneously with the execution of the virtual plant, the RTO system was able to respond to applied disturbances, improving the profit. This response implies to clean the noisy data, identify the beginning of the steady state, calculate the new setpoints using an optimization algorithm, and implement the new setpoints through the control system. In this work, RTO performance under typical process disturbances was assessed and for all the studied cases, RTO leads the process to better operational conditions. The integration of RTO with PID control improved the profitability of the FCCU in 35% in a comparison with a scenario

without RTO, and it was observed a profit variation no greater than 7% after the execution of each RTO cycle.

Highlights:

- RTO is a promissory technique in the optimization of FCCU profitability.
- The study of the RTO stages separately does not guarantee its successful implementation.
- The RTO actions improved the FCCU profitability in all the analyzed cases.
- Different strategies for each RTO stage were implemented and evaluated.
- A FCCU virtual plant was simulated using a dynamic deterministic model.
- To simulate data from a real plant, the typical noise of real data was added to the FCCU model.

Contents

List of figures

Page

List of tables

Page

Chapter 1. Introduction

The industry interest in online process optimization has emerged as a promissory technology for operating cost reduction and product quality improvements. The current market requires increasing efficiency, effectiveness, product quality, process safety, and environmental impact reduction, so online process optimization is an excellent alternative to achieve these goals. Historically, the idea of chemical processes optimization has been focused on the design phase; nonetheless, since the nineties, this approach has been complemented with strategies for enhancing the profitability during operation [1]. To achieve this purpose the industry has been working on the implementation of advanced control strategies that improve the processes control through hierarchical decision levels. These strategies have gained high relevance due to significant profitability improvements and the ability to be mainly applied for large scale and complex processes [2], [3].

The hierarchy control approach makes a successive refinement of time scales decisions, from top to bottom, as a cascade of interconnected solvable problems [4]. It implies the interaction among different control levels (planning, scheduling, optimization, control and automatization) for the execution of important decisions in accordance with the plant requirements (Figure 1.1).

The idea of the first decision level (planning) is to determine the feedstocks to purchase, and the products and quantities to manufacture. At this stage, an overall profit objective function is usually solved using linear or successive programming. The next level (scheduling) corresponds to necessary actions and events that will be executed to reach the targets defined at the planning level. In scheduling, some issues as timing of feeds deliveries, products lifting, operating mode changes, and storage problems must be solved through simulation models, rules, and optimization [4].

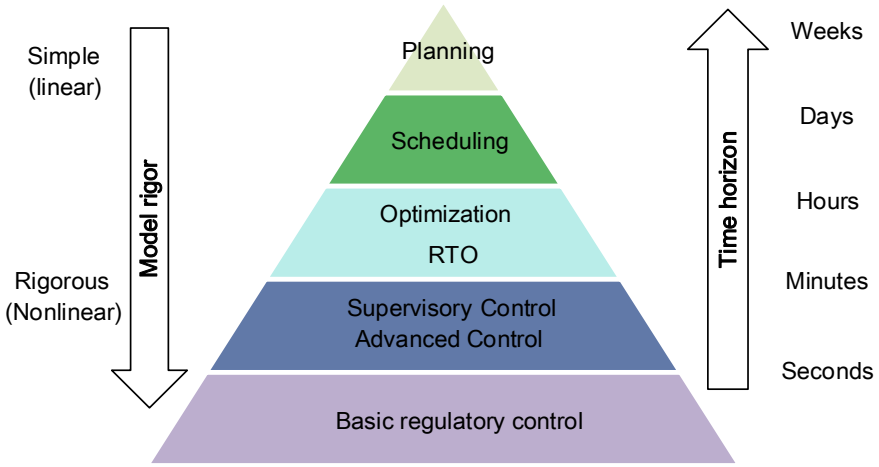

Figure 1.1 *Process automation hierarchy. Adapted from* [5],[6].

In the following layer, Real-time optimization (RTO) implements the business decisions, based on a non-linear steady-state model. It is executed in real time together with the below levels (multivariable and regulatory control) but at a different frequency. In the RTO level, the online calculation of optimal set points allows either profit maximization or cost minimization, while operating constraints are satisfying [1]. For this layer, appropriated optimization techniques and steady-state models are employed. Frequently, a steady state model is utilized to describe the plant performance and to optimize an economic objective function. Once the set points are calculated they are passed to the multivariable control layer, commonly MPC (model predictive control) that provides a minute to minute dynamic control of the plant [4]. Finally, the lowest layer, distributed control system (DCS), is in charge of regulation and control, which is executed on a second time scale.

A traditional scheme for RTO implementations is presented in Figure 1.2 In an automated plant, the control system calculates an error value from the difference between the output of the process variable and a desired value (set point), and implements control actions (using the manipulated variables) to bring the system to the desired conditions. The setpoint (SP) is usually established by an operator within an operating window, but in a RTO system the SP is defined by sequential steps that calculates the best operational plant conditions according to the output of the process variable. Then, the process output data is not only fed to the control system, but also to the first stage of the RTO system.

The first stage of the RTO corresponds to data validation and parameter estimation. This stage includes a data cleaning (denoising) that eliminates noise and gross error from the

original signals; steady state detection (when dealing with stationary RTO), to ensure that the plant is in a steady condition; a data reconciliation (DR) to get consistent measures using mass and energy balances; and a parameter estimation (PE) in which the parameters of the plant are updated from the reconciled values. Once the data are validated and the parameters are estimated, the information is sent to the optimization system where an economic objective function (subject to a first principle model and process constraints), compute the optimum operating conditions. Finally, the optimal setpoints are fed to the control system to perform the necessary actions that reach the new optimum operating conditions.

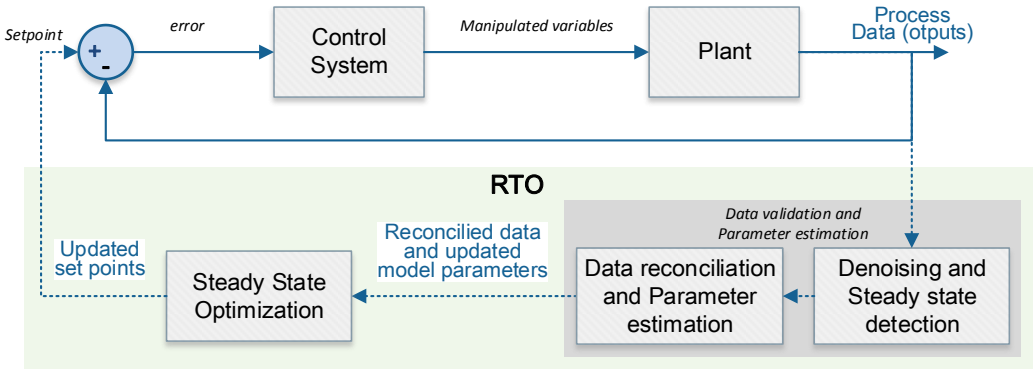

Figure 1.2 *A block diagram for RTO and regulatory feedback control. Adapted from [1].*

The basic structure of RTO in cascade with control system has become the standard approach for implementing steady-state online optimization in plants that operate around nominal steady states. However, this scheme has revealed some limitations. Although many RTO applications try to improve accuracy through model updating, there are from time to time some problems such as plant-model mismatch and suboptimal operations during the dynamic between the current steady states and the next ones. The plant-model mismatch occurs as a result of many assumptions and simplifications in the mathematical models of the process used in the hierarchical structure, mainly in optimization and advanced control levels [7]–[9].

In the other hand, the suboptimal dynamic operation is due to the fact that the RTO system must wait until the plant reaches a steady state, starts to find the next optimum point, and updates the set points in the control system [10]. This causes the system to undergo a transient period where it is not carried out in an optimal way, but in a sub-optimum way from the previous to the new optimum state. To diminish these inconvenient, dynamic real-time optimization (D-RTO) optimization methodology has been formulated. It optimizes the

economic performance of a process over a prediction horizon and calculates the control actions. This formulation essentially solves a Non-linear Model Predictive Control (NMPC) problem with an economically-oriented objective function based on first-principle dynamic models [11]. Nonetheless, D-RTO implementations still have some issues related to solution time and synchronization between plant and control [10]. This is why the steady-state approach with multiple layers continues being an attractive option for many process systems, mainly in the petrochemical industry where process automation leads to improve energy efficiency and overall economic performance.

Despite the promising results, there is no agreement around the RTO technology benefits as a strategy to increase the process in the plants' operation, due to the uncertainties of each RTO approach, and the lack of experimental and theoretical works that assess the benefits, costs of implementation, modification, and updating of instruments [4], [12]. For that reason, RTO has received important consideration in the industrial and academic literature [4] mainly on industries where the variability of the process appears all the time.

The most common RTO implementations are found in oil refining, where the continuous variation in the operational conditions, market competition, increased production cost, environmental restrictions, safety conditions, and the rising troubles associated to oil processing has encouraged using optimization and advanced control strategies. As a result, steady-state RTO technologies have been employed in numerous projects in the refinery industry [13] such as ethylene production, hydrocracking, hydrotreating, fluid catalytic cracking, catalytic reforming, and gasoline blending [14].

Within these units, one of the most complex and perhaps the most important economically in any refinery is the fluid catalytic cracking unit (FCCU). This unit converts heavy oils from the vacuum unit into more valuable products such as diesel, liquefied petroleum gas (LPG), and naphtha as a higher fraction in the gasoline pool. The high price of valuable products and the high quantities processed into these units make the FCCU a good candidate for RTO applications as an economic attractive tool. Consequently, the use of RTO in FCCU is an important topic of interest in the industry. However, its implementation is not trivial and it is difficult to find documentation that presents a study of all stages of a traditional RTO and its behavior as a whole. Currently, it is necessary to generate user-friendly RTO tools capable of modeling processes in detail, in order to understand its performance, facilitate its construction and promote its industrial implementation.

Therefore, the general objective of this work is the implementation and performance assessment of a real-time optimization system on a virtual fluidized-bed catalytic-cracking plant, through:

- Selection and programming of methods and strategies for the plant data analysis suitable for the catalytic cracking unit.
- Definition of a mathematical model that predicts the steady state of the FCCU and is consistent with the model established in the dynamic virtual plant.
- Choice and implementation of the optimization and control algorithm for the implementation of the RTO.
- Integration and evaluation of the RTO system implemented in the FCCU virtual plant.

In that way, this thesis is divided into six more chapters, each one sequentially presenting the different stages that comprise the implementation of an RTO. Thereby, Chapter 2 presents a review on RTO; the rise, development, current status, and trends; and the steps to perform the RTO, such as data analysis, optimization, and control strategies. In Chapter 3, a general description of the case study is presented. It includes the description, operation, and importance of the FCCU, as well as previous RTO implementations in such units. Chapter 4 presents the algorithm's assessment for each analysis into the validation stage. The evaluated algorithms with the best performance for the RTO implementation are the wavelet-based method for denoising, the deviation method for steady state detection, and the Hampel estimator for data reconciliation. In chapter 5 the optimization methods for this kind of problems are discussed and the optimization problem is presented. Considering this analysis, a genetic algorithm was selected for the RTO implementation. In Chapter 6, control methods tendencies and the most common control strategy is analyzed and implemented to the case study. In Chapter 7, all the strategies with the best results are integrated into the virtual plant to evaluate their performance into the RTO. Finally, conclusions and recommendations are presented.

Chapter 2. Real-Time Optimization

Abstract

The searching for the highest profitability in processes of high variability, as a result of market requirements and the inherent process disturbances, is one of the most important engineering challenges. This has motivated the use of optimization strategies as real-time optimization (RTO) which uses an online calculation of optimal setpoints from the process through the maximization of an economic cost function. As RTO can bring high economical earnings besides increased energy efficiency and reduced emissions, it is considered a powerful tool for searching the most profitable way to operate petroleum and petrochemical processes. This chapter aims to give a general perspective of RTO, its role in hierarchical control, and optimization decision making. RTO structure, applications, and some different approaches are examined, and some conclusions and perspectives for future research works are presented.

Keywords: hierarchical control, data validation, online optimization, RTO, control.

2.1 Introduction

In recent years, optimization has received special attention as a useful tool for growing competition in terms of effectiveness, energy efficiency, production cost reduction, product quality improvement besides the fulfillment of safety requirements, and strict environmental regulations. The increase of energy consumption and the volatility of the prices have promoted the use of better advanced control and optimization technologies that improve the profitability and stability in industrial plants [15]. The rise of computer processing capability to solve complex optimization problems and the use of more advanced solvers (as sparse matrix SQP) have allowed solving large problems with efficiency and confidence [4]. The availability of distributed control systems (DCS) for process control and data acquisition, and the application of multivariable controllers have made large scale online

optimization feasible. This is mainly true because a DCS is able to provide current plant measurements that do not just allow the updating parameters in plant models but also ensure a quick and accurate response to find new optimal set points [16].

As the process conditions normally change over time, the optimum values of the process variables need to be re-calculated and optimized every moment of the time (e.g. every hour, every day). For this purpose, optimization strategies as real-time optimization (RTO) result in a very attractive option to the continuous search of high profitability mainly in petroleum and petrochemical processing units [17]. RTO is in charge of optimizing the process in economic terms through an objective function [18] that adjusts the process variables each time a new change is originated by any external condition (operational variables, feed compositions, process constraints, etc.). Hence, the objective function is established either as minimization of energy consumption or maximization of products depending on market availability, safety and environmental constraints, product prices, feed costs, and product specifications.

RTO systems are model-based and they become part of closed-loop process control systems that keep the process as close as possible to the optimal operating point. This is achieved thanks to the use of rigorous process models and economic updated information in order to predict the optimal process operating conditions [18]. According to estimates from [4], nowadays 250-350 implementations of RTO use commercially available rigorous models. These models include detailed component mass and energy balances, detailed molecular kinetic reaction schemes, and their use would seem the most accurate in the RTO implementation. Nevertheless, in practice, the models at this level of detail are not necessary to reach the desired economic objective. It is because even if they would give more value than a simplified model, the rigorous model may be harder to match with the plant and more difficult to maintain. Therefore, the main consideration is to decide if the model is able to represent the process with enough detail and rigor such that the model reflects the key economic tradeoffs and operating constraints, and reaches a valid economic optimum.

Economic RTO benefits can be direct or indirect [18]. The direct benefit (online benefit) is referred to the economic performance improvement, or in other words, the increment of the plant profit by the reduction of energy consumption and the pollutant emissions. In the other side, the indirect benefit is related to a better understanding and knowledge of the process.

For example, stages included in RTO (as gross error detection) can help to detect the plant instrument errors; parameter estimation is useful for evaluating the equipment conditions and the identification of the bottlenecks and problem sources; and rigorous model process can be useful for maintenance, advanced process control, process design, and process monitoring. The RTO implementation has been motivated by the increase of computer processing capability: bigger models (with 100.000-200.000 equation models for optimization with 30-40 decision variables) and faster convergence (in less than 40 minutes). Therefore, RTO technology is essentially online optimization based on product scheduling and production control that seeks to maximize the plant's profit.

In the following sections, the place of RTO in control layers hierarchy and some RTO approaches under investigation are considered. Afterward, the methodology used in the standard RTO approach or RTO in steady state is explained. Finally, some industrial applications of traditional RTO technology are discussed, and some conclusions and suggestions are mentioned.

2.2 Control layers hierarchy

In a plant, the control hierarchy is usually a common solution to manage complex decisions and distribution decision making. It uses a successive refinement of time scales from top to bottom in a way that it breaks down complex problems into a cascade of interconnected solvable problems [4]. Control hierarchy and decision making are usually stratified in several layers that have different response times and control objectives that allow to determine what is important for specific decisions at any level of the hierarchy. These layers include planning, scheduling, RTO, supervisory control, and regulatory control. A general representation of these plant scales in optimization is given in Figure 2.1.

Control hierarchy and decision-making layers are configured as follow:

- **Planning:** This layer determines what and how the products of interest will be produced based on market demand. Among the decisions are what raw material to buy, and what and how many products to make. This layer is also an optimization task with a plant profit objective function solved by linear programming (LP) or successive programming.

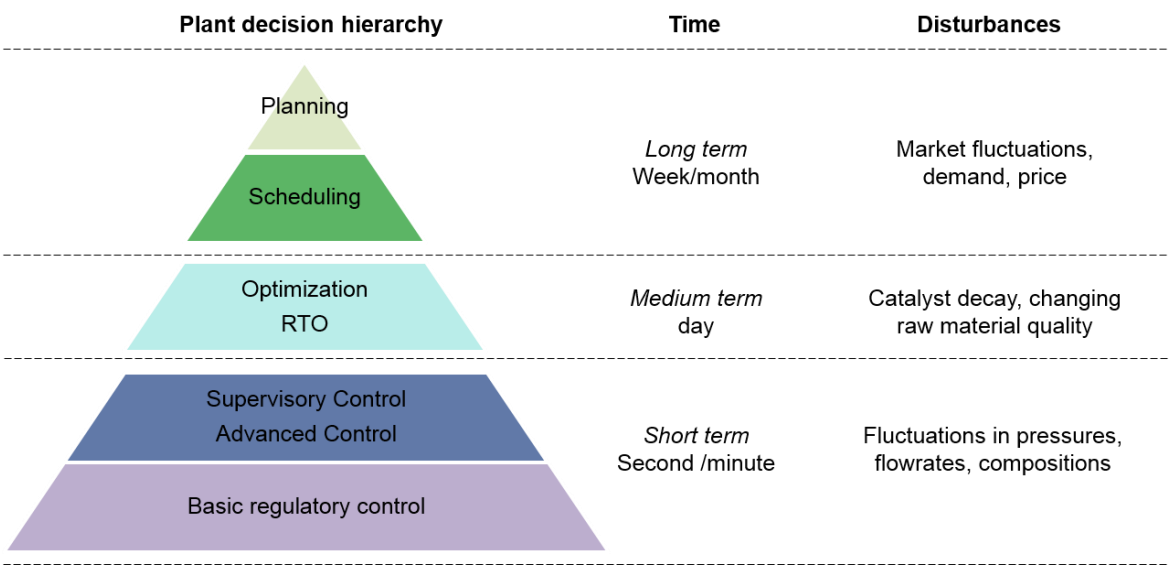

Figure 2.1 *Structure of Plant decision hierarchy depending on time and disturbances* [5].

Planning group can also provide the price (based on LP results) to RTO applications if the yield or stream properties do not change considerably.

- **Scheduling:** The results from this layer assign the best production rates for the plants [16]. This means that scheduling decides when actions and events will be executed for the plant: delivery feeds, product lifting, operating mode changes, and so on, in order to avoid storage problems. Linear optimization is commonly used for problems at this level, and the frequency of this optimization can be weekly or monthly.

- **RTO:** The main interest of this layer is the implementation of online business decisions according to a calibrated non-linear steady-state model. Then, this layer must maximize the profitability of the process under steady state by determining the optimal conditions: optimal setpoints and targets for the manipulated variables. The RTO disturbances are usually related to changes in economics, efficiencies, equipment fouling, and catalyst deactivation that can occur at low frequencies but have to be updated in real time, and it can be extended to typical process disturbances.

  The optimal conditions are found by solving an optimization problem which can be easy to solve when it is close to the optimal point. For this kind of problems, most commercial predictive controllers have LP or QP (quadratic programming) integrated layer. Nevertheless, in more complex processes it is essential to use a nonlinear optimizer that leads the system towards a better operation region. When ideal economic target

set points are provided by the RTO, they are passed to the supervisory layer which is in charge of the control process in steady state. Time scale of sampling for RTO is hours.

- **Supervisory layer**: This layer is in charge of ensuring the quality of the final product following specifications within the operating limits of the process. There are two main alternatives in this layer**:** advanced single control loop with additional fixes, and multivariable control as Model Predictive Control (MPC) [19]. The leading technology used here is MPC which acts on a minute time scale . This algorithm considers the interaction between control loops and provides minute to minute dynamic control of the plant.

  The controlled variables at this level are related to the product quality, while manipulated variables are the set point for the regulatory layer [18]**.** Then, the outputs of this layer are usually the set points of the PID controllers, and it is configured so that if there is any failure in the advanced control level, the plant operation continues with the last PID set points in the DCS [15].

  Most industrial MPC applications are linear models developed from plant tests, and they have demonstrated to be adequate for many control problems in the process industries. On the other hand, Non-linear MPC (NMPC) combined with RTO in the same layer is an active research area; although it has been useful just in certain processes as polymerization, there is not a significant application in the industry for continuous processes.

- **Regulatory layer:** This is the lower level which is focused on basic and inventory control. It is responsible for stabilization of the process in the time scale of seconds. The main objective of this layer is implementing the control actions computed by the supervisory control layer. These actions ensure a safe unit operation and prevent disturbances that can propagate in the plant. PID controllers (SISO) [18] is the most common control algorithm in this layer , and it is configured in digital systems (DCS-distributed control system or PLC –Programmable logical controllers)[15].

As it was mentioned above, the overall control architecture applies time scale separation between different layers. RTO and control layer below are executed in real time at different intervals with continual feedback from the process, whereas in planning and scheduling

levels, the feedback and updating of the model are performed intermittently and the human intervention is required to determine a set of objectives of the next level. These decisions have a significant impact on plant operations and each level may affect the organization in different ways. Then, the success of RTO needs the support of the whole organization to avoid conflicts between layers and failures in the RTO system.

2.3 RTO approaches

RTO strategies can be classified depending on the layers between optimization and regulatory control (one, two, or three layers), and according to the type of the model used (static or dynamic model).

2.3.1 One, two, and three layers

When RTO (based on a rigorous model) is not used, the optimization is made through simplified linear economic function in a linear optimization layer in which a linear programming (LP) or quadratic programming is solved. In this case, the upper layer provides approximated optimizing targets to the control layer (Figure 2.2). Sampling time is usually one minute [20].

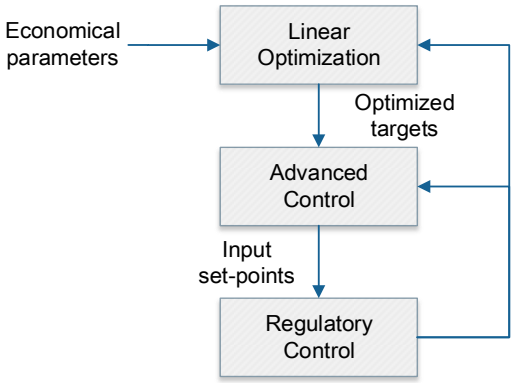

Figure 2.2 *Two-layer hierarchical structure without RTO* [20].

This approach is usually not the most suitable economically. Then, as it was mentioned before, the use of more rigorous strategies have been formulated. In this way, when RTO is included in the control structure, three main approaches have been considered:

Two layers (traditional RTO)

In a two-layer structure, RTO sends optimum values to the control layer which computes the required control actions to reach those optimum values and stabilize the process [20].

RTO uses a rigorous non-linear steady-state model while APC (Advanced Process Control) usually employs a linear dynamic model (Figure 2.3). Set points may be implemented via model predictive control (MPC) scheme or, alternatively, regulatory control [21]. Since sometimes the targets can be unreachable for APC, the operating points must be driven as close as possible to points defined by the optimization targets.

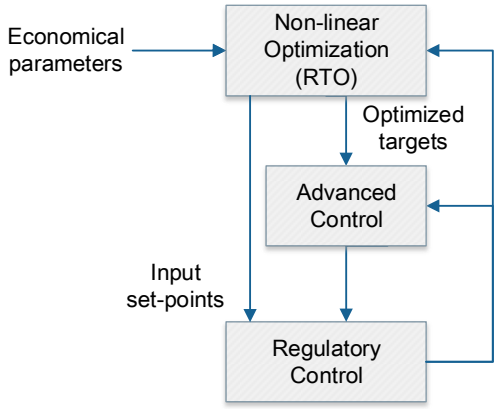

Figure 2.3 *Two-layer hierarchical structure with RTO. Adapted from* [20].

Because the model used in the optimization stage and the control layer can present mismatches between them, two approaches have arisen: three layers and one layer.

Three layers

In this approach, a linear optimization layer is included in the two-layer structure (Figure 2.4). The addition of this layer is made the linear dynamic model of the controller compatible with the non-linear model of the RTO layer [20]. This new addition allows that the difference between the control targets and RTO targets is minimized. However, this approach is not usually employed since the addition of another model can make the system more complex.

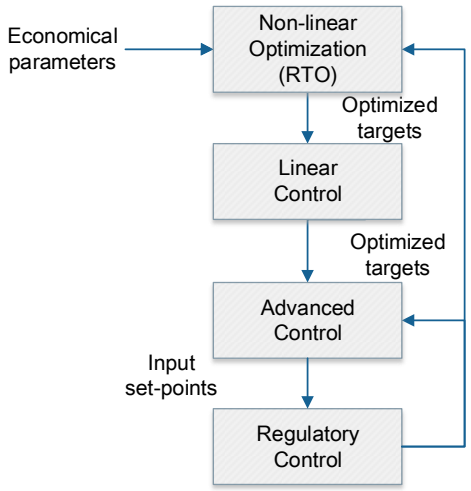

Figure 2.4 *Three-layer hierarchical structure with RTO* [20]

One layer (DRTO)

For this approach, optimization and advanced control problems are solved together in a one-layer structure (Figure 2.5). That means that an economic optimization problem term is included in the MPC objective function, which lets that plant operate close to the best operational condition [22]. Unlike the traditional MPCs, economic MPCs optimize the process operations rather than maintain the process variables around a few desired steady states [23].

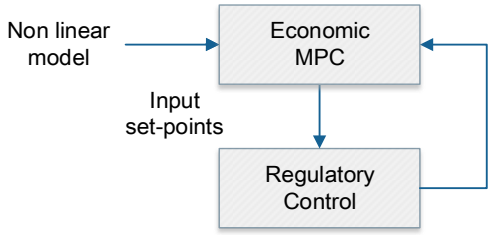

Figure 2.5 *One layer hierarchical structure (economic MPC).*

This approach uses a unique dynamic model; this is why a mismatch between models is not a problem. Nevertheless, it requires a high computational effort and does not guarantee a global optimum [20].

2.3.2 Static and dynamic models

The main goal of RTO is to reach the optimal operation of the plant through model-based numerical optimization. Depending on the type of process, the model based optimization can be classified as static optimization (RTO) and Dynamic optimization problem (DRTO):

- ***Static optimization problem (classic RTO)*:** optimizes the steady-state performance of a (dynamic) process while satisfying a number of operating constraints. In this case, the optimization problem can be formulated as:

$$\begin{aligned} \min \quad & J(u) = \phi(u, y) \\ s.t: \quad & F(u, y) = 0 \\ & G(u) = g_i(u, y) \leq 0 \end{aligned} \qquad \textit{Equation 2.1}$$

  where u corresponds to decision or input variables, y_p measured output variables, ϕ cost function to be minimized, F the process model, and g_i inequality constraints on the input and output variables.

- ***Dynamic optimization problem (D-RTO):*** optimizes the dynamic performance of a dynamic process while satisfying a number of operating constraints. This is commonly applied to batch processes; although some continuous process has also been studied. The DRTO problem can be formulated as:

$$\begin{aligned} \min_{u[0,t]} \quad & J = \phi\big(x(t_f), t_f\big) \\ s.t: \quad & dx/dt = F(x, u), \qquad x(0) = x_0 \\ & S(x, u, \theta) \leq 0 \\ & T(x(t), \theta) \leq 0 \end{aligned} \qquad \textit{Equation 2.2}$$

  where J is the scalar performance index to be minimized, x the n-dimensional vector of states with the known initial conditions x_0, u the vector of inputs, S the vector of constraints, T the vector of terminal constraints, F the dynamic model, and t_f the final time that is finite, but can be either fixed or free.

From the approaches mentioned before, the most applied in the industry has been two-layer RTO (traditional RTO). Although this has brought many benefits, its implementation, in some processes, has presented three main drawbacks [24]. First, RTO needs more complex non-linear steady-state models than the supervisory layer, due to the fact that it

requires an accurate process model to yield good performance. Second, models used in the lower feedback layer have discrepancies with models used in the RTO layer. That means that the RTO model can calculate an operating point that is unreachable by the feedback control layer, and that this leads to an offset between the actual operating steady state and the desired operating steady state. And third, a “re-optimization” after a steady state is detected, because of the inherent dynamic of the process and the presence of the disturbances. This can be complemented with the low frequency of execution which can affect the performance of the process. However, an increase in frequency can lead to stability problems of the closed-loop system.

Furthermore, for some chemical processes that are never in steady state (i.e. batch processes, processes with load changes, and grade transitions), the typical approach is not able to reach the optimal operation through time. Then, the steady-state strategy has been questioned in terms of being the best operating strategy for time-varying process economics and the non-linear characteristics of the process.

In an effort to integrate economic process optimization and process control, and make improvements in the performance when the process is dynamic, transient, or time-varying operation, strategies as economic MPC (EMPC)[24]–[26] and D-RTO approaches [26]–[29] have been proposed. EMPC (Figure 2.5) incorporates a general cost function or performance index (economic cost function) to be optimized. It can operate the process in a varying mode (non-steady state) and optimize the process economics. However, a rigorous design of EMPC that can operate large scale processes in a dynamic optimal model and is able to maintain the stability in closed loop process is challenging due to the notions of stability (e.g., asymptotic stability of a steady state) [31]. DRTO has a similar structure to EMPC as the optimization problem is treated as dynamic optimization that minimizes an economic objective subject to a dynamic process model. However, DRTO is not used for feedback control, but in the RTO layer of the hierarchical structure with the process control layer. For the DRTO approach, just theoretical treatment of closed-loop stability has been done and this kind of real-time applications are usually employed for batch or semi-batch processes. Continuous process with a recurrent grade of transitions that require cyclic executions as air separation units (ASUs) has demonstrated good results [32]. On the other hand, EMPC is usually implemented for feedback control, and it results in a dynamic model that is assumed to be consistent with the optimization layer.

DRTO systems consist of the solution of a dynamic optimization problem in the continuous time domain. It is represented by a differential algebraic optimization problem that uses a model on a form of differential algebraic equations (DAE). The optimization problem is usually solved by a transformation of it into a NLP problem using control vector parameterization [27]. While some EMPC only require knowledge about economic optimal steady state with a periodic trajectory (as a terminal constraint or stability region), DRTO requires much more knowledge of optimal operating strategy and sufficient understanding of the pricing behavior to model it correctly. Actually, EMPC requires information from RTO to improve closed loop performance. The recent online dynamic optimization research has been focused on considering economic objectives including disturbance rejection and setpoint tracking simultaneously, longer time horizons with additional constraints and degrees of freedom, and incorporating multiple operation stages over the predictive horizon [33].

It is important to emphasize that EMPC does not replace entirely RTO, because tasks as data reconciliation and model updating remain as a RTO responsibility. Using EMPC will have different closed-loop trajectories, more than traditional RTO with conventional MPC, because the model in RTO will use a steady-state process model, while EMPC uses a dynamic process model. In the case of using DRTO, the closed loop economic performance is not as good as the performance with EMPC, because DRTO is typically executed at a slower frequency than EMPC. However, if DRTO is executed at the same rate as EMPC, D-RTO is essentially (one layer) EMPC. A more detailed discussion of EMPC formulation can be found in [31].

Although different alternatives for online optimization have been formulated, classic RTO continues to lead the industry applications. For this reason, stages of optimization of this type will be detailed in the next section.

2.4 Classic/traditional RTO (standard approach)

The typical RTO structure uses a rigorous model in steady state to describe the plant behavior and optimize an economic objective function subjected to the process model [34]. Although RTO is responsible for process optimization, it covers more responsibilities than just optimization [31]. In fact, the RTO loop is an extension of a feedback control system, and it is composed of a sequence of steps that drive the system to the optimal point of

operation. This structure consists of different stages: steady-state detection, data reconciliation, measurement validation, process model updating, economic optimization, and optimal setpoints implementation. The RTO cyclic algorithm is represented in Figure 2.6. When the plant operation has reached a steady state after a process disturbance, the data are collected and sent to the validation stage. Here gross errors are detected and the data are reconciled through mass and energy balances. These validated measurements are useful to determine the model parameters and to be sure the model represents the plant accurately. At each RTO sampling time, key parameters of the steady-state model are updated to reduce the plant mismatch by using plant measurements [35]. Next to validation, in the optimization stage, the optimum set points are calculated using the updated model. Once the optimum values are determined, these are sent to the control system in order to control the most important variables in the plant [18]. Finally, plant data is sampled from the DCS to feed them at the beginning of the next RTO execution when a new state is detected as a result of any change in the process. This cycle is typically updated every few hours or even days [33].

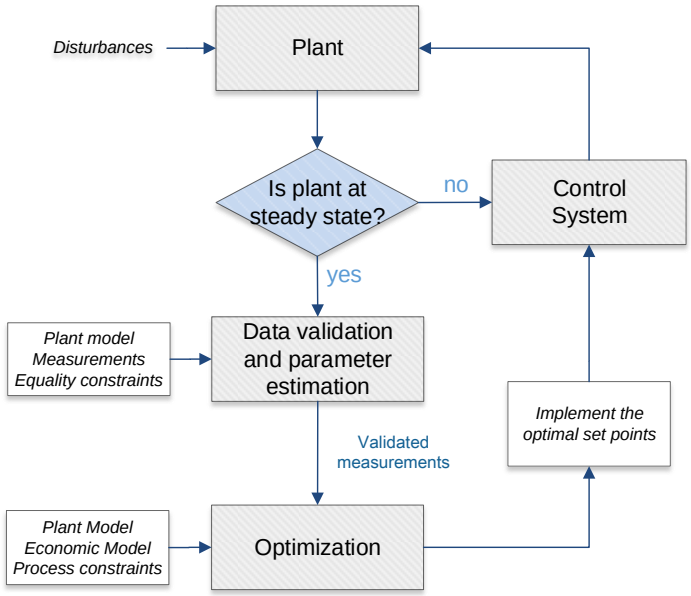

Figure 2.6 *RTO cycling algorithm Adapted from* [16]

Each execution of online optimization is determined for each of the units of the process, and it depends strongly on the settling time that can be estimated from the time constant by process step testing. Here is important to notice that the period of time between two online optimization executions must be longer than the settling time to be sure that the unit has returned to a steady state [16].

2.4.1 Steady-state detection

As RTO uses a static model, the plant must be in a reliable steady state. The most common methods include statistics terms as mean, variance, or slope of selected signals over a moving window that are compared against thresholds or previous values. Also, filters and averages of plant measurements are employed to eliminate frequencies and dynamic effects that can be present in the signals. Then, a steady state is detected if the signal passes a specific test; if not, testing continues until the process reaches steady state. When the process is in a steady state, plant measurements are sent to the data validation step.

2.4.2 Data reconciliation and gross error detection

Data reconciliation verifies data consistency: their fitting with material and energy balances. Then data validation is in charge of removing gross errors and rectify biases in the measurements (temperatures, pressures, flow rates, compositions, etc.). When data are validated, they are used to update the parameters in the plant model and be sure that the model predicts the operation of the plant. The updated plant model is used to evaluate the profit function (economic model) and determine the best-operating conditions.

2.4.3 Parameter estimation

This step includes the estimation of parameters as catalyst activity, heat exchanger factors, tray efficiencies in distillation columns, and so on. Also, in the economic model, there are parameters as sale prices, the products demand, cost and availability of raw materials, utility cost, etc. that have to be adjusted for an accurate profit.

In the parameter estimation, the plant model parameters are determined by minimizing the sum of squares of measurement errors, subject to the constraints in the plant model. After they are calculated, parameters are used for the plant simulation model to match the plant operation at the current operating conditions.

In this stage, it is important to consider which parameters are affected by unmeasured disturbances and which subset of parameters guarantees a consistent model. For example, parameters that change slower time scale may be not necessarily be updated every RTO execution. Parameter estimation is useful for evaluating the equipment conditions and to detect decreasing efficiencies and other problems in the process [18].

2.4.4 Economic optimization

This is the core of the optimization because good performance depends on both reliable input data as a reliable mathematical model. The optimal point is determined by the optimizer by using the plant model updated (measurements adjustments, parameters, constraint limits, and economic values). Once the model has been chosen, an objective function needs to be established depending on the maximization of the operating profit or minimization of the cost. The optimization problem is usually defined as non-linear programming which can be solved by successive quadratic programming (SQP). The plant model includes material and energy balances, thermodynamic and kinetic expressions; and most current RTO technologies are based on rigorous, steady state, first principles mathematical models [17]. The best conditions determined in this stage are sent to the DCS as set points for the controllers [16].

Because of the dependence of each RTO stage on the results of the previous ones, improvements in the accuracy of any of the above stages will enhance the optimization process. On the other hand, inaccuracies in those stages can lead to operating condition choices that do not improve the profitability of the plant operation. In that way, when online optimization is developed, it must ensure that the model parameters and process constraints are determined accurately to validate the process itself and to guarantee that the control target can be attained. If a real-time model process is not accurate, the control system will not be able to bring the process to the state specified by optimization. The process may seem unstable as the control system continues to move manipulated variables to reach infeasible control variable targets.

Probably, the data quality is as important as the frequency and quality of model updating. From the startup process until it shuts down, the process goes through a continuous state of degradation due to wearing in the equipment, fouling in the exchangers, decaying in the catalyst activities, plugging in lines and distributors, and some others inconvenient that will affect the value of the parameters of the model. Therefore, a real-time updating of model parameters provides realistic mathematical models in optimization systems.

2.5 RTO applications

Since the late 1980’s, several industrial applications of online optimization mainly in refineries and chemical plants have been implemented [36]. In the existing refineries is

common that shortcomings emerge as a result of market dynamics, new environmental regulations, and product specifications, mainly for continuous process. When established conditions are out of date, they may consume too much energy or not have sufficient reliability. To maintain competitiveness, oil refineries have implemented optimization strategies in the searching for the best operational conditions, and they have reported improvements in plant operations from 3% to 20% [16]. Typically, profitability gains due to better scheduling quality (provided by computer-aided decision-making technology) have been projected as ranging from US$ 0.10 to US$ 0.15 per crude oil barrel processed [37]. Maybe one of the reasons for the increased optimization use in refineries has been the stagnation in the expansion capacity as a result of the recent world economic slowdown and the optimization of the existing plants, which has lost priority in favor of the design of new ones [38].

In 2003, Oil & Gas Journal [39] reported that RTO use has been increased with around 100 worldwide large-scale refining applications. Furthermore, RTO can also be used for offline studies as a tool for debottlenecking and evaluating changes in feed, catalyst, equipment configuration, operating modes, and chemical costs.

RTO applications in refining process have been hampered by the lack of reactor models for major refining units, property estimation techniques for petroleum streams, the availability of equipment models, and the lack of understanding about how it works. Continued technology advancement has removed many of these difficulties and the number of reported RTO successes continues to grow [14]. Some economic benefits can be observed in Table 2.1.

Table 2.1 *RTO benefits in some refinery units* [14].

Process unit	Benefits* ($/bbl)
Crude unit	0.03-0.05
Hydrocracking	0.10-0.20
Hydrotreating	0.10-0.20
FCC	0.07-0.15
Catalytic reforming	0.10-0.40
Gasoline Blending	0.05-0.25

*Benefit values vary according to process design and operating conditions. Offline benefits not included.

This table reports different refinery units in which RTO has been applied. Although ethylene plants have had the most successful results, there are other applications where RTO has had a significant impact [40], [41]. The reported results have motivated companies to invest in RTO developments, but the methodology employed is not detailed because they belong to companies. Moreover, due to the strong interest in developing online optimization projects, many companies have set up partnerships to develop these tools and maintain a competitive advantage.

Some successful cases are also reported. In 1998 Honeywell Hi-Spec Solutions successfully implemented a utility optimization system at Repsol's Cartagena (Spain) Refinery Complex. The Utilities Optimization System was implemented using Honeywell's Hi-Spec Solutions ProfitMax RIOO system for Real-Time Optimization (RTO) which runs on an NT-based workstation. ProfitMax uses the NOVA modeling system from DOT Products Inc. for non-linear modeling and optimization. The utility system at Repsol's Cartagena refinery is a cogeneration system that supplies both electricity and steam to the site. The optimization problem involves optimization of the gas turbine loading and steam injection rate, header pressures, deaerator pressure, turbo-generator loading, and dual-driver settings [42].

Petrobras has been another company benefited from RTO implementations [15]. They define RTO technologies as "high sustainability" in the downstream process, proving economic benefits as a result of RTO technologies implemented in units as crude distillation column and FCCU. According to this, the profitability can increase around 6-10% when RTO and Advanced Process Control (APC) work together [17]. Although, they conclude that for a successful RTO application a good integration among different corporate teams: process analysis, production and planning program, optimization and automation, instrumentation, laboratory, production, and so on, is required.

Other major oil companies as ExxonMobil, Shell, and BP have invested in RTO research as a strategy to improve their business [17], [43], [44]. In the ExxonMobil olefins plant (Beaumont, TX), the detailed model contained about 200,000 variables and equations, and optimization is used to obtain the values of about 50 targets or set points. The key optimization variables are conversion, feed rate, and steam/oil ratio, subject to feedstock availability and equipment constraints. This RTO implementation has led to benefits in the range of millions of dollars per year [1].

Table 2.2 *Some industrial applications of online optimization* [13].

Company	Process	Location	Capacity	RTO Technology	Benefit Reported	Year	Pay-back	Reference
Sriracha Refinery	Refinery Utility	Thailand	Not report	Emerson (AMS suite)	1M$ /yr	Not report	Less than 3 months	www.pmo.assetweb.com
Borelais Group technology	Ethylene plant	Finland	300000 tpy	Neste Jacobes	12.5 M$/y	2004-2005	One month	www.hydrocarbonprocessing.com
No reported	Low sulfur gasoline HDS Plant	France	870000 metric tpy	Axens	1.1 M€/y	2006	Not report	www.hydrocarbonprocessing.com
Eastman Chemical	Utility plant	USA	3.6 M lb/h of steam, 176 MW	Emerson (AMS suite)	1 M$/y	No report	Not report	www.pmo.assetweb.com
ConocoPhillips	Alkylation's plant	USA	Not report	Emerson (AMS suite)	1.2 M$ / yr	Not report	Not report	www.pmo.assetweb.com
BASF, Seal Sands	Chemicals Optimization (acrylics & nylon polymer)	U.K.	Not report	Emerson (AMS suite)	Not report	Not report	Less than 1 year	www.pmo.assetweb.com
Shell Nederland Chemie Moerdijk	Petrochemicals Optimization	Nederland	Not report	Emerson (AMS suite)	Not report	Not report	Less than 6 months	www.pmo.assetweb.com
Sannazzaro refinery	Refinery (FCC unit)	Italy	200000 barrels per day	Aspen Tech Inc (ASPEN HYSYS)	10 cents/barrel	Not report	Not report	www.aspentech.com
Refineria Isla, Curacao	Crude Unit	Nederland	180000 bbl/d	SimSci& Foxboro (ROMeo &MRA)	2 M$ / yr	2 M$ / yr	Not report	www.eptq.com
Yeosu Yeochun	Ethylene Utilities	Korea	Not report	Emerson (AMS suite)	1.038M$ / yr	Not report	Not report	www.pmo.assetweb.com
Hyundai Petrochemical Co.	Olefins Plant	Korea	350000 ton/yr	M.W.Kellog Co.	12%(increased profit)	Not report	Not report	Oil & gas journal
ConocoPhillips	Refining Closed-Loop Optimization	U.S.A	Not report	Emerson (AMS suite)	Between 600,000 $ - 1.2 M$/yr	Not report	Not report	www.pmo.assetweb.com
Not report	Boiler Performance Monitoring Entergy	U.S.A	Not report	Emerson (AMS suite)	240,000$/yr	Not report	Not report	www.pmo.assetweb.com

Most recently, in 2015, Evonik reported being one of the first chemical companies to use process control systems with real-time optimization in some of its plants. The aim is to increase the savings potential of €50 million by the year 2025 by expanding the use of real-time optimization. For them, real-time optimization results in an estimated savings potential of €50 million and they hope to realize by the year 2025 [45]. Today, companies like SimSci offer real-time optimization system services with a potential refinery value of 6-40 MM USD/year [46].

Although many applications have been successful and the benefits in RTO solutions have been important, the RTO acceptance in the industries is not global; this is because some companies still consider RTO as an immature technology that needs to be investigated before being implemented [4]. Additionally to this, negative changes have impacted the RTO applications: staffing reduction have influenced the support groups responsible for RTO maintaining and global competitivity have to bring continuous changes to plant operation (equipment modifications and operating conditions). As a consequence, keeping RTO performing well has been a great challenge, and the difficulties that have arisen can be attributed to the lack of accurate support and maintenance on the RTO system. [40] suggest that the problems of the RTO applications can be overcome if the companies acquire a commitment and allow access to engineering expertise.

Additional to these, the lack of a modeling culture is an impediment to RTO. [4] mention that good results are obtained when the organization is committed with the RTO functionality, because besides the online benefits, it is also useful to understand the impact of any variation in the process. Then, RTO results in a good tool to get yield information in the planning and to understand the impact of independent variables on the profit.

It is important to note that RTO is only implemented where it is economically justified. One of the key requirements for RTO use is the variability of the optimal operating points due to changes in operating conditions, changes in feedstock, variable constraints, and changes in product and feedstock prices. When the variability is not so high, RTO results unnecessary because it can be determined offline avoiding closing the loop on the RTO system.

2.6 Conclusions

Online optimization has considerably improved the profitability of a plant operation and the emission reduction, besides providing a better understanding of the process. Many processes' profitability has increased in a range of 5-10%. The fast development in hardware and software tools, and automation technology have allowed that online optimization is considered as a strategy in the chemical plant profit improvements without substantial capital investment. These facts have motivated that many companies adopt this technology to their process, mainly in the oil and gas industry.

Nowadays, there are many tools in the market to maintain regulatory control; however, they usually require well-trained engineers to interpret, analyze and define appropriate actions as change control valves, tune PID controllers or implement a new strategy in case of faults. Many times, industries spend more time and money with actions that will not carry good results. So, the challenge here is to incorporate tools that help engineers (that know very well the process) in making decisions that prioritize the actions of each process and perform an automatic diagnosis and assessment of the regulatory control system.

Other RTO challenges are associated with its successful implementation, maintenance, convergence problems by numerical failures, and conflict with the decision hierarchy as a result of a model mismatch between different optimization levels. Then, due to the fact that RTO in steady state is still more common in industrial applications, an improvement of each of their different stages could bring important benefits in the current RTO implementations.

It has been mentioned that a traditional RTO scheme frequently leads to suboptimal operation because RTO updates only occur when a new steady state is detected. Consequently, other approaches as DRTO and EMPC (based on first-principle dynamic models of processes) have become as emerging technologies. The use of these dynamic models for large scale applications avoids the requirements of steady-state detection procedures and allows the simultaneous solution of optimization and control problems. However, the high computational effort that is required, stability problems and numerical issues have been the main reasons why its industrial application is limited.

Chapter 3. Fluid Catalytic Cracking Unit

Abstract

Despite the strong growth of renewable energy sources in recent years, fossil fuels continue to dominate global energy demand. This has resulted in an increasing number of petroleum refining investments, mainly for conversion units dedicated to producing transportation fuels. Among them, one of the most relevant is the FCCU which is employed for the conversion of high molecular weight hydrocarbon fractions of petroleum into more valuable olefinic gases, gasoline, and other products. Although the FCCU has been widely studied, it is still a subject of interest in the industry as a result of changes in the market, new specifications in the product, and the growing need to crack increasingly heavy crudes. This chapter gives a general description of the FCCU, its importance and its place in the refinery, typical loads and products, a description of each section of the unit, as well as FCCU common reactions and catalyst features. Some control strategies including PID and APC strategies employed by the industry in this unit are discussed. Finally, the study case for RTO application is presented along with an analysis of the studied model behavior.

Keywords: FCCU, Gasoline, FCC model, virtual plant.

3.1. Introduction

The Fluid Catalytic Cracking Unit (FCCU) is considered one of the most important conversion technologies in a refinery. Global fluid catalytic cracking (FCC) market demand was around 617.9 kilo-tons in 2014 [47]. It is the major producer of gasoline in the world, middle distillate olefins (LCO) or light olefins, as well as the main producer of an important fraction of propylene for the polymer industry [48].

The FCCU was used for the first time in 1937, but just until 1942, in the United States, the first unit was installed. At that time, thermic cracking was the main technology used, but it

was replaced by catalytic cracking which is able to obtain better yields in naphtha with a high gasoline's octane number. It is estimated that approximately 350 catalytic crackers operate around the world, which 102 are in the United States with a total capacity of over 14.7 MMBPD of oil processed in the world [49].

In a general way, the typical FCCU process breaks down ("crack") heavy crude fractions into lighter refinery streams for further processing or blending [50]. The cracking is made by the action of a catalyst which promotes the reactions at a lower temperature than that required for the thermal cracking. The reactions produced are much faster and selective than thermal cracking. However, the reactions generate an amount of carbon that is deposited on the catalyst surface and deactivates the catalyst. Hence, cracking processes are continuously developed by a circulation of the catalyst that is intimately contacted with the load in the riser. Subsequently, the catalyst is regenerated by burning coal produced in the regenerator [51].

In the following sections, a brief overview of the main FCCU characteristics is presented. First, a more detailed process description, cracking reactions, catalyst features are introduced, and RTO developments are mentioned. Finally, a short description of the FCC model used for the FCC virtual plant implementation is presented.

3.2 Fluid catalytic cracking unit

For many refineries, FCCU plays a central role in the oil process conversion. In fact, almost all major fuel refineries have a FCCU. The typical capacity of this unit is usually 1/3 of the capacity of the atmospheric distillation and brings the largest contribution to the gasoline pool (Figure 3.1).

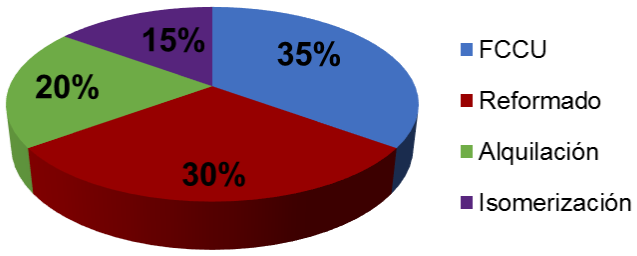

Figure 3.1 *Refinery units contribution in the gasoline pool (%vol)* [52].

FCCU takes desulphurized feedstocks to crack them into lighter, mainly high octane gasoline. The feedstock usually comes from atmospheric distillation (a mixture of paraffins, naphthenes, and aromatics), or distilled and/or bottoms from the vacuum tower; although many refineries mix streams from both distillation stages. The charge can be hydrotreated, partially treated, or totally unhydrotreated depending on the feed components. Although in a typical refinery, a FCCU is mainly installed to produce gasoline, the FCCU also produces olefins ($C_5^=$ and $C_4^=$) and LPG. Olefins can be used for alkylation and MTBE production. In some cases, FCCU can be dedicated to the production of petrochemicals, as in the UOP petro-FCC process [53]. A scheme for a typical high conversion refinery is presented in Figure 3.2 *A typical high conversion refinery [49].*

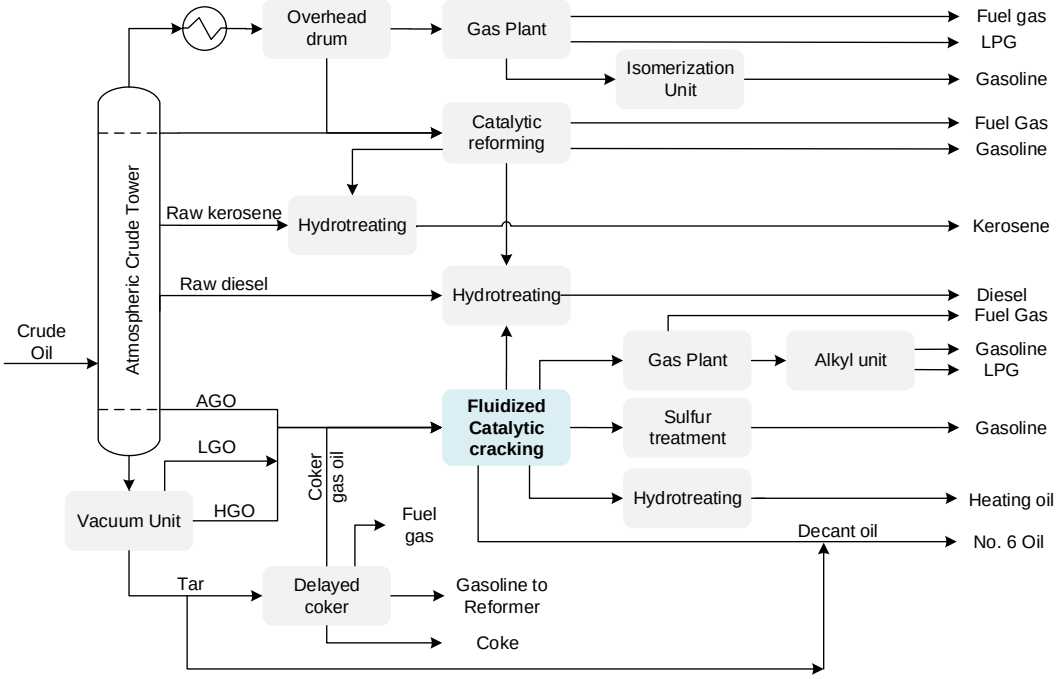

***Figure 3.2** A typical high conversion refinery [49].*

3.2.1 Process description

The FCCUs are usually composed of 4 sections (Figure 3.3):

- Feed preheating section
- Riser and stripping section
- Regeneration section
- Main fractionator section

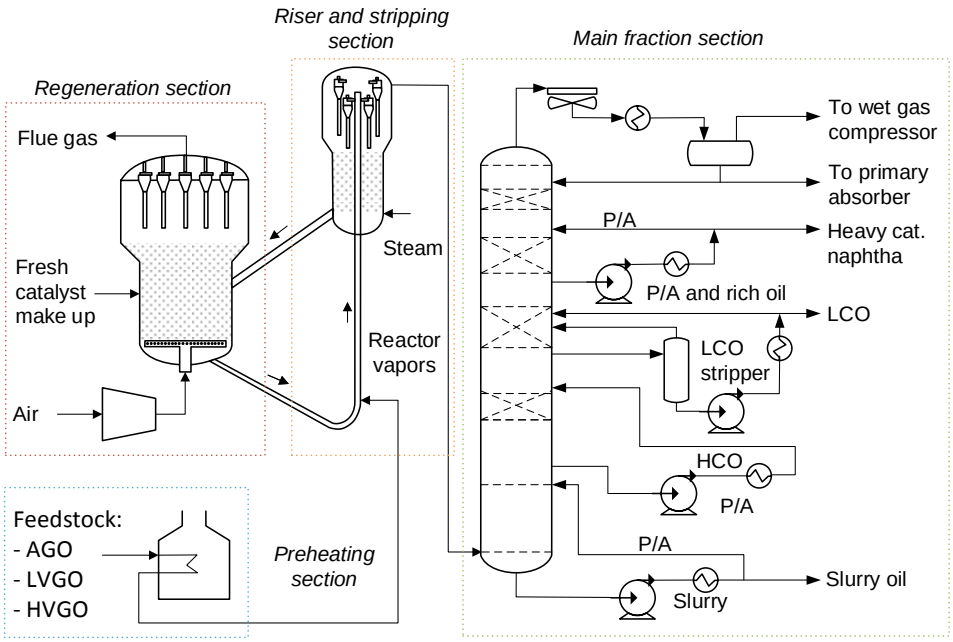

Figure 3.3 *Fluid catalytic cracking unit (basic scheme). Adapted from* [49], [54].

Feed preheating section

Gas oil feed to FCCU is commonly preheated before reaching the riser through heat exchangers that use hot streams from the main fractionator: pump around (P/A), light cycle oil (LCO) product or bottoms P/A. The range of the temperature is normally between 479-1023 K (205 - 400°C) [49].

Riser and stripping section

This section is composed of riser, catalyst separation, and stripper.

- **Riser:** In the riser, an efficient contact between the feed and the regenerated catalyst is critical to achieving the desired cracking reactions, whereby feed nozzles are used to atomize the feed and steam. As soon as the feed comes into contact with the catalyst, the feed is vaporized and the cracking reactions begin. Average cracking reactions occur in the range of 755-811K with oil feed temperatures from 533-700K. The necessary heat to vaporize the gas oil feed and reach the desired temperature for cracking reactions is provided by the hot regenerated catalyst. The resulting vapors carry the catalyst upward to the riser, so that when it reaches the top of the riser, the cracking reactions have finished. As cracking reactions are endothermic, the additional energy necessary to compensate the internal cooling is also provided by the hot catalyst. The ratio of catalyst to oil is normally in the range of 4:1 to 10:1 by weight. The

cracking process produces carbon which deactivates the catalyst rapidly decreasing its activity. Consequently, the catalyst is continuously moved from the reactor to the regenerator and back to the reactor, in order to be regenerated and recover the catalytic activity.

- **Catalyst separation:** After the mixture of catalyst and hydrocarbon cracked exits from the riser, it is separated to avoid secondary reactions above 783K (510°C). This separation is made in a vessel that contains cyclones that separate approximately 75-99.9% of the catalyst from product vapors. Product vapors are driven to the FCC main fractionator to be separated into gaseous olefins, FCC gasoline, and cycle stocks; while cyclones collect and sent the spent catalyst to the stripping section.

- **Stripper**: In spite of catalyst separation, some hydrocarbons adsorbed in the catalyst surface can remain on the spent catalyst. Then, a countercurrent flow steam is used to take away these hydrocarbons, avoid hydrocarbons losses, and reduce coke production into the regenerator. Once they are separated, the catalyst goes to the regeneration section.

Regeneration section

This section includes regenerator and catalyst handling facilities.

- **Regenerator:** In the regenerator, the coke produced in the cracking reactions and deposited on the catalyst is burned off to reactivate the active sites from the catalyst [55]. Regenerator also supplies the heat for cracking reaction and delivers fluidized catalyst to the riser [49]. To do these, the regenerator uses air blowers to allow combustion reactions. The energy produced as a result of combustion reactions is used for supplying sensible heat to the circulating catalyst, such that the hot regenerated catalyst satisfies the thermal requirements for the cracking section (heat balance). Traditional regenerators consist of two sections: the dense phase (at the bottom) and the diluted phase. The diluted phase is the region above the dense phase and has a substantially lower catalyst concentration than the dense one [49].

  The regenerator can operate in two different conditions depending on the requirements: complete combustion (no CO is produced) or partial combustion (CO is converted to CO_2 in an external boiler). Complete combustion can generate more energy and

decrease the coke yield, but requires low catalyst-oil ratio while partial combustion generates less energy and increases the coke yield. The choice of partial versus full combustion is determined by FCC feed quality. If it is “clean” full combustion is the choice, but if it has low quality or residue, partial combustion (possible with heat removal) is the choice [49].

The flue gas contains an important quantity of energy, so it has been used for different schemes. In some partial combustion units, the flue gas goes to a CO boiler to generate high-pressure steam, while in others, the flue gas is used to produce steam by a shell/tube heat exchanger.

- **Catalyst Make up:** As not all the active sites can be regenerated by impurities presence and catalyst lost from the system with the flue gas, fresh catalyst is introduced into the circulating catalyst system. Fresh catalyst is stored in a fresh catalyst hopper to be added to the regenerator through a catalyst loader.

Main fractionator section

This section consists of the main fractionator and the gas plant.

- **Main fractionator:** the purpose of this fractionator is to recover liquid products from the output reactor stream. The overhead gas products, light gases, and unstabilized gasoline are cooled and partially condensed in the overhead condensers. After this, they flow to the wet gas compressor to get wet gas. At the bottoms, the product is called slurry which is used to make No. 6 fuel oil or carbon black feedstocks when it has low sulfur, low metals, and low ash content. Besides overhead and bottoms products, the main fractionator is often designed to get three sidecuts used as P/A streams: HCO, LCO, and heavy naphtha. HCO is used as recycle to the riser and rarely as a product; LCO as absorption oil in the gas plant and (after a stripping) as a product for diesel/heating oil blending; while heavy naphtha is used as absorption oil in the gas plant and for blending in the gasoline pool.

- **Gas plant:** the gas plant takes the main fractionator overhead gas products (unstabilized gasoline and light gases) and it separates them into fuel gas, C_3 and C_4, and gasoline. C_3 and C_4 include propane, propylene, n-butane, i-butane, and butylenes. Some refineries use alkylation units or a depropanizer tower to separate C_3 from C_4.

3.2.2 Load and products features

The FCC unit function is to convert heavy gas oil (HGO), vacuum gas oil (VGO), or residue feedstock into useful products. A general scheme of feedstock and products in FCC based on models presented by [56], [57] is presented in Figure 3.4.

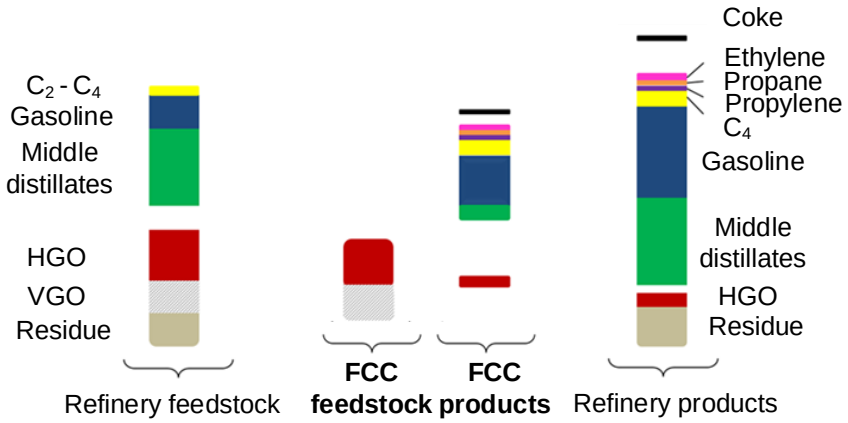

Figure 3.4 *The effect of FCC conversion on total refinery product. Left: Atmospheric distillation frees up about 50% of the feedstock (middle distillates, gasoline, and light gases). Heavy gas oil (HGO) and vacuum gas oil (VGO) are converted in the FCC unit. The products from FCC are combined with the initial products from crude distillation in the column on the right* [48].

- **Load**: the crude quality used to feed the FCC unit can vary as a result of the different type of crudes in the refinery and the fluctuation of the market conditions. The load supplied to the FCCU is mainly composed by Heavy Gas Oil (HGO) from atmospheric distillation, Vacuum Gas Oil (VGO), including HVGO and LVGO, and sometimes GO from visbreaking or coking in small quantities.

- **Products:** The typical products from this conversion are dry gas (hydrogen, methane, ethane, ethylene), LPG (propane, propylene, i-butane, n-butane, butylenes), gasoline, light cycle oil (LCO), HCO (in few FCCs), slurry, and combustion coke [49]. Normally, the objective is to maximize the conversion to gasoline (because it gives about 35% of total gasoline pool), LPG, and more recently diesel production.

3.2.3 FCC reactions

When gas oil molecules come in contact with the catalyst, many complex reactions take place, and the product distribution is mainly dependent on the nature and the strength of the catalyst acid sites. Large number/part of them are cracking reactions, although thermal

reactions also occur due to non-ideal mixing in the riser and poor separation of cracked products in the reactor.

Thermal reactions or thermal cracking generates free radicals and is mainly induced by the temperature and poor distribution of heat in the reactor. The sequence of reactions forms a product containing mainly C^1 and C^2 (dry gas), as well as the generation of highly branched alpha-olefins, which do not contribute to increasing the octane number in gasoline. The main drawback of thermal cracking is that a high percentage of olefins produced during the intermediate reactions are polymerized and directly condensed in coke. For that reason, catalytic cracking is preferred because it leads to a more valuable product distribution.

Cracking reactions of heavy hydrocarbons in an FCCU occur through a mechanism known as "carbonium ion" in the presence of an extreme acid strength catalyst (zeolites). In an initial stage, the hydrocarbon molecule is adsorbed on the acid center of the catalyst to extract the proton. This generates the formation of a hydride ion (H +) and a carbenium ion (R +). The carbenium ion is highly unstable, so the chain breaks down into an olefin and a new carbenium ion (beta cleavage). During this process, isomerization reactions and hydrogen transfer can also occur with the generation of aromatics and paraffins.

3.2.4 Catalyst features

Commercial cracking catalysts used in FCCU are microspherical particles that when they are properly fluidized, they behave like a liquid [49]. FCC catalyst is prepared from acid-treated natural aluminosilicates, amorphous synthetic silica-alumina combinations, or crystalline synthetic silica-alumina catalysts known as zeolites or molecular sieves [55]. The most used are either zeolites or mixtures of zeolites, and amorphous synthetic silica-alumina, because zeolites have higher activity, give higher gasoline yields, encourage gasoline with a large percentage of paraffinic and aromatic hydrocarbons, have lower coke yield, increase the i-butane production, and reach higher conversions without over-cracking.

3.3 RTO applied on FCCU

Control and optimization of an FCCU have been subject of numerous studies through more sophisticated techniques as MPC [58], steady-state RTO [59], [60], NMPC [61], and by

integrating optimization and advanced control layer (one layer approach also called DRTO) [28].

Among them, one of the most attractive has been DRTO, because it integrates the economic optimization problem with the optimization of control actions. This optimization is made in real time and in a dynamic state, which is very interesting for complex dynamic processes. An example is mentioned by [27]. where a comparison between DRTO and RTO applied to a FCCU is made. The DRTO is implemented by using a mechanistic dynamic model and the large scale NLP solving the problem through IPOPT solver. The results reveal significant benefits in DRTO application to FCCU. However, although many studies of DRTO have been developed in the last years, its application in FCC plants has been limited due to its complex structure and two sides have never been seamlessly integrated [62]. Only successful real applications have been reached for batch and semi-batch processes [63].

On the other hand, traditional RTO has been more successful. In 1977, [64] described a real-time optimizer (RTO) for the Residual Catalytic Cracker plant at the Statoil Mongstad refinery. The predicted economics (objective function) is calculated under the restriction of entire plant mass balance satisfaction, while the constraint predictions are based on delta values from the current operating point. A commercially available sequential quadratic programming (SQP) routine solves the optimization problem. The optimization system was coded in FORTRAN and implemented in a plant computer along with model-predictive control (MPC) applications; both interact with the real-time process database. Optimized independent RTO-variables are implemented on the plant as set-points for the MPC controlled variables or as desired values of the MPC manipulated variables.

Another example of successful RTO implementation was reported by Petrobras. They used RTO in FCCU by equation oriented approach [17] and an international bid was created. It used Invensys and Romeo including a reactor/regenerator section, a main fractionator, and a gas recovery plant. The system was running in closed-loop and the average gain was evaluated in US$ 0.12/bbl of FCC feed by comparing the unit performance with and without RTO. As a conclusion, they make some comments related to the implementation: lack of instrumentation on preheat train (FCC) implied simplifications that directly impact the main fractionator balance, reason why it needs to be evaluated from time to time; and the necessity of estimating feed characterization due to low feed lab analysis frequency and

non-convergence problems by instrumentation faulty and/or out of service of any piece of the equipment. These issues force to have a fully dedicated RTO engineer for each application, so that the engineer can assess its results, make sure they are being implemented, and keep the system running in spite of the daily issues.

Another rewarding application of RTO in a FCC was presented in October, 2012 at the SimSci-Esscor User Group Meeting, Houston TX. They implemented a Real-Time Optimization (RTO) in ROMeoTM using SimSci-Esscor'sTM to a Fluid Catalytic Cracking (FCC) reactor model. According to ExxonMobil Research and Engineering, some of the RTO benefits applied to this unit were: RTO directly manages fuel gas production up to a specified cushion limit, MPC provides tight control of fuel gas cushion by fine-tuning the RTO temperature target between RTO solutions; RTO optimizes the reactor temperature against fuel gas cushion while accounting for day/night operation, seasonal differences, and as feed quality and other constraints change; and RTO significantly improved conversion at similar or higher rates than the previous operation.

3.4 FCCU virtual plant

The RTO implementation is developed in a dynamic virtual plant in Matlab ® that generates data under different scenarios. The virtual plant considers a dynamic simulation of a FCCU using a phenomenological model and error addition to data to resemble it as a real plant. Noise is unavoidably present in plant signals and is usually caused either by data acquisition process (instrument miscalibration or malfunction, power supply fluctuation, wiring, and process noise) or due to environmental effects.

3.4.1 FCC model

The equations for a continuous riser reactor and regenerator model are coupled in Matlab®. The ordinary differential equations and non-linear algebraic equations for material and energy balances are solved by using ode15s solver. The solution of these equations started with initial guesses of regenerated catalyst temperature (T_{rgn}), coke fraction on the regenerated catalyst ($C_{coke,rgn}$) and oxygen mole fraction leaving regenerator dense bed (xO_2) from steady state. In searching for the FCC steady state, initial conditions reported by [65], [66] were used. The FCC model implemented in the virtual plant is presented in Appendix B.

Steady-state sensitivity

In order to study the effect of changes in independent variables on the reactor performance, variations of the independent variables are presented as increases or decreases of the steady-state reference conditions. The independent variables include:

- Flow rate of air to the regenerator (F_{air}).
- Catalyst circulation rate (F_{cat}).
- Flow rate of oil in the feed (F_{feed}).
- Feed oil temperature (T_{feed}).
- Air temperature (T_{air}).

As follows, the profiles of gas oil, gasoline and temperature along the riser in the reference steady state, and the effect of changes in independent variables on the riser and regenerator temperatures; mass fraction of gasoline (G) gas oil (GO) and coke in the riser outlet; oxygen and coke in the regenerator, and the ratio CO_2/CO are presented. For assessing the effect of these changes, the steady-state conditions were plotted vs the percentual variation on the independent variable.

- ***Riser profiles***

The model predictions for gas oil and gasoline concentration along with the riser temperature profile at steady state conditions are shown in Figure 3.5.

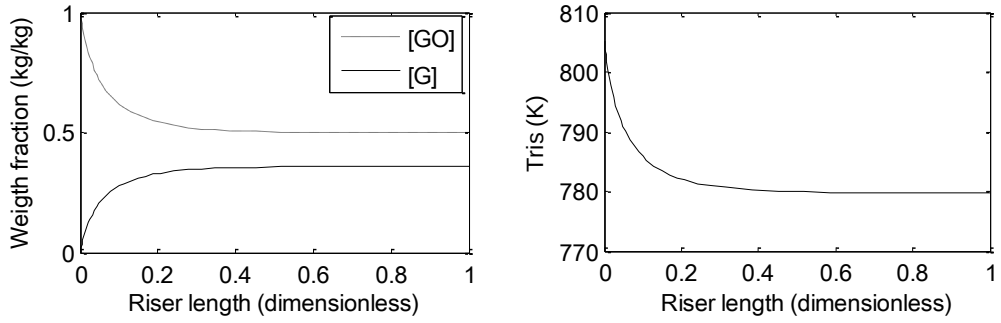

a) Weight fraction riser profile *b) Temperature riser profile*

Figure 3.5 *Concentration and temperature riser profile at steady state conditions.*

In Figure 3.5a, it can be seen how the concentration of gas oil (GO) decreases while the gasoline concentration (G) increases as a consequence of cracking reactions. For these steady-state conditions, it is observed that the maximum gasoline fraction (0.3585 kg/kg)

can be obtained from a riser dimensionless length of approximately 0.7. On the other hand, in Figure 3.5b a decrease in temperature is observed as a result of the cracking reaction. The initial temperature is 805 K, but as the reaction proceeds, the temperature decreases to 780 K making endothermic reactions evident.

- ***Effects of changes in the air flow rate to the regenerator***

The more oxygen availability increases the combustion reactions rate as the energy production is enhanced by a higher oxygen concentration. The catalyst delivered to the riser carries a greater amount of heat, which increases the temperature of the riser. This increase in temperature is accompanied by an increase in the production of gasoline, but also in coke as can be seen in Figure 3.6a and Figure 3.6b

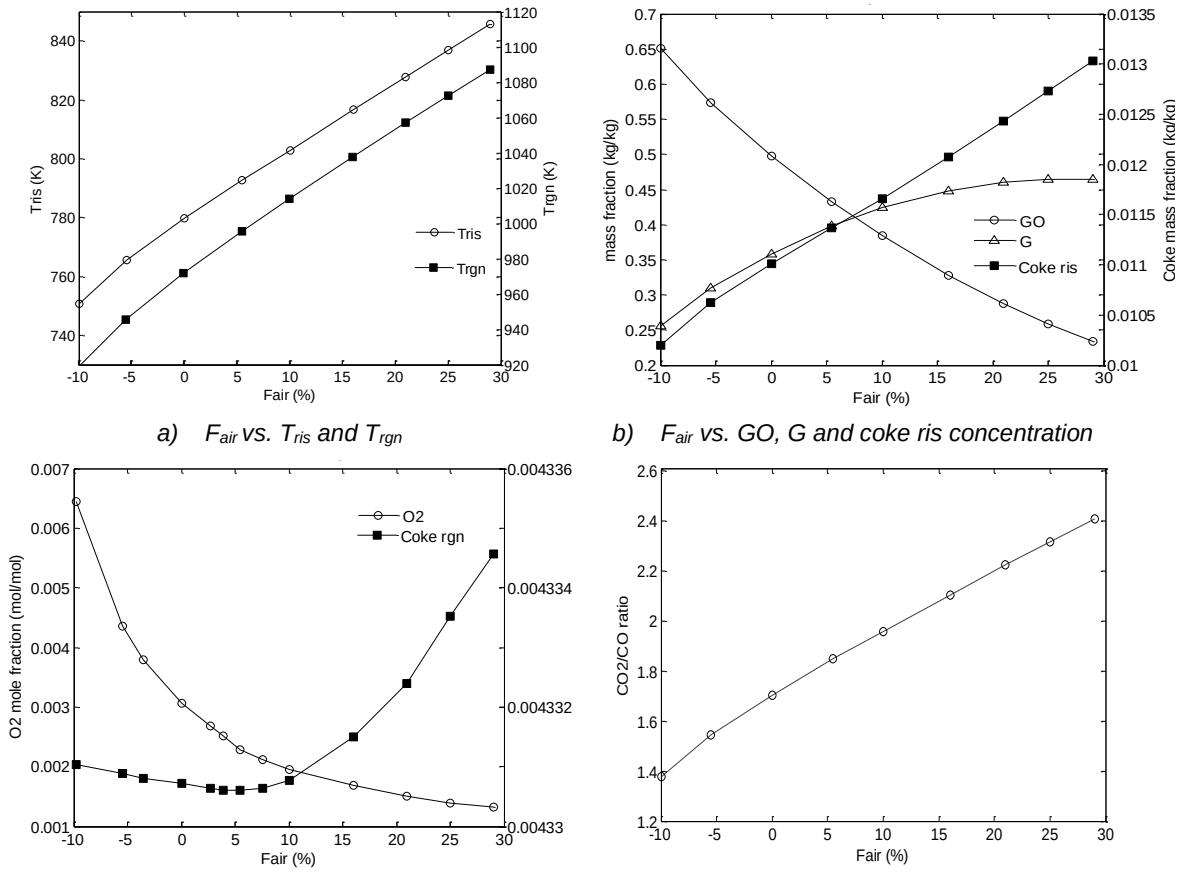

a) F_{air} vs. T_{ris} and T_{rgn}

b) F_{air} vs. GO, G and coke ris concentration

c) F_{air} vs. O_2 and coke in the regenerated catalyst

d) F_{air} vs. CO_2/CO ratio

***Figure 3.6** Changes in steady state by changes in air flow rate.*

If the air flow increases, the amount of oxygen consumed is higher and complete combustion reactions are promoted (CO is converted to CO_2). This is evidenced in Figure

3.6d, where sigma value (CO_2/CO) increases with rises in air flow. A particular behavior is observed with the amount of coke present in the regenerated catalyst (Figure 3.6c). As the air flow in the regenerator increases, the coke in the catalyst decreases as a result of combustion. However, for an increase in air flow greater than 10% of the steady-state condition, the amount of coke in the regenerated catalyst starts increasing significantly. Then, from this value of air flow, the amount of coke generated in the riser is so high that the regeneration stage is not able to eliminate this coke by combustion.

- ***Effect of changes in catalyst circulation rate***

Results of changes in catalyst circulation rate for the FCC system are depicted in Figure 3.7. The increase of the catalyst circulation rate (increase in the valve opening) derives in higher riser temperatures (Figure 3.7a) associated with more heat in the input and more active sites available for the endothermic cracking reactions. However, the increase in the riser temperature also raises the rate of cracking reactions making large quantities of coke and favoring the catalyst deactivation (Figure 3.7b). Likewise, the increased heat removal rate from the regenerator cause a decrease in the regenerator temperature (Figure 3.7a). This effect is due to the fact that the catalyst, which is in continuous circulation, is the vehicle for the transfer of energy between the two reactors [67].

As the coke produced in the riser increases, the oxygen consumed in the regenerator for the coke combustion is greater. This is reflected in Figure 3.7c where the amount of oxygen in the flue gas decreases with the catalyst flow increase.

Despite more oxygen is consumed for combustion, the oxygen in the regenerator is not enough to burn all the coke and then, the amount of deposited coke in the regenerated catalyst increases gradually. The decrease in the regenerator temperature also affects the combustion products. In Figure 3.7d the CO_2/CO ratio decreases with increases of the catalyst flow which favors a higher production of CO over CO_2.

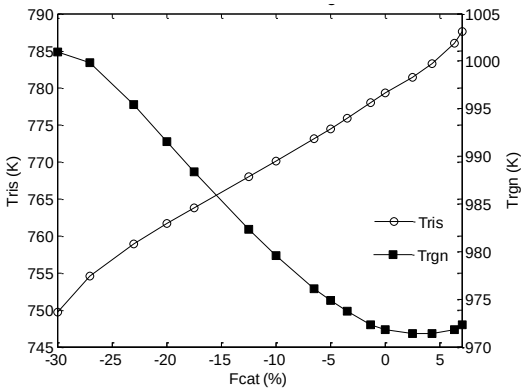

a) F_{cat} vs. T_{ris} and T_{rgn}

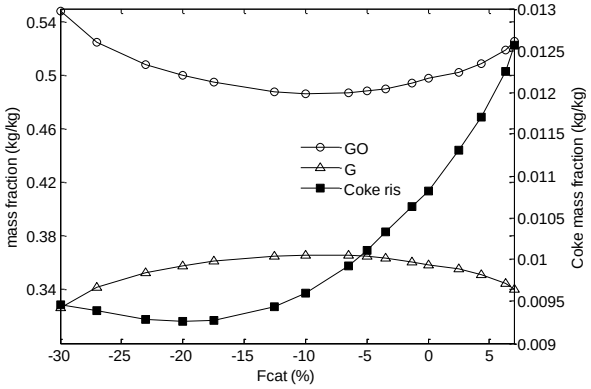

b) F_{cat} vs. GO, G and coke ris concentration

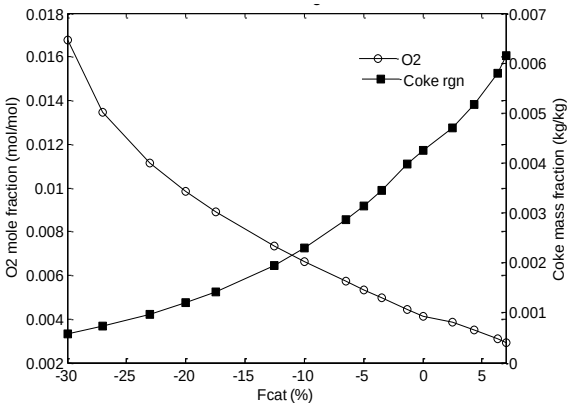

c) F_{cat} vs. O_2 and coke in the regenerated catalyst

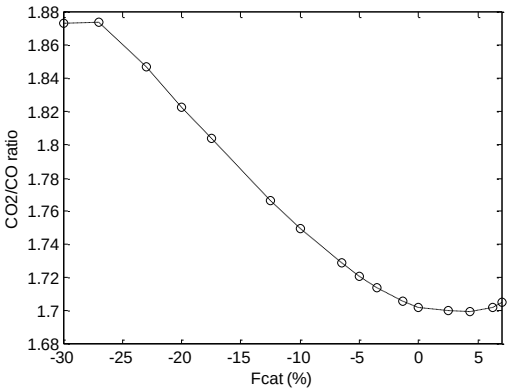

d) F_{cat} vs. CO_2/CO ratio

Figure 3.7 *Changes in steady state by changes in catalyst circulation rate.*

- ***Effects of changes in the feed circulation rate***

The increase of feed flow rate in the system leads to a decrease in reactor temperature since most of the energy to reach the cracking temperature is supplied by the regenerated catalyst (Figure 3.8a). Therefore, if the quantity of preheated feed is greater and the regenerated catalyst remains constant, the cracking temperature decreases, as well as the production of gasoline and coke since there are less catalyst area available for cracking reactions (Figure 3.8b).

Now, if the produced coke decreases, the amount of coke to burn in the regenerator is lower and less oxygen is consumed. This leads to a decrease in the regenerator temperature (Figure 3.8a) and more oxygen be released in the flue gas (Figure 3.8c). This decrease in the regenerator temperature encourages the CO production over CO_2 as shown in Figure 3.8d.

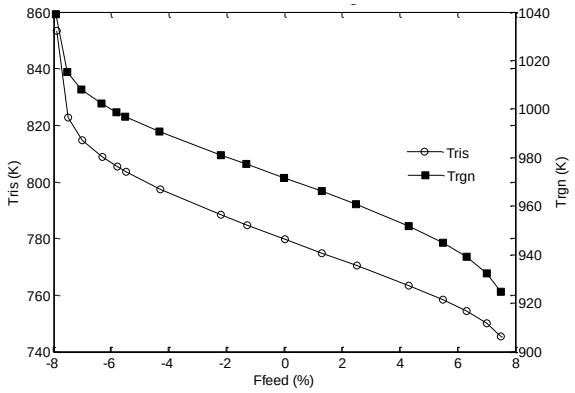

a) F_{feed} vs. T_{ris} and T_{rgn}

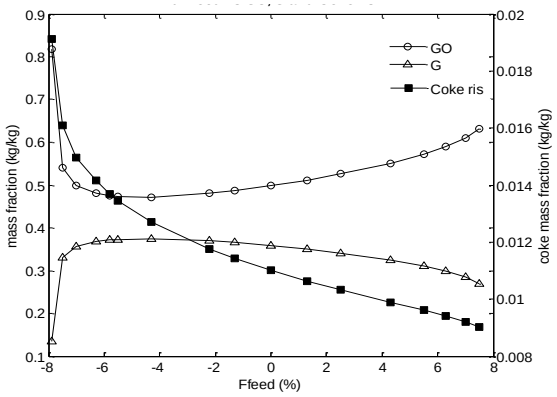

b) F_{feed} vs. GO, G and coke ris concentration

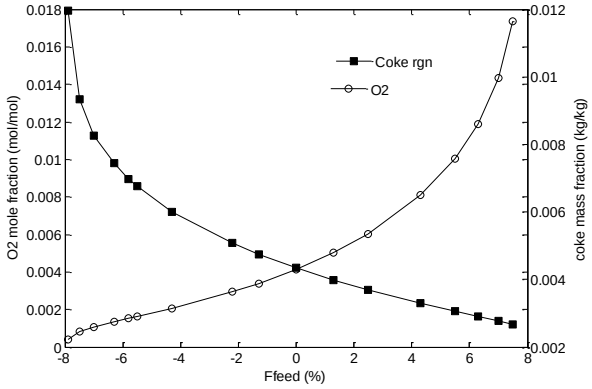

c) F_{feed} vs. O_2 and coke in the regenerated catalyst

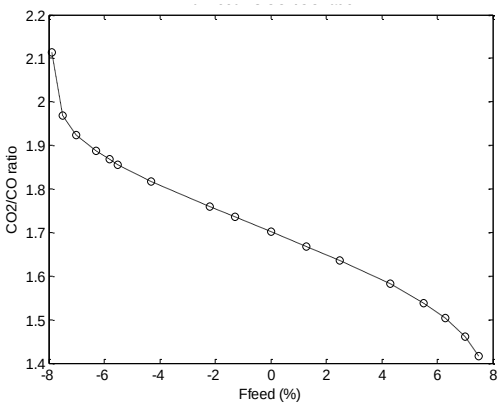

d) F_{feed} vs. CO_2/CO ratio

Figure 3.8 *Changes in steady state by changes in feed flow rate.*

- *Effect of changes in the feed oil temperature*

Figure 3.9 shows the effect of changes in the feed oil temperature on the FCC system.

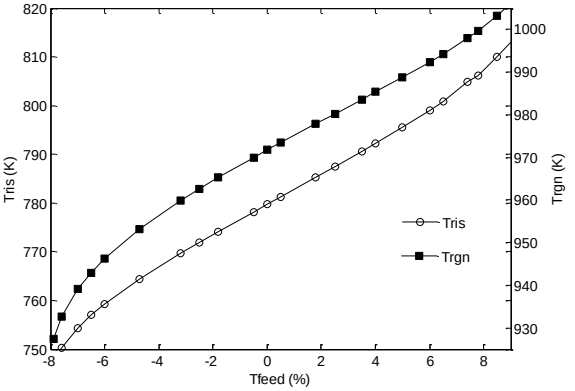

a) T_{feed} vs. T_{ris} and T_{rgn}

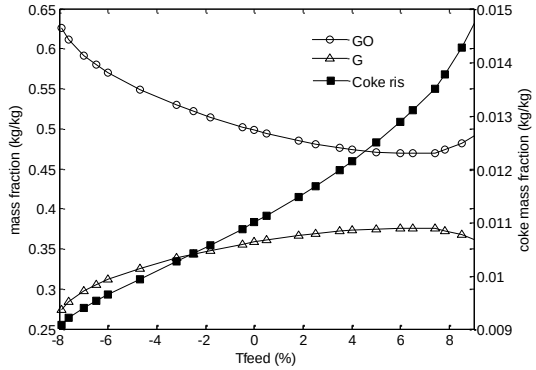

b) T_{feed} vs. GO, G and coke ris concentration

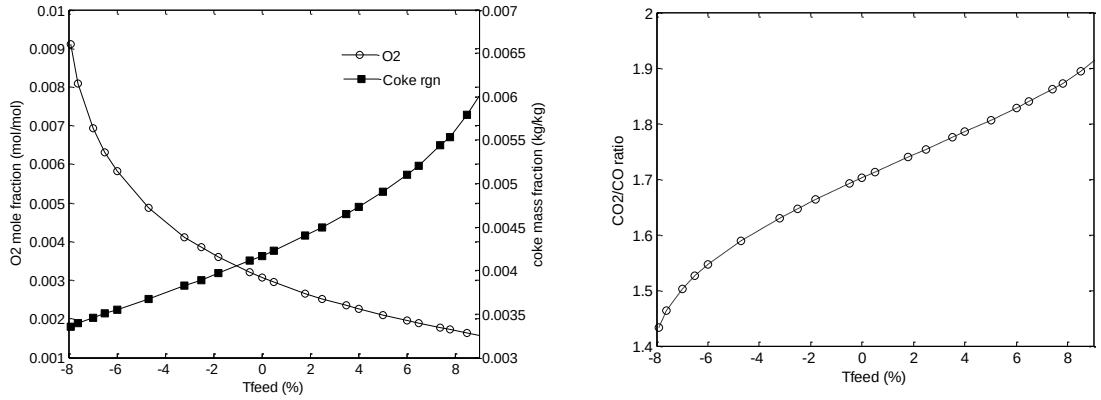

c) T_{feed} vs. O_2 and coke in the regenerated catalyst *d) T_{feed} vs. CO_2/CO ratio*

Figure 3.9 *Changes in steady state by changes in feed oil temperature*

Increases in feed temperature elevate riser temperatures (Figure 3.9a) and improve cracking reactions: gasoline production, but also coke formation (Figure 3.9b). As more coke is produced, more coke is deposited on the catalyst, and then more oxygen is used to burn the coke in the regenerator (Figure 3.9c). This leads to a regenerator temperature increase (Figure 3.9a) that favors the complete combustion reactions: increment of the CO_2 produced in the flue gas (Figure 3.9d).

- ***Effect of changes in the air supply temperature***

Figure 3.10 depicts the effect of changes in air temperature in the FCC systems. Increases in air temperature promote total combustion reactions in the regenerator rising the oxygen consumed and CO_2 produced (Figure 3.10c and Figure 3.10d). This elevates the regenerator temperature and the regenerated catalyst temperature as well (Figure 3.10a). The quantity of energy that is transferred by the catalyst from the regenerated to the riser, step up the cracking temperature and the gasoline production, but also that of coke (Figure 3.10b).

The more the coke produced in the riser, the more the coke deposited in the catalyst. Then, when the spent catalyst reaches the regenerator, the available oxygen in the regenerator is not able to eliminate all the coke deposited (Figure 3.10c). In fact, over 40% above the reference steady state temperature, the amount of gasoline produced begins to decrease (Figure 3.10b). This may be due to an increase in the riser temperature and a decrease in the available active sites of the catalyst by coke deposition.

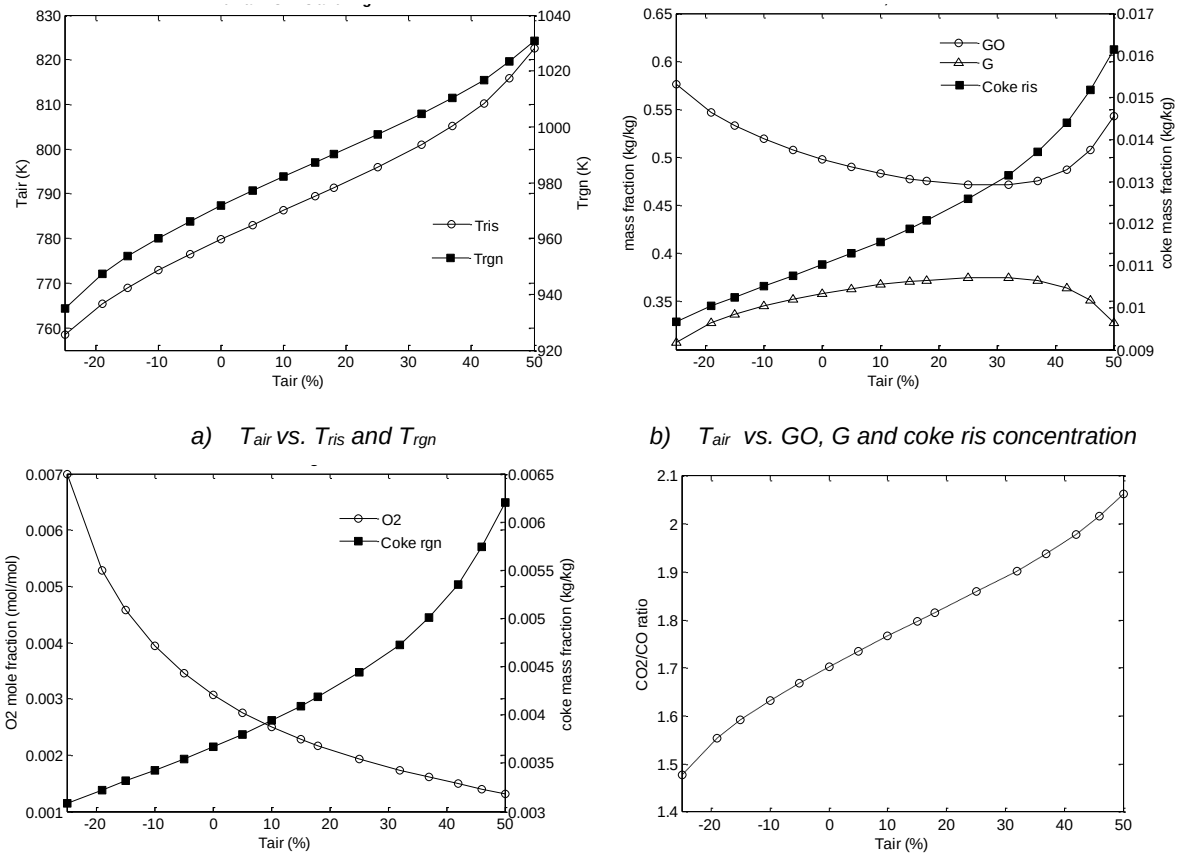

a) T_{air} vs. T_{ris} and T_{rgn}

b) T_{air} vs. GO, G and coke ris concentration

c) T_{air} vs. O_2 and coke in the regenerated catalyst

d) T_{air} vs. CO_2/CO ratio

Figure 3.10 *Changes in steady state by changes in air temperature*

3.4.2 Data contamination

In order to simulate a real plant, dynamic output data from FCC solution were contaminated using a Gaussian error with a signal-noise ratio 50 (SNR 50), gross error in a set of 15% of the overall random data, and errors from 0 to 5% of the maximum values. Measured variables also were contaminated with random bias errors between 2σ and 50σ in order to simulate real plant measurements. Some signals after data contamination are depicted in Figure 3.11

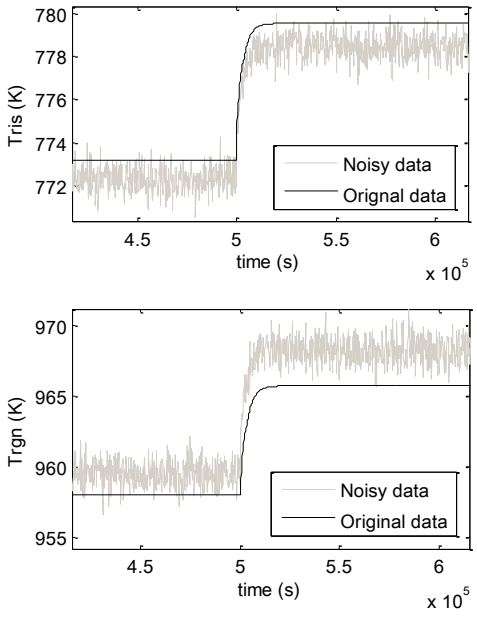

Figure 3.11 *Dynamic simulation from FCCU virtual plant.*

3.5 Conclusions

An industrial FCC unit has been simulated in Matlab ® by integrating kinetic models for riser reactor and regenerator. The coupled model equations were solved using ode15s solver. The results obtained were used to study the effect on the system when independent variables are changed.

Increases in F_{air}, T_{air}, T_{feed} and F_{cat} have an important influence on gas oil conversion, but from them, for this steady state conditions, F_{air} has a stronger one. This is a consequence of the fact that the amount of regenerated catalyst is much higher than in the other cases, and therefore, the catalyst that reaches the riser has more active sites available for the cracking reactions. From the analysis, it appears that decreasing T_{feed} leads to higher gasoline conversion as it enhances cracking reactions.

So, as FCC is defined as a MIMO (multiple input and multiple output) system, it is necessary to find the optimal operation changing multiple variables of the system. Searching for a greater amount of gasoline and a smaller amount of coke using the lowest possible energy in the process is covered in Chapter 5, where an optimality analysis is presented for the study case of the FCCU.

A noise addition was used to the model that allowed creating data similar to those obtained in a real plant which is very useful to compare the plant response and each one of the RTO stages when data are contaminated (as it happens in real plants) and when they are not (ideal data).

Chapter 4. Data Validation and Parameter Estimation

Abstract

Data validation and parameter estimation are important steps for an RTO (real-time optimization) implementation. Data validation eliminates errors and inconsistencies in data of an industrial process, while parameter estimation determines the new values of model parameters as a result of the updating operational conditions. Data validation usually include steady-state detection, data reconciliation, and gross error detection. This chapter discusses the data validation step (including a previous denoising procedure) and parameter estimation applied to FCCU data from a virtual plant. The results will be used for a later optimization stage in an RTO. Different types of wavelets and threshold methods are used for denoising. Modified F-test, wavelet transform, and standard deviation methods are compared for the steady state estimation, while WLS (Weighted least squares) and Hampel estimator are used for data reconciliation parameter estimation.

Keywords: Denoising, steady-state detection, data reconciliation, parameter estimation, RTO, FCCU.

4.1 Introduction

Online optimization is recognized as an attractive technology for increasing the profit of chemical plants. Although it could be believed that for real-time optimization it is enough to estimate the new set-points from a process model and implement them by using an appropriate control system, before these steps its is key to develop a data treatment that includes data validation (steady state detection, gross error detection, and data reconciliation) and parameter estimation (Figure 4.1). Data validation and parameter estimation consist of a sequence of steps which allow getting reliable and updated plant

data for the next RTO steps. Usually, data are collected when the system reaches a steady state, although there are new tendencies towards gathering data during dynamic states.

In a classical RTO, when the plant is in steady state, data are collected and sent to the stage in which gross errors are removed and data are reconciled. If the steady state is not detected, the RTO cycle is interrupted until the plant reaches a stable operation [68]. Once the data are validated, the measurements are used for parameter estimation. Sometimes, data validation and gross error detection can be substituted by a simpler data validation using bounds checking [4].

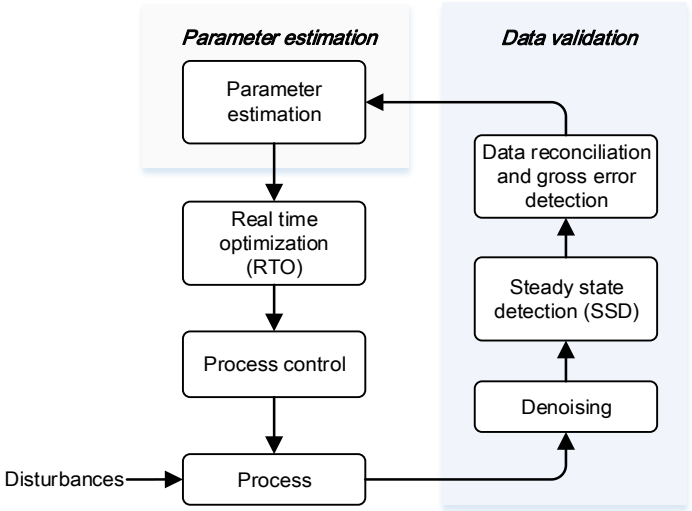

Figure 4.1 *Data validation stages and Parameter estimation in the RTO system. Adapted from* [7].

Data validation and parameter estimation are important steps in online optimization because they are crucial to acquire reliable process models [69]. Actually, quality data affects directly a suitable optimization and control process [70].

In the next sections, a brief examination of each data validations steps will be presented: steady-state detection, data reconciliation, and parameter estimation. Additional to this, and as a consequence of the unavoidable signal noise in the measurements devices, a denoising additional step will be considered. As a case study, data from the FCCU virtual plant (Chapter 3) will be used to analyze some data validation and parameter estimation strategies. Then, the methodology used for this stage will be presented in section 3, and their respective results and analysis will be presented in section 4. Finally, some conclusions will be mentioned.

4.2 Data validation

Data validation is a critical RTO stage such as it identifies serious deviations of the measurements generated by isolated errors on data values. In this way, data validation eliminates data that may be invalid or suspect, and maximizes the recoverable data. In this work, data validation consists of denoising steady-state detection, data reconciliation, and parameter estimation.

4.2.1 Denoising

In a real plant, measurements are unavoidably contaminated with noise at high frequency [71]. This noise is caused either by data acquisition process (instrument miscalibration or malfunction, power supply fluctuation, wiring, and process noise) or because of environmental effects. Noise presence decreases data analysis performance, making it difficult to get reliable information and leading to errors in process optimization. To avoid this, noise elimination is required. The process of noise removal is known as noise reduction or denoising [72].

Denoising can be represented by the following equation:

$$s(t) = f(t) + \sigma e(t) \;\; t = 0,1,\dots,n-1 \qquad \textit{Equation 4.1}$$

where $s(t)$ is the measured signal (noise signal), $f(t)$ the true process signal (noise free), $e(t)$ are independent random variables, and σ the intensity of noise or variance in $s(t)$.

Typically $e(t)$ is given either by Gaussian white noise, gross errors, or both. Gross errors can be outliers and bias. The former includes some abnormal behavior of measurement values (process leaks or malfunctioning instruments). The latter refers to the situation in which the measurement values are systematically too high or too low [73]. According to this, the goal of the denoising process is to remove the noise component from the measured signal $\sigma e(t)$ and recover the true signal $f(t)$ [74].

Many strategies have been applied in denoising processes: Moving Average Filter, Exponential Smoothing Filter, Linear Fourier Smoothing, Multifractal Approach, Simple Non-Linear Reduction, General Matching Pursuit, Wavelets Denoising, and so on. Moving average filter is one of the oldest methods, and it can be seen as a convolution with a plateau function. This method considers an average over neighbor values of discrete time

series. Although this is one of the simplest methods, the length of the filter affects the results and the quality of the denoising [75]. Exponential smoothing filter uses an infinite impulse response filter depending on a parameter which can be between 0 and 1 [75], this parameter defines the filtering strength. Linear Fourier smoothing employs Fourier filter methods based on Fourier transform that decomposes a signal into its frequency components. High-frequency components are suppressed such that a denoising effect is achieved by low pass filtering [75].

In the Multifractal Approach, the signal is analyzed through the "multifractal spectrum" which gives either geometrical or probabilistic information. Here, the idea for denoising is to get rid of insignificant irregularities while keeping meaningful singularities. After denoising, most points should lie in smooth regions [76]. Wavelet denoising transforms the noisy signal into the wavelet domain, thresholds the wavelets coefficients, and determines the inverse wavelet transform to get the denoised signal [77]. One of the advantages of the wavelet method over classical methods (like Fourier transform) is that in wavelets, data are analyzed in time and frequency domain, while in the others data is just analyzed in frequency only [78]. The knowledge of time-frequency characteristics allows a better understanding of signals features [79].

The nonlinear wavelet shrinkage method is based on the discrete wavelet transform. The noise reduction is done by reducing the magnitude of the coefficients in a nonlinear way. Then, wavelets result in good approximating signals with sharp spikes or discontinuities [80] and therefore it is a good option for denoising signals in data collection systems.

[81] review some existing denoising algorithms, such as filtering, wavelet-based, and multifractal approaches, and performs a comparative study. They conclude that the wavelet-based approach finds applications in denoising images corrupted with Gaussian noise while the multifractal approach has better results when the noise characteristics are complex.

From the strategies mentioned above the most used due to its high applicability in data analysis and signal processing is denoising by Wavelet transform. It has been found to be a powerful tool in noise removal from a variety of signals [79], [80], especially in time-varying and non-stationary signals [78]. An important feature of this method is that it does not require any particular assumption of the nature of the signal, allowing the presence of

discontinuities and spatial variations. Due to the recent interest in this technique, it will be explained in more detail in the next section.

Wavelets based denoising

The wavelet transform is a multiresolution analysis developed by [82]. The term wavelet (small wave) is a function of a finite length. A wavelet can be seen as a wave-like oscillation with an amplitude that starts out at zero, increases and decreases back to zero representing a brief oscillation [83], [84]. Different wavelets types are shown in Figure 4.2.

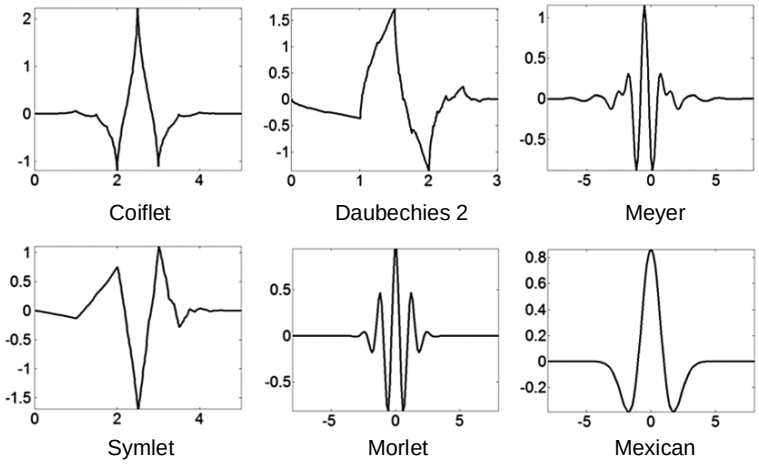

Figure 4.2 *Different types of Wavelets* [85].

The wavelet shape can vary from one to another. The more common ones are haar, daubechies, biorthogonal, coiflets, symlets, morlet, mexican hat, and meyer. A more detailed description of wavelet families can be found in [84].

Wavelets are used in the signal processing to remove noise in a signal, preserving the signal characteristics and its frequency content [86]. Wavelets use different scales of resolution (large and small windows) of the function. These scales let to notice both gross and small features in a signal or a function. The wavelet analysis procedure consists in selecting a wavelet prototype function called mother wavelet. The basis functions in a wavelet are the result of scaling and translation operations in mother wavelet. Then, the signal is expanded onto basis functions which are created by expanding, shrinking, and shifting prototype mother wavelet [81]. Temporal analysis is performed with a contracted, high-frequency version of the mother wavelet, whereas frequency analysis is performed with a dilated, low-frequency version of the same wavelet. With this procedure, a signal can

be represented in terms of a wavelet expansion, using coefficients as a linear combination of the wavelet functions [87]. The wavelet transformation theory and its use in data processing can be found in [88]–[90].

Mathematically, Wavelet Transform (WT) comprises the signal decomposition in wavelet functions $\psi(t)$ given by [91]:

$$\psi_{(\tau,s)}(t) = \frac{1}{\sqrt{|s|}}\psi\left(\frac{t-\tau}{s}\right), \forall\ \tau, s \in \mathbb{R} \qquad \textit{Equation 4.2}$$

Where ψ is the transforming function (mother wavelet). The transformed signal is a function of two variables: τ and s which corresponds to translation and scale parameters, respectively. The term translation is related to the location of the window (that is generated by the mother wavelet), as the window is shifted through the signal. Translation refers to time information in the transform domain.

On the other hand, scale or scaling is used to dilate or compressed a signal. Larger scales correspond to dilated (or stretched out) signals and small scales correspond to compressed signals. As this parameter is used in the denominator, $s > 1$ dilates the signal while $s < 1$ compresses the signal. According to [92], if scales are chosen by powers of two (dyadic scales), the analysis results more efficient and accurate. Then, for discrete WT it must satisfy that $n = 2^J$, where J is some positive number and n is the length of the signal.

There are several types of discrete WT algorithm implementation, but in general, the discrete WT noise eliminations can be implemented in three steps [93]:

1. Signal decomposition: Wavelet transforms the noisy signal. In this step, a wavelet is chosen at level N, and wavelet decomposition of the signal s at level N is computed.
2. Determination of threshold contraction coefficients. For each from level 1 to N, a threshold is selected, and a soft threshold to the detailed coefficients is applied.
3. Signal reconstruction: a wavelet reconstruction is calculated applying the inverse wavelet transformation to modified wavelet coefficients. This is done based on the original coefficients approximation of level N and modified detailed coefficients of levels from 1 to N.

There are a variety of methods used to choose the threshold level λ. They can be divided into two categories:

- *Global threshold*: this implies choosing a single value of λ to be applied globally to all empirical coefficients.
- *Level-dependent threshold*: this applies different possible threshold values for each resolution level.

Both of them require an estimate of the noise level $\hat{\sigma}$. This value is usually estimated by [94]:

$$\hat{\sigma} = \frac{median(\{|\widehat{d}_{J-1,k}|: k = 0,1, \dots, 2^{J-1} - 1\})}{0.6745} \qquad \textit{Equation 4.3}$$

The most known optimal threshold selection algorithms for wavelet shrinkage proposed by Donoho and Johnstone are:

- Minimax
- Rigrsure
- Heursure
- Sqtwolog

Minimax

The Minimax is a principle used in statistics for the design of estimators which seeks to minimize a possible loss in the worst of scenarios (maximum loss) [94]. In this way, Minimax threshold value uses a fixed threshold to yield Minimax performance for mean square error against an ideal procedure. In this case, the denoised signal can be assimilated to the estimator of the unknown regression function, and the Minimax estimator is the option that realizes the minimum over a given set of functions of the maximum Mean Square Error [79], [84]. The algorithm of the threshold selection is given by [91], [95], [96]:

$$threshold = \begin{cases} \sigma(0.3936 + 0.1829 \log_2 N) & N > 32 \\ 0 & N < 32 \end{cases} \qquad \textit{Equation 4.4}$$

where $\sigma = median\left(\frac{|\omega|}{0.6745}\right)$, ω is the wavelet coefficient vector at unit scale and N is the length of the signal vector.

Sqtwolog (Universal Thresholding)

Donoho and Johnstone also suggest thresholding by empirical wavelet coefficients using universal threshold. The threshold values are calculated by universal threshold (square root log) method, which is given by:

$$Threshold_j = \sigma_j \sqrt{2\log(N_j)} \qquad \textit{Equation 4.5}$$

where N_j is the length of the noisy signal at j^{th} scale and σ_j is defined as:

$$\sigma = median(|\omega|/0.6745)$$

and ω represents wavelet coefficients at scale j.

Rigrsure

Rigrsure or sure shrink chooses a threshold λ_j by minimizing the Stein Unbiased Risk Estimate for each wavelet level j. Rigrsure threshold selection rule can be expressed as [91], [95]:

$$Threshold_j = \sigma_j \sqrt{\omega_b} \qquad \textit{Equation 4.6}$$

where σ_j is the standard deviation of the noisy signal, and ω_b is the b^{th} squared wavelet coefficient (coefficient at minimum risk). ω_b is chosen from a vector W. $W = [\omega_1, \omega_2, \dots, \omega_n]$ is a vector that consists of the square of wavelet coefficients from small to large. For each coefficient, the risk is calculated by:

$$R = \{r_i\}_{i=1,2,\dots,N} = \frac{\left[N - 2i + (N-i)\omega_i + \sum_{k=1}^{l} \omega_k\right]}{N} \qquad \textit{Equation 4.7}$$

The minimum value of risk $r_b(b^{th}r)$ is chosen and related to its wavelet coefficient. The wavelet coefficient will be ω_b.

Heursure

Sometimes the SureShrink method does not perform well. For these cases, Donoho suggested a combination of the Universal Threshold (Sqtwlog) and the SureShrink (Rigrsure) methods. This hybrid method is known as Heursure and its threshold is defined as [91]:

$$threshold = \begin{cases} \lambda_1 & A > B \\ \min(\lambda_1, \lambda_2) & A \geq B \end{cases} \qquad \textit{Equation 4.8}$$

where, $A = s - N/N$ and $B = (log_2 N)^{\frac{3}{2}}\sqrt{N}$ where N is the length of the wavelet coefficient vector and s is the sum of square wavelet coefficients given as $s = \sum_{i=1}^{N} \omega_i^2$.

4.2.2 Steady-state detection (SSD)

Accurate steady-state detection of the signals is really important for the performance of data reconciliation, process optimization, and process control. False detection of steady state can lead to misinterpretation of the true process features, and subsequently, partial correction of gross errors or false input to data reconciliation. This explains the need for steady-state detection procedures in RTO applications.

For steady-state detection, several techniques have been developed. F-test [97], T-test called direct approach, (CST) Statistical Composite Test [98], Mathematic Evidence Test (MTE) [99], extended period strategy [100], polynomial interpolation [101], and approaches based on wavelets transforms [71], [89], [102].

Among the techniques used in the detection of steady state, modified F-test and wavelets based approaches have provided good results. The F-test involves the calculation of the filtered value for the online measurements, and the variance of the filtered values by two different approaches: one using the filtered mean-square deviation from the previously filtered value, and the other using the filtered mean-square difference of the successive data [97], [103]. The wavelets technique proposes a methodology for the steady-state detection that allows filtering the high-frequency noise and correcting abnormalities from modules of the maximum wavelet transform. The state of the process is determined according to the module of first and second order wavelet transform to analyze accurately the components of the high-frequency anomalies [71].

Modified F-Test

This test is a modification of the original F-test and it was proposed by [97]. The method applies a relation (R) between two estimates of the variance of the system noise, one of the original data and another from filtered data. To filter data, three parameters are used (L_1, L_2, L_3). For these parameters (or filters), values from 0 to 1 are defined to give a value

of importance to the current values compared to the values passed, so R is calculated in each step. The discrete filtered value of the measurement value X given by [7]:

$$X_{f,i} = L_1 X_i + (1 - L_1) X_{f,i-1} \qquad \textit{Equation 4.9}$$

where $X_{f,i}$ is the filtered value of X at time i, L_1 is a filter factor, X_i is the process measured variable at time i, and $X_{f,i-1}$ is the filtered value of X at time $i-1$.

The filtered mean square deviation from the previous filtered values, defined as $v_{f,i}^2$, is defined as:

$$v_{f,i}^2 = L_2\left(X_i - X_{f,i-1}\right)^2 + (1 - L_2) v_{f,i-1}^2 \qquad \textit{Equation 4.10}$$

where, $v_{f,i}^2$ is the current filtered mean square deviation, L_2 is a filter factor and $v_{f,i-1}^2$ is the previous filtered mean square deviation.

The filtered mean square difference between successive data $d_{f,i}^2$ is given by:

$$d_{f,i}^2 = L_3 (X_i - X_{i-1})^2 + (1 - L_3) d_{f,i-1}^2 \qquad \textit{Equation 4.11}$$

Here, $d_{f,i}^2$ is the current filtered square difference of successive data, L_3 is a filter factor and $d_{f,i-1}^2$ is the previous square difference of successive data. According to this, it is possible to calculate the R-statistic, which is used to assess the existence of the steady state. R is calculated as follows:

$$R = \frac{(2 - L_1) v_{f,i}^2}{d_{f,i}^2} \qquad \textit{Equation 4.12}$$

This value (R) is compared with some critical values of the R-statistic (R_{crit}). R_{crit} is selected and determined by the level of significance α. Therefore, the system is in a stable state if the R value has a distribution of values close to R_{crit}. Then, if $R > R_{crit}$ the process is in unsteady state $(SS = 0)$, while if $R < R_{crit}$ the process is in steady state $(SS = 1)$. With this method, the tuning of parameters $L_1, L_2, L_3$is very important, since they determine how sensitive the steady state detection of the signal is made. [97] proposed that the parameters of the method must be tuned empirically. [103] recommend that this tuning must be done by trial and error according to the following:

1. Select a value of L_3 (say 0.01).
2. Select a value of L_2 (say 0.05).

3. For these values of L_2 and L_3, start with a low value of L_1 (say 0.02) and calculate R_{crit}, type II errors, and the delay in detection of the steady state.
4. Increment L_1 by 0.02, and repeat calculations of step 3 until an allowable type II error limit is crossed.
5. Increment L_2 by 0.05, and then return to step 3. Go on incrementing L_2 until the local minimum in terms of an earlier detection of the steady state is obtained corresponding to the given value of L_3.
6. Increment L_3 by 0.01, and return to step 2 until a global minimum is obtained for a given number of data points being averaged.

The analysis presented above is only valid in a single variable analysis. Consequently, an extension of a multivariable analysis must take into account that if at least one process variable is not at steady state, the system is not at steady state, and clearly the system is at steady state only if all variables are at steady state.

To assess the steady state in the process, $SS_{process}$ is defined as [7]:

$$SS_{process} = \prod_{i=1}^{N} SS_i \qquad \textit{Equation 4.13}$$

which need to be equal to 1. In another case, the system will not be at steady state.

Wavelet Transform Based Method

[102] proposed a methodology based on wavelet-transform for steady-state detection. In this, the elimination of noise or denoising is done by thresholding. Next, a shape change detection is made from the first wavelet transform since the local end corresponds to an inflection point. If a maximum module of $|W_j f(t)|$ is detected, then there is a corresponding change of form. This signal change over time can be represented using the first derivative with respect to time. Since the first order wavelet transform $Wf(t)$ is proportional to the first derivative of $f(t)$, it can be said that the function is at steady-state when $W_j f(t) = 0$ ($W_j f(t) > 0$ indicates increases in the signal while $W_j f(t) < 0$ indicates a decrease in the signal). Nevertheless, there may exist zero crossing points which are a result of inflexion points, peak values instead of steady-duration points.

These points can be identified calculating the WT on $W_j f(t)$ which means:

$$WW_j f(t) = W_s f * \psi_j(t) \qquad \textit{Equation 4.14}$$

where $WW_j f(t)$ is called the second-order and $\psi_j(t)$ is the first-order wavelet.

[102] establish a steady-state index to measure the degree of steady state. In this way, $\beta = 0$ indicates the unstable status and $\beta = 1$ indicates that the steady state is reached. Therefore,

$$\text{if } |W_s\, f(t)| > T_u, \text{ then } \beta = 0. \qquad \textit{Equation 4.15}$$

or,

$$\text{if } |W_s f(t)| < T_s \text{ and } |WW_s f(t)| < T_w, \text{ then } \beta = 1. \qquad \textit{Equation 4.16}$$

$T_s, T_u\, T_w$ are threshold values which are determined according to the fluctuation of the measurements and the sensitivity of variables to process operation.

T_u is the WT modulus threshold for identification of unsteady status, T_s is the WT modulus threshold for the identification of steady state, and T_w is the second-order WT modulus threshold for identification of the zero-crossing point of the WT. They are calculated as follows:

$$\begin{aligned} T_s &= \sigma_{W_f} \\ T_u &= 3\lambda\, \sigma_{W_f} \\ T_w &= \sigma_{WW_f} \end{aligned} \qquad \textit{Equation 4.17}$$

where σ_{W_f} is the standard deviation of the wavelet modulus, σ_{WW_f} is the median of the second-order WT modulus, and λ is an adjustable parameter that usually can be assumed as 1. S is the characteristic scale and it is determined based upon the process dynamic behavior and the zooming property of dyadic WT. S is calculated as [102]:

$$S = j = int\left(\log_2 \frac{\tau}{t_s} + 0.5\right) \qquad \textit{Equation 4.18}$$

where t_s is the sampling interval and τ is the response time constant.

For a multivariable system, it must be fulfilled that:

$$B(t) = \prod_{i=1}^{N} [\beta_i(t)]^{w_i / \sum w_i} \qquad \textit{Equation 4.19}$$

where β_i is the calculated individual index of the ith critical variable, and w_i indicates the contribution of the ith critical variable (usually assigned 1.0 as default).

Standard Deviation Method

A new methodology based on the standard deviation is proposed for steady-state detection. It is based on a comparison between the standard deviation of the five previous values of the signal (α) and a tuning parameter (β). This comparison is done for each time of the signal.

The α parameter is calculated for each time point using the standard deviation of the result of dividing the five previous points by the time interval of these five points, as follows:

$$\alpha_{t=i} = std\left(\frac{Signal_{t=i-4}}{\Delta t}, \frac{Signal_{t=i-3}}{\Delta t}, \frac{Signal_{t=i-2}}{\Delta t}, \frac{Signal_{t=i-1}}{\Delta t}, \frac{Signal_{t=i}}{\Delta t}\right) \quad \textit{Equation 4.20}$$

where $\Delta t = t_i - t_{i-4}$.

The β parameter has two different values depending on the system state:

- $\beta = S_1$ when $SSD = 1$
- $\beta = S_2$ when $SSD = 0$

where $S_1 \geq S_2$. $S_1$and S_2 are tuning parameters and depends on each signal. If $\alpha < \beta$ the process is in steady state $(SSD = 1)$ and $\beta = S_1$. In contrast, if $\alpha > \beta$ the process is in unsteady state $(SSD = 0)$ and the β will be updated by S_2. For better understanding, the algorithm for this procedure is depicted below.

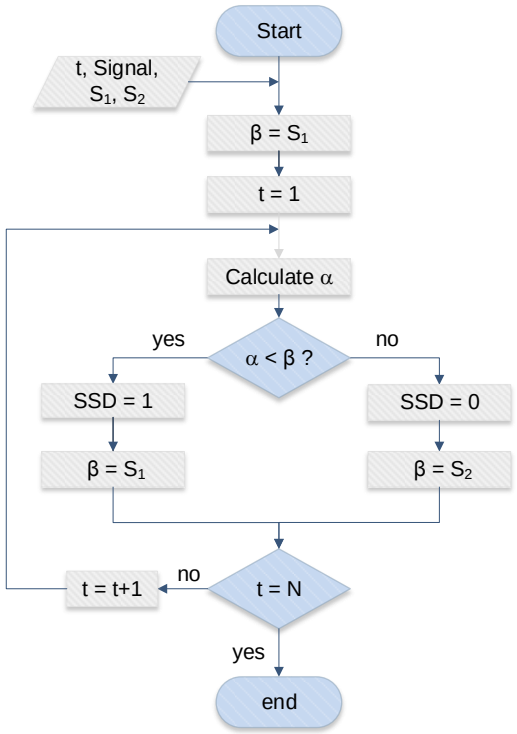

Figure 4.3 *Standard deviation method algorithm for SSD. N quantity of signal data.*

S_1 value finds the time in which the disturbance occurs, whereas S_2, a more sensitive parameter, finds when there is a new steady state after the disturbance occurs. Similar to Modified F-Test, the completely steady state $SS_{process}$ can be evaluated using Equation 4.13.

4.2.3 Data reconciliation and parameter estimation (DRPE)

Accurate process data are the foundation for optimization and control in RTO. In data collection, measurements are unavoidably contaminated not just with noise, but also with measurement errors (gross and random error), as a result of sensor faults and sensor biases. This causes inadequacies in the model of the process and inconsistencies with the mass and energy balances/conservation laws of mass, energy, etc. Although the previous techniques (as denoising) are needed as a first step to attenuate the effect of the high frequency of noise in the measurement, they do not ensure consistency of the data that obey the mass and energy balances [104]. This is the principal difference between data reconciliation and other filter techniques.

Data reconciliation (DR) is then responsible for raw data processing and its transformation into reliable information (Figure 4.4). The DR procedure is carried out by means of the

minimization of measurement errors subject to the model constraints. In addition to reconciliation, parameter estimation (PE) is used to establish the values of the parameters from the reconciled values.

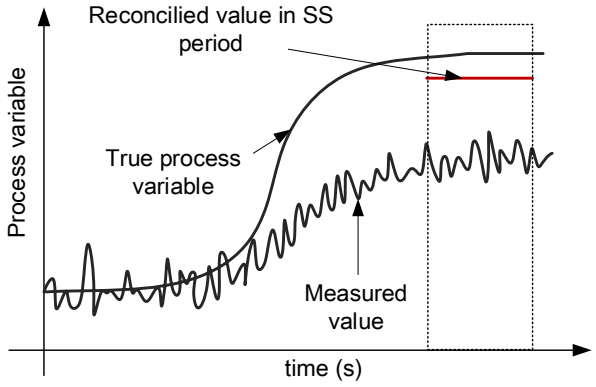

Figure 4.4 *Data reconciliation representation* [71].

These two steps can be integrated by means of the formulation of a DRPE problem which aims to minimize the errors of the measures subject to the model constraints.

Then, the DRPE problem can be defined as:

$$\begin{aligned} &\min \sum \left(\frac{x_i^M - x_i}{\sigma_i} \right)^2 \\ &\text{subject to: } h(x,u,p) = 0 \\ &\qquad g(x,u,p) \leq 0 \\ &\qquad x^L \leq x \leq x^U \\ &\qquad pL \leq p \leq p^U \\ &\qquad u^L \leq u \leq u^U \end{aligned}$$

Equation 4.21

where x^M is the set of measured data of the corresponding variable x, ρ is the estimator function, x_i is the solution of the DRPE problem, h is the set of equality constraints, u is the set of unmeasured variables, and g is the set of inequalities.

This equation represents a minimization of a quadratic error between the measured value and that determined by the minimization. To solve this, many strategies have been proposed. One of the most efficient, not only because of its results but also because it simultaneously includes the parameter estimation, is the use of robust estimators. These estimators reduce the gross error effect and give less biased estimates. From robust

estimators, maximum likelihood estimators or M-Estimators such as Hampel estimator are well known [105], [106].

The main advantage of the Hampel estimator is that an exploratory data analysis is not necessary for the outliers' estimation. These estimators are also independent of the distribution, producing unbiased results as they add less weight to the isolated measures and protect other measures from being contaminated.

The DRPE problem with a maximum likelihood objective function is defined by [107], [108] as:

$$\begin{aligned} \min & \sum_{i=1}^{H}\sum_{j=1}^{n} \rho^{M}\left(\frac{x_{ij}^{M}-x_i}{\sigma_i}\right) \\ \text{subject to: } & h(x,u,p)=0 \\ & g(x,u,p)\leq 0 \\ & x^{L} \leq x \leq x^{U} \\ & pL \leq p \leq p^{U} \\ & u^{L} \leq u \leq u^{U} \end{aligned} \qquad \textit{Equation 4.22}$$

where ρ_i^j is the maximum likelihood estimator and $\varepsilon_i = (x_{ij}^M - x_i)/\sigma_i$, is the standard error, n is the number of measured variables and H is the size of the horizon which is fixed to adjust data to a real-time system.

The maximum likelihood objective function (ρ) can also be defined as WLS, Contaminated Normal. Cauchy, Logistic, Lorentzian, Fair, Hampel's redescending estimator, and so on.

4.3 Methodology

The methodology followed for this chapter is presented in Figure 4.5. Each of those stages is detailed below.

4.3.1 Data source

Dynamic data to carry out data analysis were obtained from a FCC virtual plant developed in Matlab ®. The output data were contaminated using a Gaussian error with a signal-noise ratio 50 (SNR 50), gross error in a set of 15% of the overall random data and errors from 0 to 5% of the maximum values. Measured variables also were contaminated with random bias errors between 2σ and 50σ in order to simulate real plant measurements.

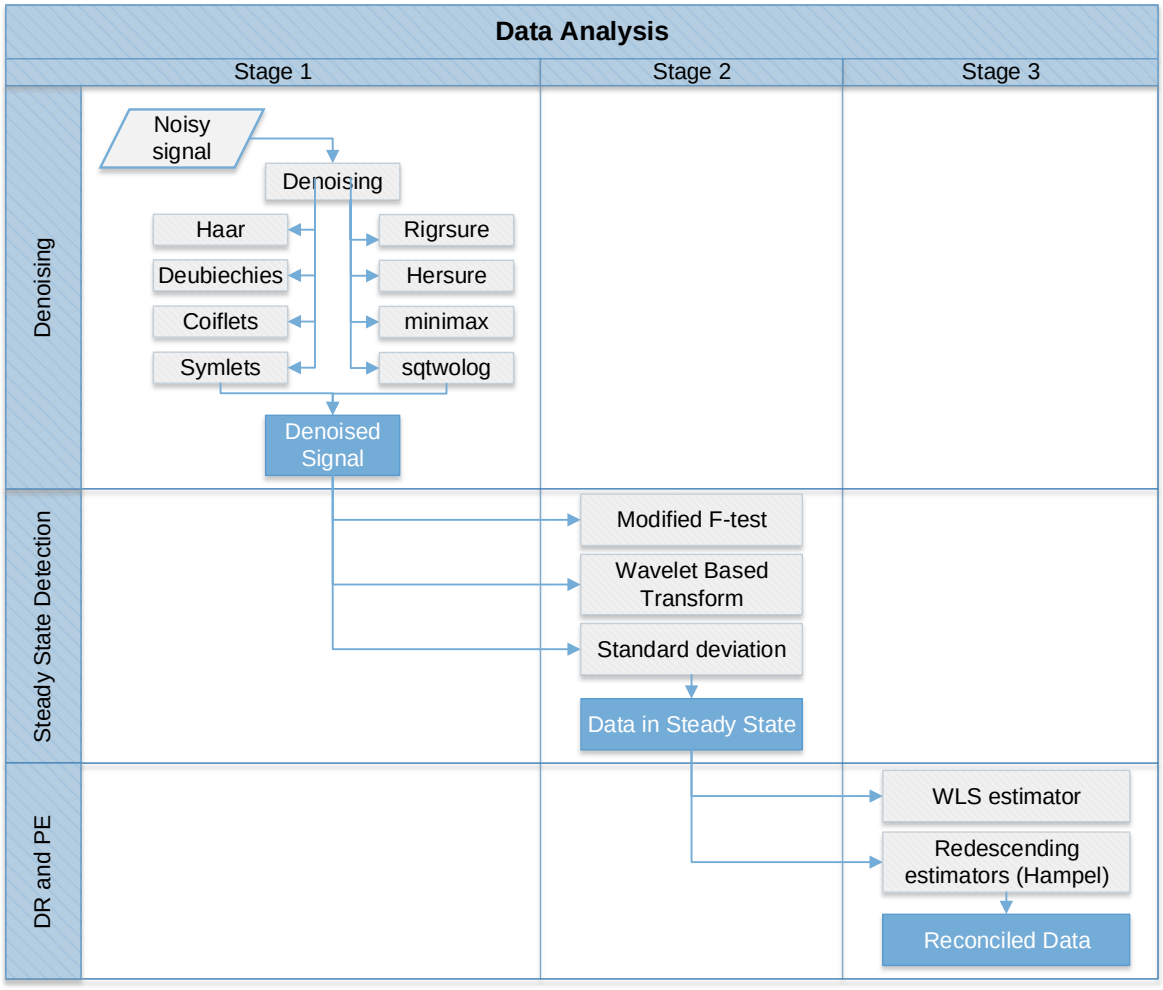

Figure 4.5 *Methodology followed for Data Analysis.*

4.3.2 Denoising

Wavelet Shrinkage Threshold (WST) was used to denoising contaminated signals from virtual FCC plant, using haar, daubechies, symlets, and coiflets basis functions. WST was developed following three steps: decomposition of the signal, thresholding, and reconstruction of the signal. The first step was implemented through wavelet transform, the second one was developed through the evaluation of the most common wavelets and filters (rigsure, heursure, sqtwolog, minimaxi), and the third one, the signal reconstruction, by means of inverse wavelet transform and retained coefficients.

The basis functions used for denoising purposes were chosen through qualitative criteria by observing and evaluation of the better approximations to the signal. The basis functions chosen in Matlab® are mentioned in Table 4.1.

Table 4.1 *Basis functions used for denoising*

Basis function	Matlab name
Haar	*haar*
Daubechies	*db11**
Symlets	*sym7**
Coiflets	*coif5**

* In symN, dbN and coifN *N* is the number of vanishing moments which indicates the shape of the wavelet (softness).

The algorithm developed for denoising is depicted in Figure 4.6.

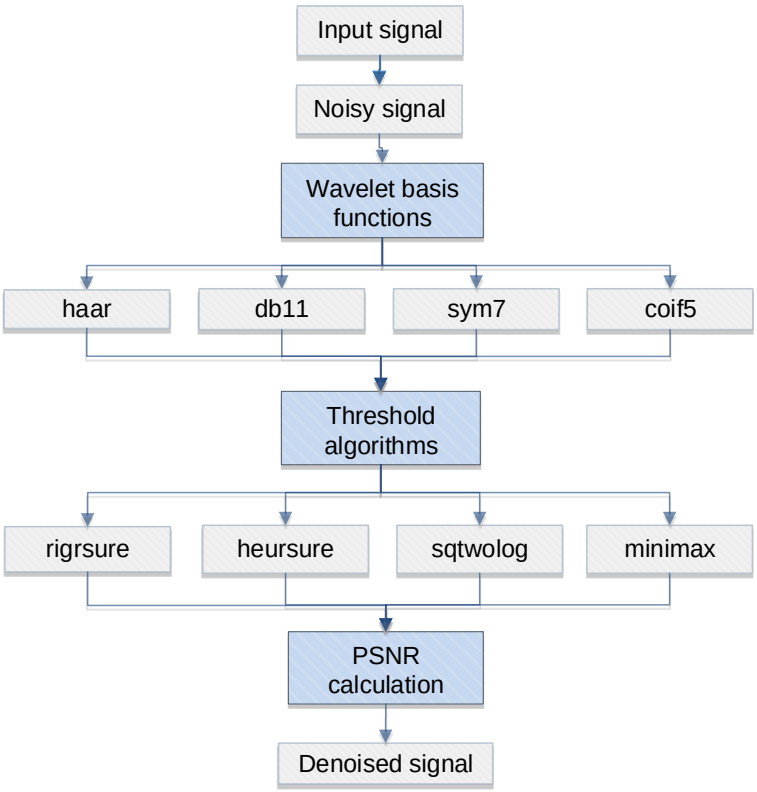

Figure 4.6 *Methodology followed for denoising.*

In order to evaluate the performance of wavelet basis functions matched with threshold algorithms, peak signal to noise ratio (PSNR) is employed. PSNR is the ratio between the maximum possible value of a time series and the maximum value of the noise. It is a measure of how noisy a signal is, and then, how effective a denoising algorithm is [72]. PSNR is given by:

$$PSNR = 10 * log_{10}\left(\frac{\left(\underset{i}{max}\{y_i\}\right)^2}{MSE}\right) \qquad \textit{Equation 4.23}$$

where MSE, mean square error is:

$$MSE = \frac{1}{N}\sum_{i=0}^{N-1}(\hat{y}_i - y_i)^2 \qquad \textit{Equation 4.24}$$

and $\hat{y}_i$ corresponds to denoised value and y_i to the noise-free real value.

4.3.3 Steady-state detection

For steady-state detection, three techniques programmed in Matlab® were compared. The first one was the F-like test, developed by [97], which employs a relation between two estimates of the noise variance of the system (R). Data filtered depends on three parameters λ_1, λ_2, λ_3 which vary from 0 to 1. The tuning parameters were developed according to [103] guidelines. The maximum acceptable variability is defined by means of a critical value, (R_{crit}). The variances ratio (R) are evaluated in each step. If $R > R_{crit}$the process is not at steady state, $SS = 0$; and if $R < R_{crit}$ the process is at steady state, $SS = 1$.

The second technique for SSD was carried through by the wavelet method proposed by [102]. In this one, the changes of a signal in the measurement from the system can be represented through the first order wavelet $Wf(t)$ and the zero crossing points is considered through second order wavelet, $WWf(t)$. Therefore, a steady state is detected from first and second module wavelet transform with a steady state index $0 \leq \beta \leq 1$. Thereby, when $\beta = 0$ an unsteady state is identified, and when $\beta = 1$ a steady state is achieved.

The threshold values T_u, T_s and T_w are determined according to the degree of fluctuation of the measurements and the sensitivity of variables to process operation. In this case, they are calculated from the historic measurements selected under steady state, by using the equations defined for T_s, T_u and T_w.

The third technique used for SSD is related to standard deviation calculation as was explained in section 2.3. This consists of the α and β parameters comparison for each time of the signal. α is the result of the standard deviation value of the five previous points over the time interval of these five points, while β can have two possible values S_1 and S_2 depending on the SSD state. Then, $\beta = S_1$ when $SSD = 1$ (steady state) and $\beta = S_2$ when $SSD = 0$ (unsteady state).

S_1 and S_2 are tuning parameters and can be calculated as follows:

1. Initialize S_1 as the standard deviation of the signal in steady state.
2. Increase or decrease the S_1 value until the time of disturbance is detected.
3. Initialize S_2 as less value as S_1.
4. Increase or decrease the S_2 value until it adjusts the steady-state detection.

4.3.4 Data reconciliation and parameter estimation

Data reconciliation and parameter estimation are developed according to the procedure presented in [105]. The data reconciliation problem begins with the acquisition of the process data measurements of system variables for which sensors are available.

From the measurement session (data from the DCS), a horizon of data is generated by sampling process data at various time intervals. These data are organizing into a matrix as:

$$X^M = \begin{bmatrix} x_{11}^M & x_{12}^M & \dots & x_{1H}^M \\ x_{21}^M & x_{12}^M & \dots & x_{2H}^M \\ \vdots & \vdots & \ddots & \vdots \\ x_{n1}^M & x_{n2}^M & \dots & x_{nH}^M \end{bmatrix}$$

where x_{ij}^M is the ith measured variable in the jth time period, n is the number of measured variables and H is the size of the horizon which is fixed to adjust data to a real-time system. As was mentioned in section 2.3, the DRPE problem is written as:

$$\begin{aligned} \min & \sum_{i=1}^{H} \sum_{j=1}^{n} \rho^M \left(\frac{x_{ij}^M - x_i}{\sigma_i} \right) \\ \text{subject to: } & h(x,u,p) = 0 \\ & g(x,u,p) \leq 0 \\ & x^L \leq x \leq x^U \\ & pL \leq p \leq p^U \\ & u^L \leq u \leq u^U \end{aligned}$$

Equation 4.25

where x^M is the set of measured data of the corresponding variable x, ρ is the estimator function, x_i is the solution of the DRPE problem, h is the set of equality constraints, u is the set of unmeasured variables, and g is the set of inequalities.

For maximum likelihood objective function, WLS (weight least squares) estimator, and Hampel estimator are used. WLS is defined as [105], [109]:

$$\rho_{WLS}{}_i^j = \frac{1}{2}\varepsilon_i^2 \qquad \textit{Equation 4.26}$$

where Hampel estimator ρ^M is defined as:

$$\rho_{Hampel}{}_i^j = \begin{cases} \dfrac{\left(\varepsilon_j^j\right)^2}{2} & 0 \le \left|\varepsilon_j^j\right| \le a_H \\ a_H\left|\varepsilon_j^j\right| - \dfrac{a_H^2}{2} & a_H < \left|\varepsilon_j^j\right| \le b_H \\ a_H b_H - \dfrac{a_H^2}{2} + (c_H - b_H)\dfrac{a_H^2}{2}\left[1 - \left(\dfrac{c_H - \left|\varepsilon_j^j\right|}{c_H - b_H}\right)^2\right] & b_H < \left|\varepsilon_j^j\right| \le c_H \\ a_H b_H - \dfrac{a_H^2}{2} + (c_H - b_H)\dfrac{a_H^2}{2} & c_H < \left|\varepsilon_j^j\right| \end{cases} \qquad \textit{Equation 4.27}$$

Hampel estimator depends on three parameters: a_H, b_H and c_H. [108] report tuning parameters with 95% of efficiency as $a_H = 1.35, b_H = 2.37, c_H = 5.4$.

In order to compare the estimators' performance, a relative error is calculated and defined as:

$$\%error = \frac{(real\ value - reconcilied\ value)}{real\ value} * 100\% \qquad \textit{Equation 4.28}$$

Then, for the FCCU case study, the measured variables to reconcile are depicted in Figure 4.7.

Measured variables are classified as redundant and non-redundant. Data reconciliation uses redundancy to adjust the measurements to the constraints of the process. This concept is not limited to the same variable that is simultaneously measured by several sensors, but also used spatial redundancy. Spatial redundancy refers to the fact that a single variable can be estimated by several independent ways such as algebraic constraints from mass and energy balances.

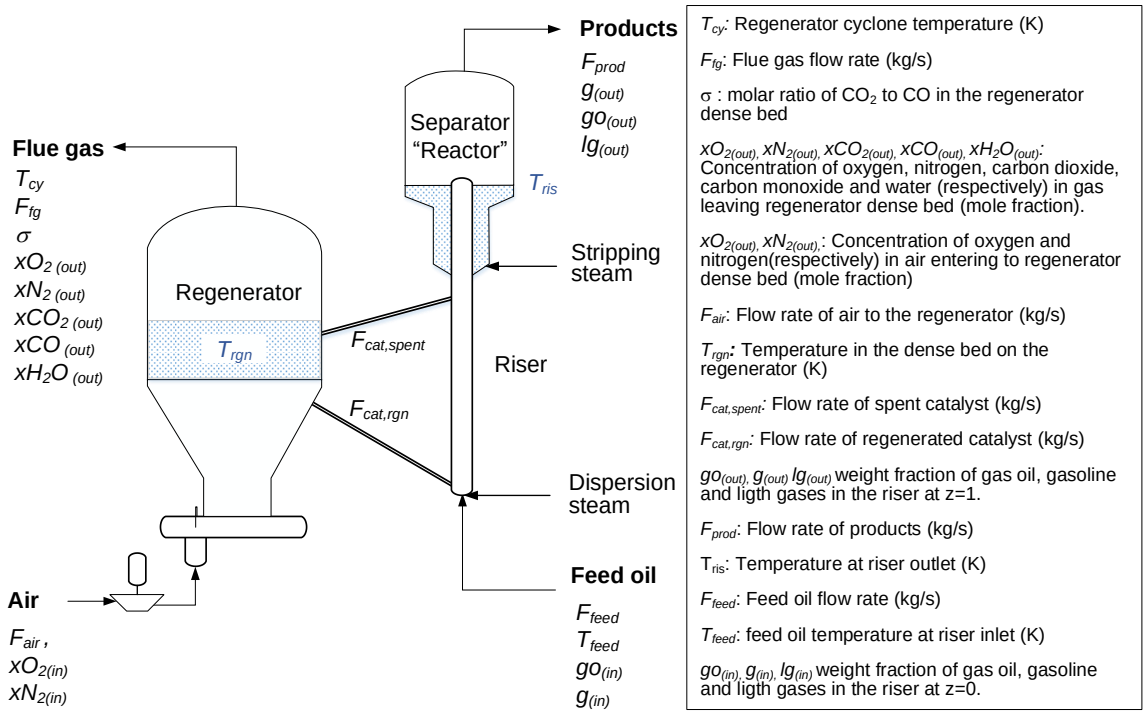

Figure 4.7 *Measured variables in FCCU for data reconciliation.*

FCCU redundancy is obtained from the data source and material and energy balances presented in Appendix B. Then X^M matrix is defined as follows:

$$\mathrm{X^M} = \begin{bmatrix} xO_{2_{(in)}}{}^{M}_{t=1} & xO_{2_{(in)}}{}^{M}_{t=2} & \dots & xO_{2_{(in)}}{}^{M}_{t=H} \\ F_{air}{}^{M}_{t=1} & F_{air}{}^{M}_{t=2} & \dots & F_{air}{}^{M}_{t=H} \\ \sigma{}^{M}_{t=1} & \sigma{}^{M}_{t=2} & \dots & \sigma{}^{M}_{t=H} \\ xO_{2_{(out)}}{}^{M}_{t=1} & xO_{2_{(out)}}{}^{M}_{t=2} & \dots & xO_{2_{(out)}}{}^{M}_{t=H} \\ F_{fg}{}^{M}_{t=1} & F_{fg}{}^{M}_{t=2} & \dots & F_{fg}{}^{M}_{t=H} \\ T_{cy}{}^{M}_{t=1} & T_{cy}{}^{M}_{t=2} & \dots & T_{cy}{}^{M}_{t=H} \\ T_{rgn}{}^{M}_{t=1} & T_{rgn}{}^{M}_{t=2} & \dots & T_{rgn}{}^{M}_{t=H} \\ F_{feed}{}^{M}_{t=1} & F_{feed}{}^{M}_{t=2} & \dots & F_{feed}{}^{M}_{t=H} \\ T_{ris_{(1)}}{}^{M}_{t=1} & T_{ris_{(1)}}{}^{M}_{t=2} & \dots & T_{ris_{(1)}}{}^{M}_{t=H} \\ F_{prod}{}^{M}_{t=1} & F_{prod}{}^{M}_{t=2} & \dots & F_{prod}{}^{M}_{t=H} \end{bmatrix}$$

where H is referred to horizon length defined as 17 measured points after steady state is detected.

The data reconciliation problem is solved using “interior-point algorithm” from the *fmincon* function available in Matlab ®. Constraints are defined by material and energy balances from Appendix B. Upper and lower bounds for measured variables are shown in Table 4.2.

Table 4.2 *Upper and lower bounds for measured variables used in the minimization problem.*

Lower bound	Variable	Upper bound
0	$xO2_{(in)}$ *(mole fraction)*	0.2136
22	F_{air} *(kg/s)*	32
1	$\sigma_{(1)}$	2.423
0	$xO2_{(out)}$ *(mole fraction)*	1
22	F_{fg} *(kg/s)*	35
810	T_{rgn} *(K)*	1090
37	$F_{feed_{(5)}}$ *(kg/s)*	44
755	$T_{ris\ (1)}$ *(K)*	840
37	F_{prod} *(kg/s)*	44

A scheme for DR methodology is depicted in Figure 4.8.

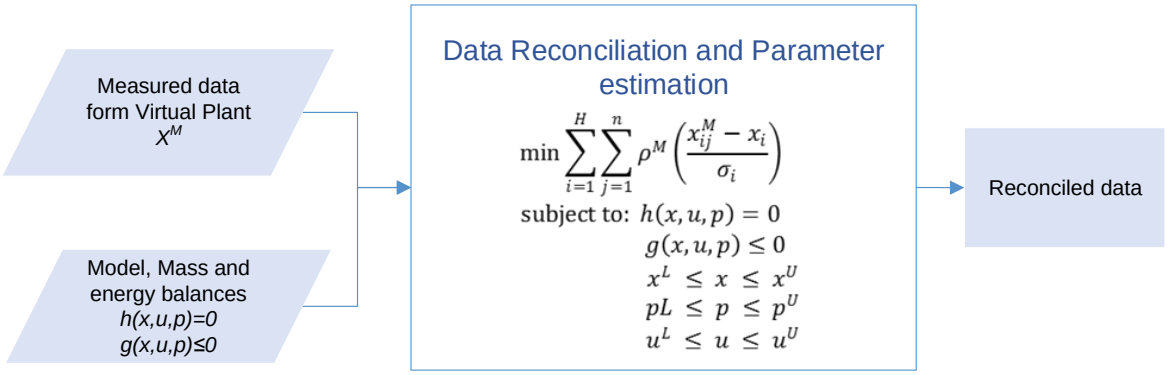

Figure 4.8 *Methodology followed for data reconciliation.*

4.4 Results and discussion

4.4.1 Denoising

In order to establish the best performance in the denoising procedure, a comparison between basis functions and filters was made. To do this the PSNR was calculated for a riser temperature profile (Table 4.3). Every wavelet with all filters studied in this work was plotted. According to this, sym7-heursure (PSNR=26.033) and coif5-heursure

(PSNR=26.773), generates the better PSNRs indicating that those wavelet parameters fit the data satisfactorily.

Table 4.3 *PSNR for a riser temperature profile.*

	Rigrsure		Heursure		Sqtwolog		Minimaxi	
	PSNR	**MSE**	**PSNR**	**MSE**	**PSNR**	**MSE**	**PSNR**	**MSE**
haar	-10.202	10.477	-10.204	10.480	-10.289	10.689	-10.290	10.690
db11	25.513	0.003	24.904	0.003	20.257	0.009	19.945	0.010
sym7	25.809	0.003	26.033	0.003	18.211	0.015	18.452	0.014
coif5	25.689	0.003	26.773	0.002	22.303	0.006	23.746	0.004

The denoising signals obtained with sym7 and coif5 using heursure threshold are depicted in Figure 4.9.

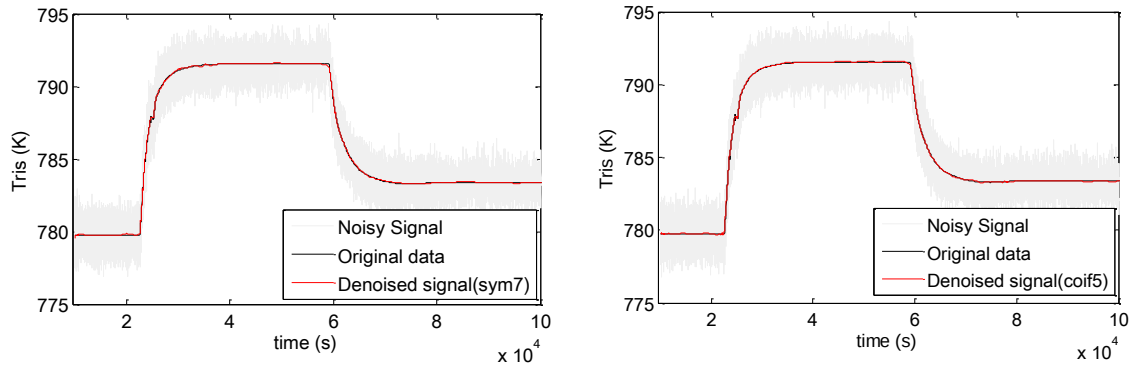

a) Denoised signal using Symlets and heursure

b) Denoised signal using coiflets and heursure

Figure 4.9 *Comparison of methods for signal denoising sym7 (PSNR=26.033) and coif5 (PSNR=27.733) with heursure threshold for riser temperature profile (a 5% step increase in F_{air} at 22.600s, and a 2.9% decrease in T_{feed} at 60.000s).*

Figure 4.9. shows a very good fit between the original signal and the clean signal using these two wavelet basis functions. It demonstrates that both of them can be used for the denoising procedure in this kind of signals.

Poor results are obtained for haar even testing all the thresholds used in the others basis functions. Haar works well for signals in steady state with PSNR=45.2949, while for signals with different steps the PSNR is very low (PSNR= -10.204). This result is presented in Figure 4.10.

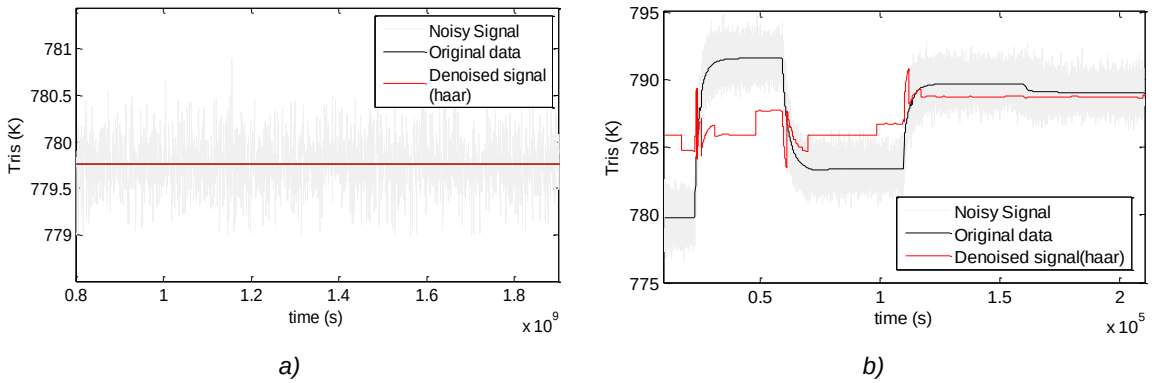

a) *b)*

Figure 4.10 *Comparison of steady state (a) and nonsteady (b) state signal denoising using haar and heursure for riser temperature profile.*

The better results of coiflets, symlets, and daeubiches with respect to haar basis functions could be consequence of the vanishing moments (db1 to db11, coif1 to coif5 and sym2 to sym8). In this sense, for a higher vanishing moment, the smooth will be better and therefore, the fit as well. This can be observed in Figure 4.11

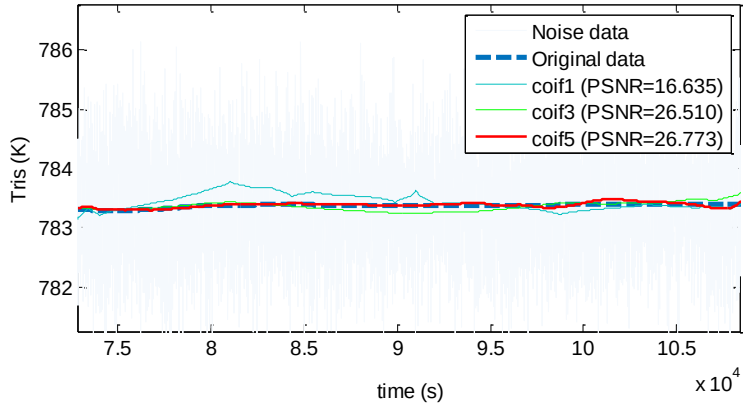

Figure 4.11 *Denoising coifllets comparison based on vanishing moments. The higher the vanishing moment, the higher the PSNR.*

From Figure 4.11, it was also observed that the denoised signal with the best fit (high PSNR) is not necessarily the smoother one. It occurs for example for the denoised signal using db11-sqtwolog (PSNR=20.257) and coif5-rigrsure (PSNR=25.689). According to the performance parameter, the coif5-rigrsure signal should have a better approximation than that of db11-sqtwolog; but as it is observed in Figure 4.12, the db11-sqtwolog results on a smoother signal than that of coif5-rigrsure.

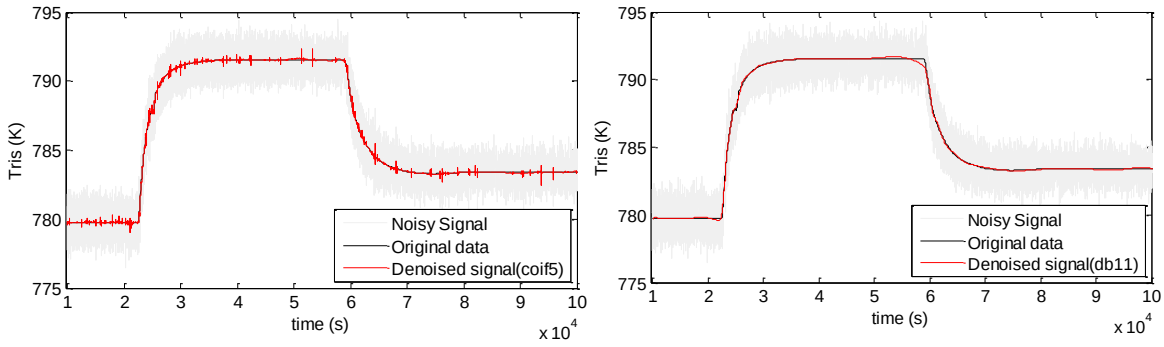

a) Denoised signal using coiflets and rigsure

b) Denoised signal using daubechies and sqtwolog

Figure 4.12 *Comparison of methods for signal denoising coif5 (PSNR=25.89) and db11 (PSNR=27.733) with rigrsure and sqtwolog threshold for riser temperature profile (a 5% step increase in F_{air} at 22.600s, and a 2.9% decrease in T_{feed} at 60.000s).*

In Table 4.3 and Figure 4.13, it is also observed that the higher PSNR is obtained for heursure threshold followed by rigrsure, sqtwolog and minimaxi. Although rigrsure has a good PSNR (better than minimax and sqtwolog) and follows the tendency of the real signal, there is some "noise" that it is not completely eliminated. On the other hand, sqtwolog follows the signal tendency, but it does not have a good PSNR. The best result is then obtained for heursure threshold as a combination of rigrsure-sqtwolog thresholds.

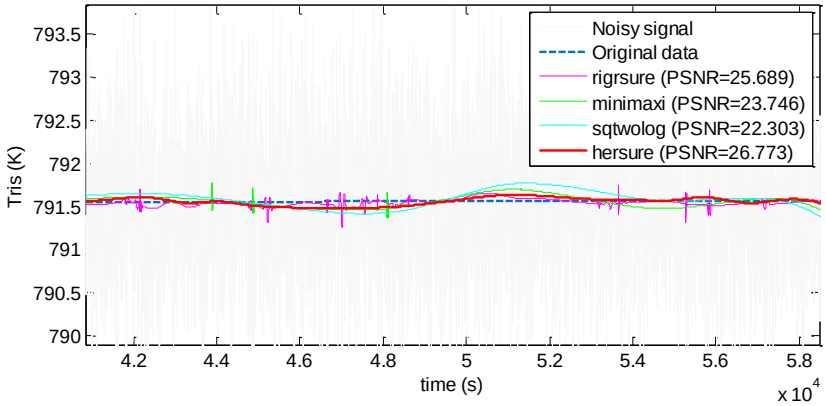

Figure 4.13 *Denoising threshold comparison for coif 5.*

4.4.2 Steady-state detection

For Steady-State Detection (SSD), F-test, Wavelets Transform Based Method, and Standard Deviation Methods were evaluated. A graphical comparison of the three methods applied to regenerator temperature is depicted in Figure 4.14 (Case A) and Figure 4.15 (Case B). The only difference between case A and B is due to the randomness in the noise added to the signal. Although the same parameters are used for the generation of noise

(SNR = 60, 15% data contaminated with gross error), the points where noise and gross errors generated randomly are different for both cases.

Figure 4.14 shows how the three methods behave with respect to steady-state detection. The SS, β, and SSD values vary from 0 to 1 and correspond to the Modified F-test, wavelet transform, and standard deviation methods, respectively.

From this figure, it can be inferred that the F-test method is able to detect the second and third steady state of the regenerator's temperature profile but not the first state. It is also observed that it identifies some false detections of steady state close to $11x10^4$ s (30.5h) and a false non steady-state detection near the same point. On the other hand, the wavelet transform method is able to detect the moment in which disturbances occur, but it is not capable of detecting the point at which the steady state is reached again.

In Figure 4.15 the same sequence of the evaluated methods for the detection of steady state is observed. Although the data generation conditions are the same, it is observed that the results of the steady-state detection using the F-test method are unsatisfactory because of the strong failures in the detection in contrast to Figure 4.14. The reason for these results lies in the effectiveness of the noise elimination stage. Although the wavelet transforms allow a good approximation of the original signal, sometimes the cleaning does not result in a completely clean signal. Then, for the F-test method, the presence of small variations can seriously affect the detection of the steady state and generates erroneous detections either of steady state or non-stationary state. On the other hand, the standard deviation method is not affected by the presence of these variations and has a good response to the expected detections.

The standard deviation method shows to be the best alternative among the three methods. Although it takes more time to detect the second and third states, this method is able to predict the moment at which the disturbance occurs. Furthermore, it does not suffer a high influence from small noise presence.

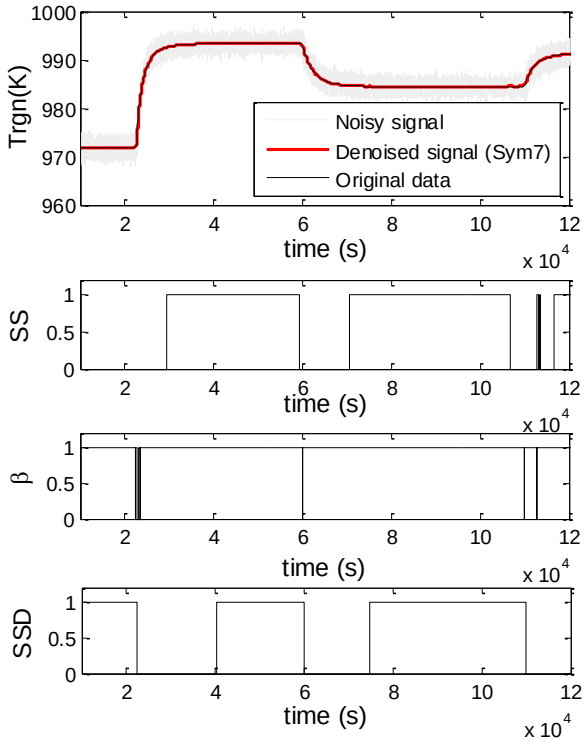

Figure 4.14 *Steady-state detection methods comparison for regenerator temperature profile (Case A). SS: Modified F-test, β: Wavelet transform based method, SSD: Standard deviation method.*

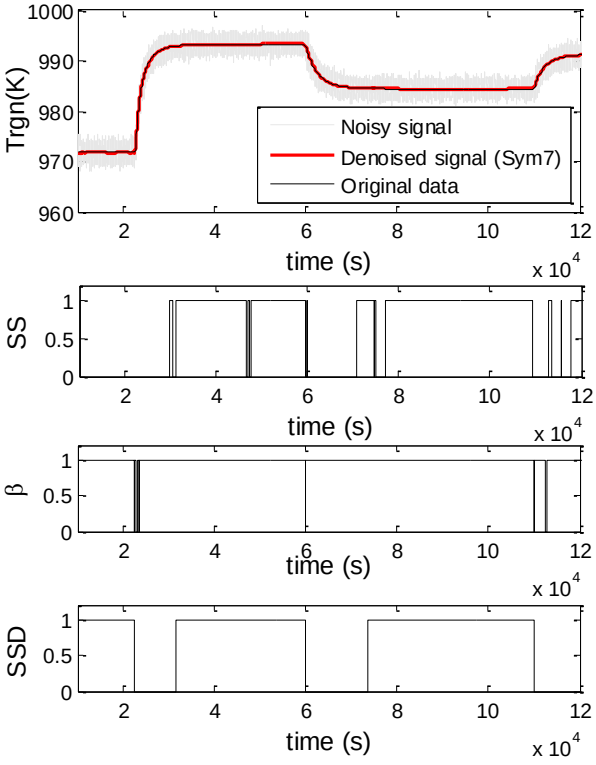

Figure 4.15 *Steady-state detection methods comparison for regenerator temperature profile (Case B). SS: Modified F-test, β: Wavelet transform based method, SSD: Standard deviation method.*

Another important aspect for the RTO implementation is the run time for each method. They are reported in Table 4.4.

Table 4.4 *Run time for F-test, wavelet transform and standard deviation methods.*

	Modified F-test	**Wavelet transform**	**Standard deviation**
Run time(s)	24.6	4.72	15.3

Although wavelet transform method spends less time, it is not appropriate for steady-state detection in these signals. In contrast, the standard deviation method results in a better time than that of the modified F-test.

From the tuning of F-test, wavelet transform, and standard deviation parameters, the best values in the riser temperature profile are reported in Table 4.5.

Table 4.5 *Parameter values for riser temperature using Modified F-test, Wavelet transform and Standard deviation methods.*

Test	**Parameter**	**Value**
Modified F-test	L_1	9.50x10-1
	L_2	3.50x10-3
	L_3	1.50x10-7
Wavelet transform	T_s	1.12x10
	T_u	3.35x10
	T_w	2.47x10-1
Standard deviation	S_1	1.50x10-4
	S_2	1.80x10-6

Despite the fact that these parameters determine the sensitivity of each method to detect the steady state, they do not have a relation between them and are independent for each method.

From the modified F-test parameters tuning, it was observed that high values of L_1 lead to detecting a steady state when it is not a steady state; low values of L_2 tend to detect steady state when it is not at steady state, and high values of L_3 tends to do detect unsteady state when it is steady state. In the S_1 and S_2 tuning for the Standard Deviation Method, low S_1 values make disturbance detection more sensitive while low S_2 makes detection more sensitive to detect the new steady state.

4.4.3 Data reconciliation and parameter estimation

Once the steady state has been detected, data reconciliation is carried out by using WLS and Hampel maximum likelihood estimator. The results of this evaluation for regenerator temperature are presented below:

Figure 4.16 depicts the comparison between WLS and Hampel estimator for the data reconciliation problem. Original data and denoised signal show the difference between values as a result of bias.

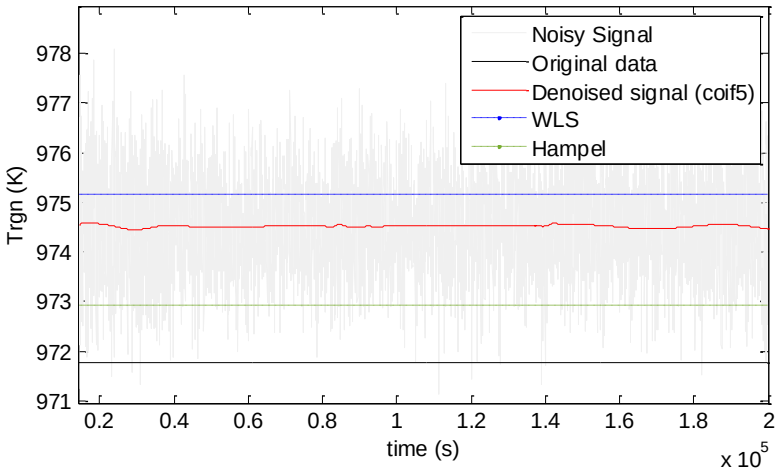

Figure 4.16 *Data reconciliation for regenerator temperature using WLS and Hampel estimator.*

From Figure 4.16, it is observed that the Hampel estimate value is closer than that of WLS with respect to the real value, so it seems more accurate for data reconciliation procedures. Minimization of DRPE was also applied over the noisy signal (Table 4.6) to see how noise can affect the reconciled values.

Table 4.6 *Data reconciliation for regenerator temperature using Hampel estimator*

	Real value	**Measured value (mean)**	**Reconciled value**	
			Noisy signal	**Denoised signal**
T_{rgn} (K)	971.76	974.52	974.24	972.92
Run time (s)*	N/A	N/A	1.31x103	2.32x103

* run time for horizon length H

From these results, it is observed that the reconciled value obtained from the noisy signal is farther away than that obtained with the denoised signal, despite spending less

computing time. Although the computation time is higher using noise elimination procedures, these significantly improve the reconciled value. Errors from WLS and Hampel estimates for the other measured and unmeasured FCCU variables were calculated, and parameters for the model were estimated. Some results are presented below:

Table 4.7 *Error percentage of data reconciliation using WLS and Hampel estimators*

Variable	Measured value	Real value	Robust estimate			
			WLS	%error	Hampel	%error
$F_{air}\ (kg/s)$	22.1	25.3780	27.027	6.50	25.594	0.851
$xO_{2(in)}$*	0.2136	0.2136	0.211	1.22	0.211	1.217
$xN_{2(out)}$*	0.7864	0.7864	0.789	0.33	0.789	0.331
$F_{fg}(kg/s)$	25.4	27.3393	29.529	8.01	27.939	2.193
$xCO_{(out)}$*	unknown	0.0531	0.0506	4.70	0.0506	4.696
$xCO_{2(out)}$*	unknown	0.0904	0.0881	2.58	0.0881	2.578
$xO_{2(out)}$*	0.0043	0.0041	0.0043	4.47	0.0043	3.759
$xN_{2(out)}$*	unknown	0.7087	0.7182	1.34	0.7182	1.340
xH_2O_{out}	unknown	0.1436	0.1387	3.38	0.1387	3.362
σ	1.6928	1.7024	1.702	0.02	1.7090	0.386
$T_{cy}\ (K)$	997.69	994.77	1100.69	10.65	996.78	0.202
$T_{rgn}\ (K)$	973.7	971.75	975.153	0.35	972.92	0.120
$F_{feed}(kg/s)$	40.63	40.630	40.543	0.21	40.53	0.224
$F_{prod}(kg/s)$	40.49	38.668	38.041	1.62	39.25	1.506
$go_{(out)}$*	0.3466	0.498	0.424	14.88	0.4850	2.636
$g_{(out)}$*	0.5168	0.358	0.404	12.69	0.3670	2.367
$lg_{(out)}$*	0.1365	0.143	0.192	33.93	0.1480	3.241
$T_{ris(1)}(K)$	776.4	779.76	776.21	0.46	780.18	0.054
$C_{coke,prod}$	unknown	0.0067	0.009	34.91	0.0070	4.928
$C_{Coke,ris}$	unknown	0.0110	0.01	9.18	0.0110	0.103
$C_{coke,sep}$	unknown	0.0110	0.01	9.18	0.0110	0.103
$C_{coke,rgn}$	unknown	0.0043	0.001	76.96	0.0040	7.837
ΔH_{cb}	unknown	-5.24E+05	-5.24E+05	0.01	-5.24E+05	0.010
$r_{cb}(kg/s)$	unknown	1.9613	2.017	2.84	1.9710	0.492

* weigth fraction

Table 4.7 confirms that errors in data reconciliation using WLS becomes higher than those of Hampel, mainly when the values are very small ($C_{coke,prod}, C_{coke,rgn}$). Actually, errors using Hampel estimator do not exceed 8% even with very small concentration values. So it

seems to be a suitable method to determine values for all steady-state variables before optimization.

4.5 Conclusions

Data validation is an important step for real-time optimization of a plant as it adjusts the measurement data of the process to satisfy process constraints, giving greater reliability of the data in the stages of optimization and control of a RTO. Data validation provides estimates of all process state variables, even if they are directly measured or not, and with the lowest possible uncertainty. In this work, denoising, steady-state detection, data reconciliation, and parameter estimation were evaluated using different methods. For the wavelet-based denoising method, a comparison between basis functions and filters was made. Symlets and coiflets basis functions combined with heursure filters gave the best results. Although PSNR is a good measure of the basis functions performance, this does not mean that the signal is the softest. So for steady-state detection procedures, it could be necessary to evaluate this visually. Noise cannot be completely eliminated using wavelet transforms, but a good approximation of the real signal can be obtained.

For steady-state detection, three methods were evaluated. From them, the standard deviation method displays the better results as it is not so sensitive to the presence of noise, and it is able to adequately detect the moment in which a disturbance occurs, as well as the beginning of a steady state. The three evaluated methods require parameters tuning according to the signal, but unlike Modified F-test and wavelet transform that require the tuning of three parameters, the deviation method only requires two.

For data reconciliation and parameter estimation, Hampel estimator was successfully used. It is able to find estimates quite close to the real values eliminating the presence of bias in the signals and ensuring agreement with the process constraints. Hence, data reconciliation is more effective when denoising procedures are applied.

The wavelet noise elimination methodologies, stationary state detection through the use of standard deviation, and the use of the robust Hampel estimator are a good combination for the validation of data in real-time optimization.

Chapter 5. FCCU Optimization

Abstract

Optimization in a refinery is used for the selection of the optimal points for the operation variables that maximize its profitability. In there, optimization of units such as the FCC is essential due to the high commercial value of its products. Within the RTO, the optimization stage plays a fundamental role since objective function, constraints and decision variables are defined in order to optimize in real time the operating conditions when they are affected by some disturbance of the system. This chapter presents the economic objective function proposed for the FCCU optimization associated with process constraints, and the parameters of the economic model such as prices, demand for products, costs of raw materials, and utility cost, as well as a sensitivity analysis to evaluate how profit is affected by system variables. Also, a comparison of deterministic and stochastic methods are presented for which SQP, Interior Point, and Genetic Algorithm were used. The results reveal that the Genetic Algorithm with an appropriate adjustment of the algorithm parameters provides satisfactory results in the optimization for an RTO implementation in a FCCU virtual plant.

Keywords: Optimization, FCC, deterministic optimization, genetic algorithm, profit, gasoline.

5.1 Introduction

Optimization has received important attention as a tool in the industry to increase competition, reduce production costs, improve quality, and satisfy environmental requirements and regulations. The use of optimization has been extended in the engineering of process systems since there are often many possible solutions in these problems, and it is not easy to find an optimal solution that leads to more profitable and

competitive operating conditions [110]. As a result, optimization techniques have been applied to problems of industrial importance, mainly in process engineering systems that include design and synthesis, separations, reactors, equipment design, and flowsheeting; and optimization problems applied to an entire company, a plant, a process, a piece of equipment in operation, or any intermediate system between them.

Optimization in process design and equipment specification is usually performed prior to the implementation of the process, and management decisions to implement designs are usually made far in advance of the process design step. On the other hand, optimization of operating conditions is carried out monthly, weekly, daily, hourly, or even, at the extreme, every minute." The first one corresponds to offline optimization as the required parameters are previously defined to the plant operation. The second one refers to online optimization which makes decisions in different levels of the organization for improving the performance of industrial processes during the process execution. Online optimization is used in the industry at various levels of the organization [111] as is presented in Figure 5.1.

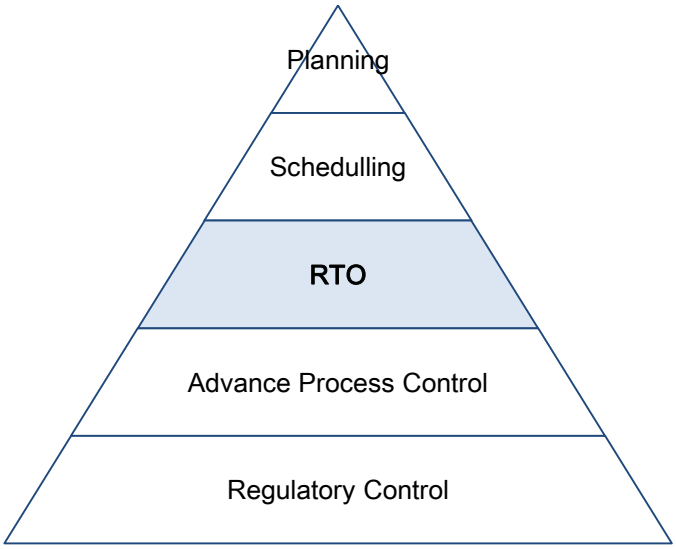

Figure 5.1 *The control and decision making hierarchy of a chemical plant. Adapted from* [6].

- *Strategic planning*, where decisions are made on opportunities and needs for priority investments, market trends, changes in legislation, etc.
- *Production planning*, which is referred to logistics, distribution, transport, and production decisions.
- *Production scheduling*, where programming is defined for on-time deliveries, reduction of storage of raw materials, and products.

- *Optimization of process units or real-time optimization (RTO)*, where it is sought to define the operation variables that provide the highest performance for the process. In this level Optimization in real-time calculates the optimal operating conditions in the at each instant of time.
- *Process control*, where the optimal conditions found through RTO are implemented in the process.

In RTO, a continuous reevaluation of any alteration of operating conditions is developed so that the economic productivity of the process is maximized. The general steps taken in one cycle of the real-time optimizer are depicted in Figure 5.2.

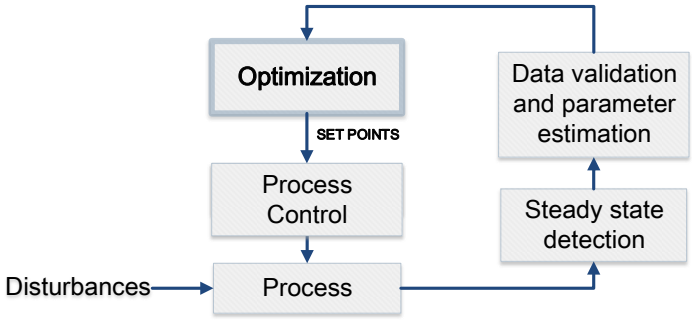

Figure 5.2 *Framework for RTO implementation. Adapted from* [112]

Steady-state detection identifies when the process is close enough to steady state for data from the process to be passed to the next stage. In data validation and parameter estimation, measured and if it is possible unmeasured variables are adjusted to satisfy the balance constraints, and the model parameters are updated. Next, the optimization algorithm is used to determine the optimum set of set points for the process. Finally, the optimizer's results are sent to the controllers of the plant. Once these set points are implemented and the plant has returned to steady-state, the loop is started again [6].

The oil and gas sector is one of the industries that has received benefits from online optimization for enhancing economic performance and reducing overhead cost. Within this industry, the Fluid Catalytic Cracking (FCC) optimization has led to a significant increase in the performance, since this unit provides the largest amount of gasoline in a refinery. In FCCU applications, the online optimization problem usually comprises the maximization the operational profit subject to a set of constraints and a non-linear programming problem (NLP) due to the complex nature and the strong interaction between riser and regenerator [113]. This is why FCCU is a good candidate for RTO applications.

In the following sections, a brief description of some optimization algorithms used in optimization is explained. Afterward, the methodology used in the FCCU optimization is presented, including a description of the proposed objective function and a sensitivity analysis of the operating variables respect to the profit. The results obtained are evaluated and compared according to the behavior of the optimization algorithms used.

5.2 Optimization algorithms

Many real-life situations lead to formulations of non-linear problems. In these cases, approximations that are commonly formulated for linear or quadratic do not give useful results and nonlinear programming (NLP) problems must be formulated. These, NLP models can be subject to a certain set of constraints that can be expressed through a system of equations or inequalities. According to this, the constrained optimization NLP problem using the process model and the objective function can be formulated as [114]:

$$\begin{aligned} \min_{(or\ max)} \quad & f(x) \\ s.t. \quad & h(x) = 0 \\ & g(x) \leq 0 \\ & x_{min} \leq x \leq x_{max} \end{aligned} \qquad \textit{Equation 5.1}$$

where x are the model variables, $f(x)$ is the objective function, $h(x)$ the vector of equality constraints (from the process model), $g(x) \leq 0$, is the vector of inequality constraints, and $x_{min} \leq x \leq x_{max}$, are the variables for upper and lower bounds.

NLP problems can be solved using deterministic and/or stochastic methods. The deterministic optimization, also known as mathematical programming, employs algorithms that are based on linear algebra, gradient calculation, and in some cases the calculation of the Hessian of the response variables [115]. These methods always start with an initial condition, and after some iterations, a better value for each variable is found. One important characteristic of these models is that they will always return the same result if the initial conditions do not vary. On the other hand, stochastic methods are based in stochastic models which incorporate probabilistic elements. The probabilistic elements imply that the final output of the model will be in some kind of confidence interval which means that unique input leads to a different output for each execution of the algorithm. Algorithms with stochastic components are known as metaheuristics, and they are described as “solution methods that orchestrate an interaction between local improvement procedures and higher

level strategies to create a process capable of escaping from local optima and performing a robust search of a solution space" [116].

5.2.1 Deterministic Methods

Some major deterministic approaches for NLP are Interior Point (IP, which uses a log barrier function; Penalty and augmented Lagrange methods that use the idea of penalty to transform a constrained problem into a sequence of unconstrained problems; Generalized Reduced Gradient (GRC) which uses a basic descendent algorithm, and Successive Quadratic Programming (SQP) that solves a quadratic approximation at every iteration. SQP and IP algorithms are discussed below.

Sequential Quadratic Programming (SQP)

One of the common methods to solve the NLP problems are Sequential (or successive) Quadratic Programming (SQP). This method is based on the gradient calculation for the objective function and the constraints. The objective function is defined as a quadratic function, while the constraints as linear functions. Once the quadratic problem is established, quadratic programming is recursively used to find a search direction that minimizes the objective function value [114]. The quadratic problem can be formulated as [117]:

$$\begin{aligned} min \quad & f_k + \nabla f_k^T\, p + \frac{1}{2} p^T \nabla_{xx}^2\, \mathcal{L}_k\, p \\ s.t. \quad & \nabla c_i(x_k)^T p + d_i = 0 \\ & \nabla c_i(x_k)^T p + d_i \geq 0 \end{aligned} \quad . \qquad \textit{Equation 5.2}$$

$$and \quad d_i = c_i(x_k + p_k) - \nabla \mathrm{c_i}(x_k)^T p_k$$

here, f_k is the objective function, ∇f_k^T is the gradient vector of the objective function, $\nabla_{xx}^2\, \mathcal{L}_k$ is the Hessian matrix (second derivative) of the objective function, c_i and $\nabla c_i(x_k)^T$ are the value of the constraint i and its gradient respectively, evaluated at the solution point of the current iteration x^k. Finally, p is a vector that represents the change in searching direction at each iteration and it is calculated from the solution of the optimization problem (Equation 5.2) in the last iteration $(k-1)$.

Once p is calculated, the size of the step a_k is determined to define how much the solution should be moved over the address already found. The new solution at the $k+1$ iteration is represented by:

$$x_{k+1} = x_k + a_k * d_k$$

The solution converges when the vector p is less than the relative tolerance $(\delta = 0.0001)$, and when the KKT conditions are satisfied [118].

Interior Point Method (IP)

The interior point method uses the basic formulation of an NLP, but here the limits are replaced by a logarithmic barrier term. The method solves a sequence of problems by decreasing the values of μ. Then for each $\mu > 0$, Equation 5.1 becomes [119]:

$$\begin{aligned} \min \quad & f_\mu(x,s) = \min f(x) - \mu \sum_i \ln(s_i) \\ s.t. \quad & h(x) = 0 \\ & g(x) + s = 0 \end{aligned} \qquad \textit{Equation 5.3}$$

There are as many slack variables (s) as inequality constraints g. The s_i must be positive to keep the natural logarithm limited. If μ decreases to zero, the minimum of f_μ must be close to the minimum of f. Equation 5.3 is a sequence of equality problems which are easier to solve than the original problem. To solve the approximated problem, IP uses direct step or conjugate gradient in each iteration.

In each iteration, the algorithm decreases with a merit function defined as:

$$f_\mu(x,s) + v \parallel (h(x), g(x) + s) \parallel \qquad \textit{Equation 5.4}$$

The parameter v can be increased with the iteration number to force the solution towards viability. If a step attempt does not decrease the merit function, the algorithm rejects the step attempt and tries a new step.

- Direct step in (x,s). This step attempts to solve the KKT conditions through a linear approximation. This is also called the Newton Step.
  To define the direct step, the Hessian Lagrangian of the f_μ is defined as:

$$H = \nabla^2 f(x) + \sum_i \lambda_i \nabla^2 g_i(x) + \sum_j \lambda_j \nabla^2 h_j(x) \qquad \textit{Equation 5.5}$$

  And the direct step $(\Delta x,\ \Delta s)$ as:

$$\begin{bmatrix} H & 0 & J_h^T & J_g^T \\ 0 & S\Lambda & 0 & -S \\ J_h & 0 & I & 0 \\ J_g & -S & 0 & I \end{bmatrix} \begin{bmatrix} \Delta x \\ \Delta s \\ -\Delta y \\ \Delta \lambda \end{bmatrix} = -\begin{bmatrix} \nabla \mathrm{f} - J_h^T y - J_g^T \lambda \\ S\lambda - \mu \mathrm{e} \\ h \\ g + s \end{bmatrix}$$

where:

J_g is the Jacobian of the restriction g function.

J_h is the Jacobian of the restriction h function.

S = diag (s).

λ is the Lagrange multiplier vector associated with the constraints g

Λ = diag (λ).

y is the Lagrange multiplier vector associated with h.

e is the vector of ones of the same size as g.

This equation is solved through a LDL matrix factorization, which is the most expensive step computing. The $(\Delta x, \Delta s)$ factorization defines if the Hessian is positively defined or not. When it is not positive, the algorithm uses a conjugate gradient step.

- C_g step or conjugate gradient: The conjugate gradient adjusts x and s, with $s > 0$. The algorithm gets Lagrange multipliers by solving the KKT equations. Then:

$$\nabla_x L = \nabla_x f(x) + \sum_i \lambda_i \nabla g_i(x) + \sum_i \lambda_i \nabla h_i(x) = 0 \qquad \textit{Equation 5.6}$$

with $\lambda > 0$. The minimization function is defined with $(\Delta x, \Delta s)$ step as:

$$\begin{aligned} \min \quad & \nabla f^T \Delta x + \frac{1}{2} \Delta x^T \nabla_{xx}^2 L \, \Delta x + \mu e^T S^{-1} \Delta s + \frac{1}{2} \Delta s^T S^{-1} \Lambda \Delta s \\ s.t. \quad & g(x) + J_g \Delta x + \Delta s = 0 \\ & h(x) + J_h \Delta x = 0 \end{aligned} \qquad \textit{Equation 5.7}$$

The algorithm attempts to minimize a rule of linearization constraints within a region with radius (R). Next, Equation (of min) is solved staying in the radius R (confidence region), and keeping s strictly positive. More details of the IP algorithm and the derivation can be found in [120]–[122]

5.2.2 Metaheuristic Methods

Metaheuristic methods are based on the imitation of simple phenomena observed in nature. These algorithms adapt the behavior of different species to highly complex problem solutions through optimization. Some of these methods include simulated annealing, tabu search, variable neighborhood search, scatter search and path relinking, evolutionary algorithms (genetic algorithms), memetic algorithms, genetic programming, ant colony optimization, multi-start methods, greedy randomized adaptive search procedure, guided local search, hyper-heuristics, and parallel metaheuristics. As Genetic Algorithm is one of the most used [123]–[126] and it is available in Matlab, it was selected as an option for the implementation of the RTO on the FCC unit.

Genetic Algorithm

Genetic Algorithms belong to the class of evolutionary algorithms and are inspired by the process of natural evolution. Genetic Algorithms (GA) are search algorithms based on Darwin's theory of evolution in which the natural selection process is used. In the GA the most suitable individuals are selected to reproduce and generate new descendants for the next generation. After a certain number of generations, the population has evolved towards an optimal solution [127].

These algorithms have been used to solve constrained and unconstrained optimization problems, as well as problems with discontinuous, no differentiation, stochastic, or highly non-linear functions. [127] present a comparison between classical algorithms (based on derivatives) and GA.

Table 5.1 *Classical and Genetic Algorithm comparison* [127].

Classical Algorithm	Genetic Algorithm
Generates a single point at each iteration. The sequence of points approaches an optimal solution.	Generates a population of points at each iteration. The best point in the population approaches an optimal solution.
Selects the next point in the sequence by a deterministic computation.	Selects the next population by computation which uses random number generators.

A genetic algorithm scheme is presented in Figure 5.3.

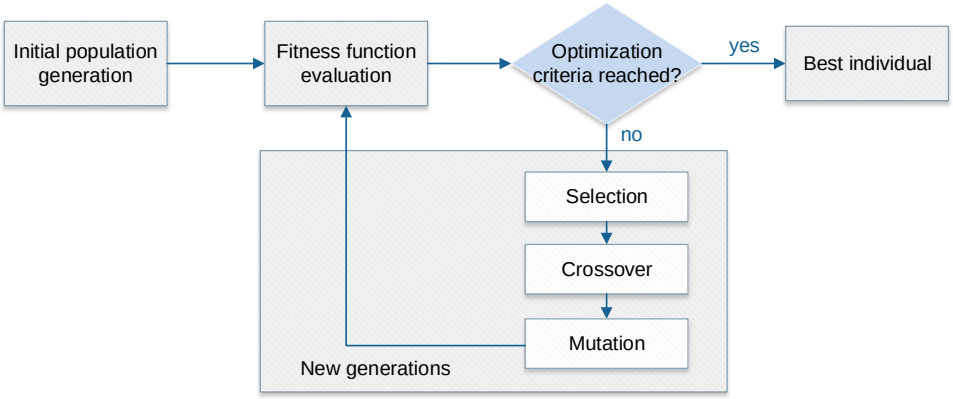

Figure 5.3 *Genetic Algorithm sequence scheme*

- **Initial Population**

The algorithm starts with a population which is made up of a set of individuals. Each individual is a solution to the optimization problem and is characterized by a set of parameters called genes which usually are represented as a string of binary values. Different genes come together to form a chromosome or problem solution as it is represented in Figure 5.4.

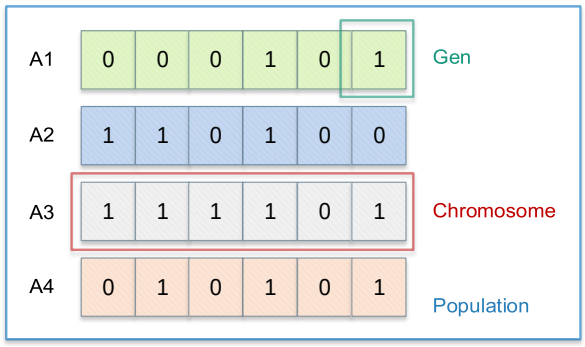

Figure 5.4 *Population, chromosomes and genes. Adapted from* [128].

- **Fitness function evaluation**

The fitness function determines how an individual fits to the desired objective. This function gives a score to each individual, and at the same time, it gives a probability score to be selected in the next generation. If the individual fulfills the criteria for optimization, it will be designated as the best individual, and the best individuals will be selected as parents of the next generation.

- **Selection**

In this step, pairs of individuals are selected based on their fitness scores. The higher the fitness, the more likely they are to be chosen as parents. As descendants inherit the characteristics of the parents, if the parents have good fitness, the children could be better than the parents and have a greater chance of survival.

- **Crossover**

In the crossover, each pair of parents is combined to create a new child. To do this, a crossover point, within the genes, is randomly chosen. Then, the genes from the parents are exchanging among themselves, and the new offspring is added to the population (Figure 5.5).

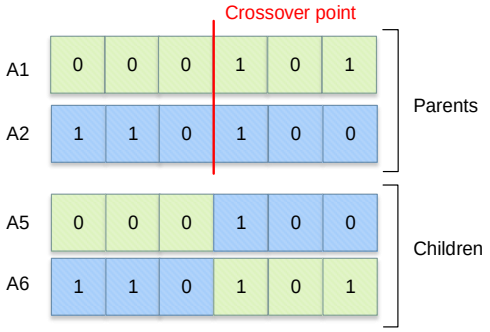

Figure 5.5 *Exchanging of genes among parents and new offspring* [128].

- **Mutation**

In mutation, some bits or genes are flipped. This occurs according to a probability defined for mutation. If a random number is less than this probability, the gen (bit) is mutated. Mutation helps to maintain diversity and prevent the problem of converging ahead of time.

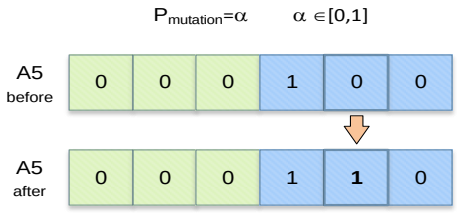

Figure 5.6 *Mutation: before and after*

Finally, this process becomes iterative until the most suitable individuals are found at the end.

5.3 Methodology

The methodology followed for this chapter is presented in Figure 5.7. Each of the stages is detailed below.

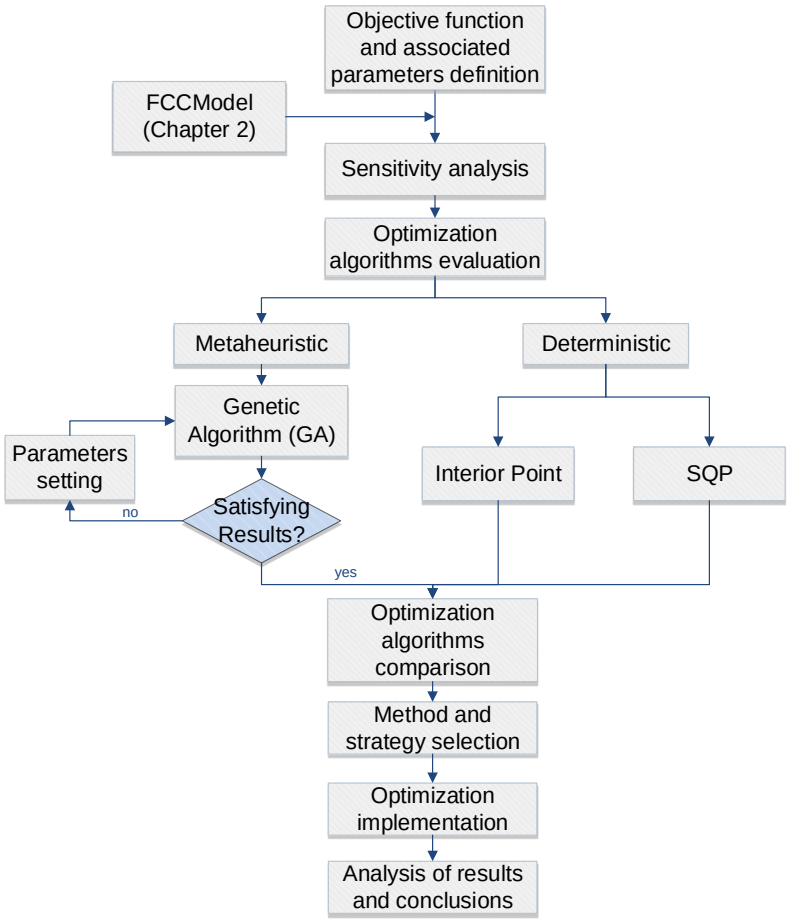

Figure 5.7 *Methodology followed for FCC optimization into the RTO implementation.*

5.3.1 Objective function development

In order to obtain the highest achievable performance for the FCC process under the constraints defined above, an economic objective function that depends on the independent process variables is considered:

$$Max: \quad FCCU_{Profit} = f(Fair, Fcat, Ffeed, Tfeed)$$

$$s.t: \quad \begin{cases} FCCU\ Model\ equations \\ upper\ and\ lower\ bounds \end{cases}$$

Equation 5.8

The FCCU profit is given by the sum of the prices for products stream, feed stream, and utilities used in the unit for the gas oil conversion:

$$FCCU\ _{profit} = \sum P_{products} - \sum P_{feedstock} - \sum P_{utilities} \qquad \textit{Equation 5.9}$$

Gasoline (G), gas oil (GO), and light gases (LG) are the products; then, the price for products is defined as:

$$P_{products} = x_{G_{(6)}} \cdot F_{prod_{(6)}} \cdot P_{G(f_{oct})} + x_{GO_{(6)}} \cdot F_{prod_{(6)}} \cdot P_{GO} + \left(\left(1 - x_{G_{(6)}} - x_{GO_{(6)}}\right) F_{feed} - F_{coke}\right) \cdot P_{LG} \qquad \textit{Equation 5.10}$$

where coke is calculated as: $F_{coke} = F_{cat}(C_{sc} - C_{rgc})$. Price for feedstock considers the fed gas oil and the catalyst reposition:

$$P_{feedstock} = F_{feed} \cdot P_{GO} + 0.005\% \cdot F_{cat} \cdot P_{cat} \qquad \textit{Equation 5.11}$$

Price for utilities is defined as:

$$P_{utilities} = F_{air} \cdot P_{air} \ + LG_{F_{Feed}\, heat} \cdot P_{LG} \qquad \textit{Equation 5.12}$$

where:

$FCCU\ _{profit}$: profit of objective function ($USD\$/s$)

$\sum P_{products}$: sum of prices of products ($USD\$/s$)

$\sum P_{feedstock}$: sum of prices of feedstocks ($USD\$/s$)

$\sum P_{utilities}$: sum of prices of utilities or variable cost ($USD\$/s$)

$x_{G_{(6)}}$: weight fraction of gasoline in the riser at $z = 1$

$F_{prod_{(6)}}$: flow rate of product stream (kg/s)

$P_G\ (f_{oct})$: price of gasoline as function of octane number ($USD\$/kg$)

$x_{GO_{(6)}}$: weight fraction of gas oil in the riser at $z = 1$

P_{GO}: price of gas oil ($USD\$/kg$)

F_{feed}: flow rate of oil in the feed (kg/s)

F_{coke}: flow rate of coke (kg/s)

P_{LG}: price of light gases ($USD\$/kg$)

Prices required for the objective function are defined in Table 5.2.

Table 5.2 *Prices for the objective function* [129] [130] [131].

Material		Price
Gas Oil (as VGO) [USD$/kg]		0.32
Catalyst [USD$/kg]		19
Power Compressor [USD$/kJ]		$1.89x10^{-5}$
Gasoline (G) [USD$/kg]	Regular	0.952
	Midgrade	1.055
	Premium	1.15
Light gases [USD$/kg]		0.184

Products cost

The product cost is defined as the revenue of gasoline production, the gas oil unconverted, and the light gases produced. For this model, there is not discrimination for other products that can also of interest in the FCC (dry gas and LPG), as they are grouped in the lump of light gases. So the main objective of the profit maximization is based mainly on gasoline production, as the higher value-added product.

As the gasoline price depends on its quality, the octane number is included in the objective function through a relationship between the octane number and the gasoline price. The gasoline price is defined based on the octane ratings of 87 (regular), 88–90 (midgrade), and 91–94 (premium gasoline) according to reported by [132]. The relationship is obtained from the curve fitting depicted in Figure 5.8.

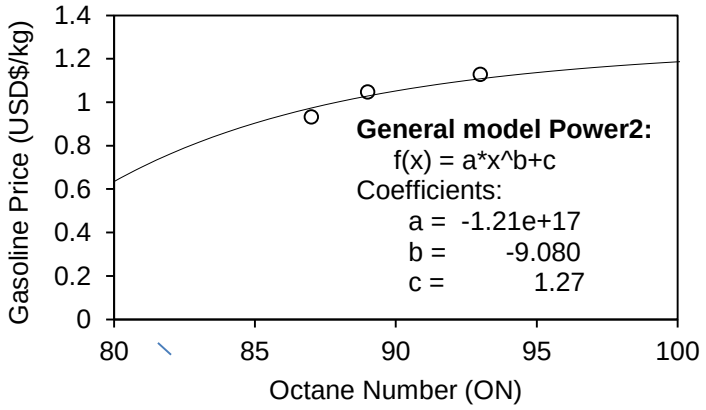

Figure 5.8 *Gasoline price curve fitting to Octane Number 2018* [131].

A second-degree polynomial function in the octane function was also considered in the evaluation of the objective function since it presented a better fit of the data ($R^2 = 1$). However, this function negatively affected the profit function at high ON values. For this

reason, a power fit with two terms is preferred. A detailed Riser Conversion and Gasoline Octane Model is described in Appendix B.

Feedstock cost

Feedstock considers the cost of gas oil (vacuum gas oil), coming from a vacuum distillation tower, as it is the typical feed of an FCCU in a refinery. The cost of a ZSM5 catalyst make up is estimated as $0.005\%Fcat$ for the commercial cost.

Utilities cost

Utilities cost depends on air feed cost and the fuel required to feed preheating.

- **Air Compression:**

The cost of air compression for the regenerator is calculated as follows:

$$P_{air} = Total\ Power\ Required\ (kW) \cdot USD\$/kW \qquad \textit{Equation 5.13}$$

here, Total Power Required (TPR) and Compression Power (CP) are given by:

$$(TPR) = Compression\ Power + leaks\ losses \qquad \textit{Equation 5.14}$$

$$CP = \frac{m_{air} \cdot H_{poly} \cdot g}{\eta_{poly}\ F_3} \qquad \textit{Equation 5.15}$$

where:

m_{air} mass air in (kg/s),

H_{poly} head required by the compressor (m)

g gravity constant (m/s^2)

η_{poly} the polytrophic compressor efficiency

F_3: conversion Factor (102)

Losses by leaks are estimated as $0.7\%CP$. More details about compression power calculation are described in Appendix B.

- **Feed Preheating**

The fuel required to feed preheating (P_{LG}) is defined as:

$$Q_{req} = F_{feed} \cdot Cp_{feed} \cdot (T_{feed} - T_{infeed}) \qquad \textit{Equation 5.16}$$

and

$$F_{fuel} = Q_{req}/CV_{fuel} \qquad \textit{Equation 5.17}$$

where:

Q_{req}: heat required to increase the feed temperature from T_{infeed} to T_{feed} (K)

F_{feed}: feed oil flow rate (kg/s)

Cp_{feed}: heat capacity of oil (VGO) (kJ/kgK)

T_{feed}: feed oil temperature (K)

T_{infeed}: battery limits temperature (K)

F_{lg}: fuel flow required for preheating (kg/s)

CV_{fuel}: heat value of fuel $(kJ/kg\ or\ kWh/kg)$

As in a refinery some products are usually used as fuels for the units supply requirements, it is assumed that the light gases produced by the FCC are used as fuel to the preheating furnace.

5.3.2 Constraints and optimization bounds

Equality constraints in the optimization problem are defined according to the FCCU process model equations presented in Chapter 2; they are evaluated in steady state to develop the steady state optimization required for RTO. On the other hand, bounds are defined according to operational conditions allowable for the FCC model Table 5.3.

Table 5.3 *Process constraints used in optimization.*

Constraint number	Lower bound	Process Variable	Upper Bound
1	20	F_{air} (kg/s)	50
2	100	F_{cat} (kg/s)	400
3	20	F_{feed} (kg/s)	60
4	400	T_{feed} (K)	670
5	300	T_{air} (K)	550
6	810	T_{rgn} (K)	1090
7	730	T_{ris} (K)	840
8	80	ON	100
9	90	RON	-
10	80	MON	-

5.3.3 Penalty function as stability criterion

Although stable state optimization meets with mass and energy balances, the optimal point may not necessarily be a stable steady state due to the multiplicity of states in a FCCU [113], [133]. In this case, the system will not be able to reach that point and will return to the nearest stable point. For this reason, a stability criterion was included within the objective function that determines whether the optimum found by the optimization is a stable state that the system can reach or not.

Consequently, a penalty is included in the objective function that discards those nodes that are not stable and punishes them as points that do not meet the optimization objective. The optimal points found by the genetic algorithm are evaluated under the stability criterion of Lyapunov (Appendix D). If the conditions found by the GA meet this criterion, the solution is part of the population with the best values, otherwise, they will be penalized and discarded as non-viable solutions of the system. Thus Equation 5.9 becomes:

$$FCCU_{\ profit} = \left(\sum P_{products} - \sum P_{feedstock} - \sum P_{utilities}\right) * penalty \qquad \textit{Equation 5.18}$$

where penalty was fixed as:

$$penalty = -1x10^{5}$$

5.3.4 Optimization algorithms

SQP, IP, and GA were tested in order to optimize the profit. First, the optimization problem was solved by SQP, followed by Interior Point algorithm (deterministic methods). GA was considered as third algorithm. Finally, the results of the three algorithms were compared to decide which of them shows a better performance. The optimization runs were developed on an Intel® Xeon® CPU E3-1241 v3 @ 3.5GHz.

5.3.5 Sensitivity analysis

To evaluate how the independent variables affect the objective function and the operation of the FCCU, a sensitivity analysis was developed. To do this, F_{cat}, F_{feed}, F_{air}, and T_{feed} were plotted against profit function. In addition, the profile of the catalyst flow vs. the riser temperature, as well as the air flow vs. the regenerator temperature were plotted to see its behavior with respect to the objective function.

This sensitivity analysis allows to visualize the behavior of the objective function and the process variables within the defined operating limits and establishes if the optimization algorithm is able to find the overall optimum of the function or gets stuck in possible local optima.

5.4 Results and discussion

5.4.1 Sensitivity analysis

A sensitivity analysis of the process variables on the profit function, in steady state, was developed in order to get a better understanding of the system behavior. The variables tested are either manipulated variables of the system or typical system disturbances for the FCCU.

Figure 5.9 shows how the air flow and the ratio of F_{cat}/F_{feed} affect the FCCU profit. Here a profit function improvement is observed from 2 to 6.8 F_{cat}/F_{feed} ratio, with a maximum in the last value. However, beyond 6.8 the profit falls from 20 to 7 US$/s. This is mainly due to the fact that increments in the F_{cat}/F_{feed} ratio generate a continuous increase in the temperature at the riser outlet (Figure 5.10).

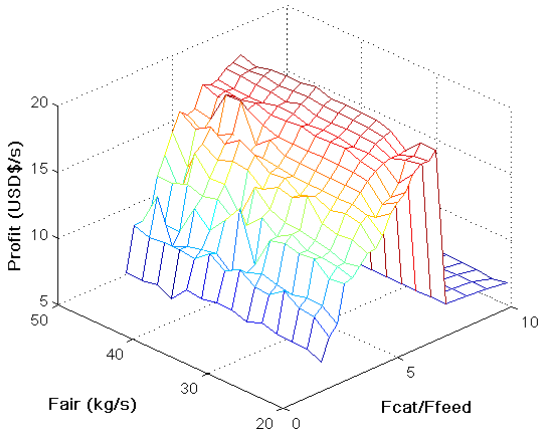

Figure 5.9 *Effect on Profit by changes in F_{air} and F_{cat}/F_{feed} ratio at T_{feed} : 660K and T_{air}: 360K.*

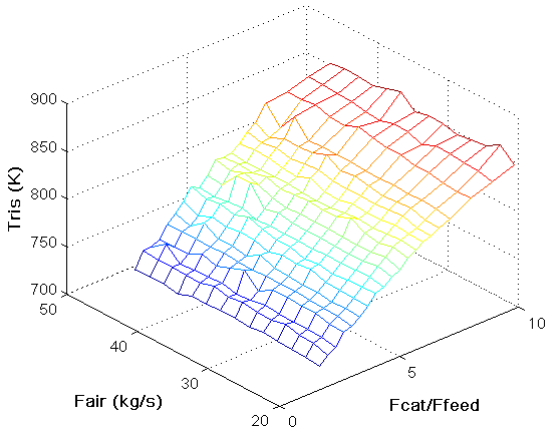

Figure 5.10 *Effect on T_{ris} by changes in F_{air} and F_{cat}/F_{feed} ratio at T_{feed}: 660K and T_{air}: 360K.*

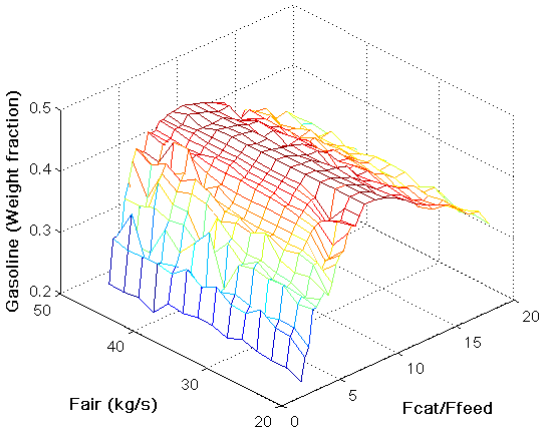

Figure 5.11 *Effect on Gasoline fraction by changes in F_{air} and F_{cat}/F_{feed} ratio at T_{feed}: 660K and T_{air}: 360K.*

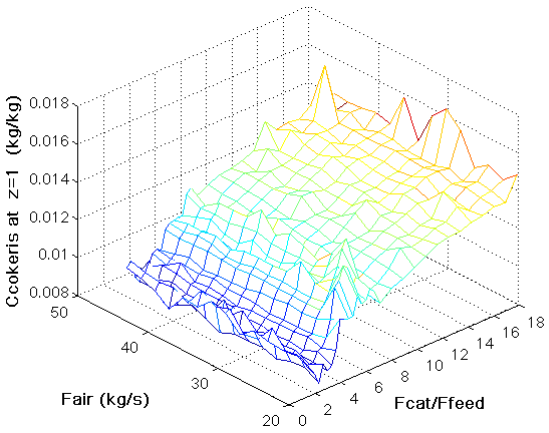

Figure 5.12 *Effect on Coke fraction in riser by changes in F_{air} and F_{cat}/F_{feed}ratio at T_{feed}: 660K and T_{air}: 360K.*

The cracking reactions that occur in the riser are endothermic, and they employ, mainly, the energy carried by the regenerated catalyst after the coke combustion process. Therefore, by increasing the F_{cat}/F_{feed} ratio, the amount of catalyst entering the riser increases as well as the available energy for cracking. Into the riser, the temperature will increase and the cracking reactions are promoted increasing gasoline production. However, even if the GO continues to be consumed, an excessive increase on the available energy favors an over cracking which increases the coke and light gases formation, and decrease in the gasoline production (Figure 5.11, Figure 5.12, Figure 5.13 and Figure 5.14).

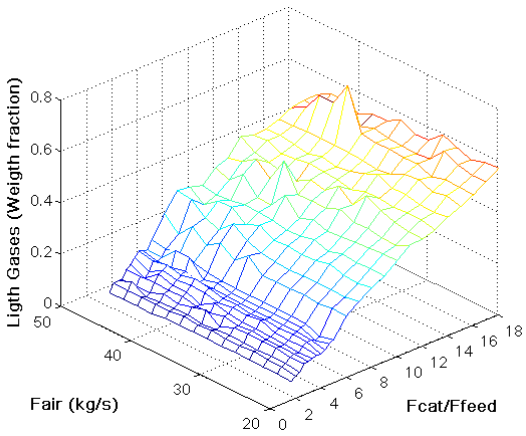

Figure 5.13 *Effect on light gases fraction by changes in F_{air} and F_{cat}/F_{feed} ratio at T_{feed}: 660K and T_{air}: 360K.*

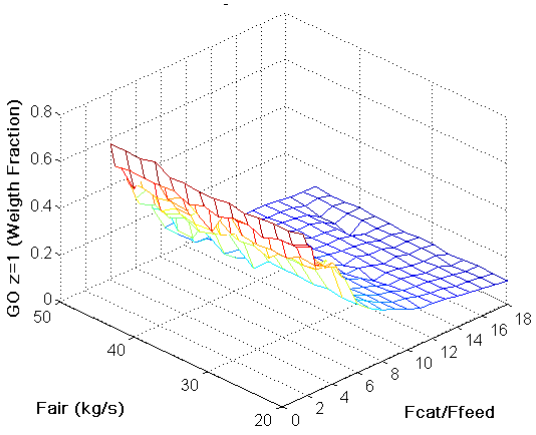

Figure 5.14 *Effect on gas oil fraction in z=1 by changes in F_{air} and F_{cat}/F_{feed} ratio at T_{feed}: 660K and T_{air}: 360K.*

On the other hand, the air flow has only a slight influence on the objective function while the F_{cat}/F_{feed} ratio is the determinant factor in the function's profit.

Figure 5.15 shows how the regenerator temperature is affected by varying both the air flow and the F_{cat}/F_{feed} ratio.

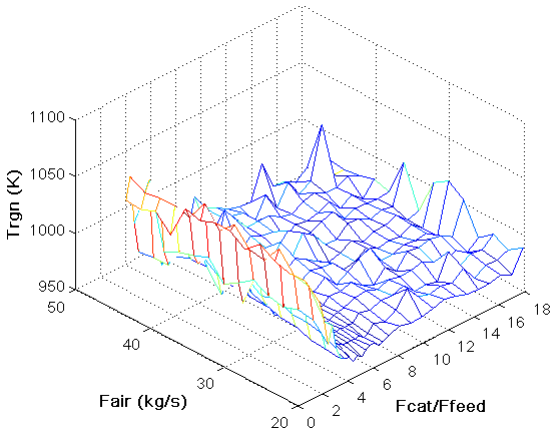

Figure 5.15 *Effect on T_{rgn} by changes in F_{air} and F_{cat}/F_{feed} ratio at T_{feed}:660K and T_{air}: 360K.*

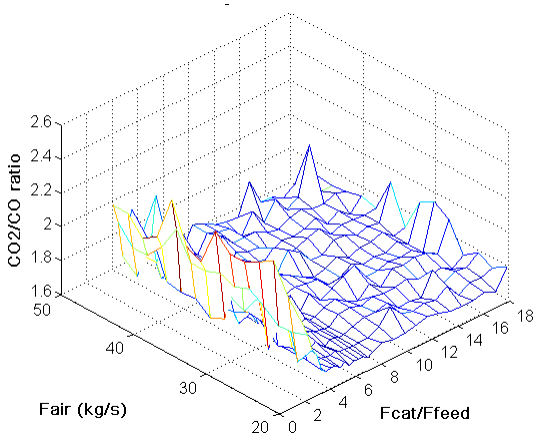

Figure 5.16 *Effect on CO_2/CO ratio by changes in F_{air} and F_{cat}/F_{feed} ratio at T_{feed}: 660K and T_{air}: 360K.*

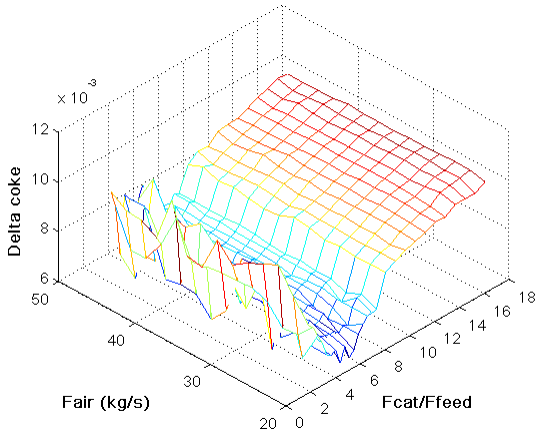

Figure 5.17 *Effect on delta Coke by changes in F_{air} and F_{cat}/F_{feed} ratio at T_{feed}: 660K and T_{air}: 360K.*

Again, for the defined conditions, the regenerator temperature is determined mainly by the F_{cat}/F_{feed} ratio, although slightly influenced by the air flow. At low F_{cat}/F_{feed}, T_{rgn} value increased to 1020K (Figure 5.15), because the available oxygen exceeds the necessary amount to coke burn. This excess of oxygen favors the conversion of CO to CO_2 rising up the regenerator temperature (Figure 5.16). This ratio is also favored when the catalyst flow is increased, but in this case, the increase in the regenerator temperature is due to the energy that the spent catalyst carries with it.

The amount of coke burned is represented in Figure 5.17. In there, the same effect mentioned above is observed. High temperatures favor the combustion of coke, but not necessarily the conversion of GO to gasoline (Figure 5.11). The effect of T_{feed} and F_{feed} on profit function, and gasoline weight fraction at F_{cat}, T_{air} and F_{air} constant is depicted in Figure 5.18 and Figure 5.19.

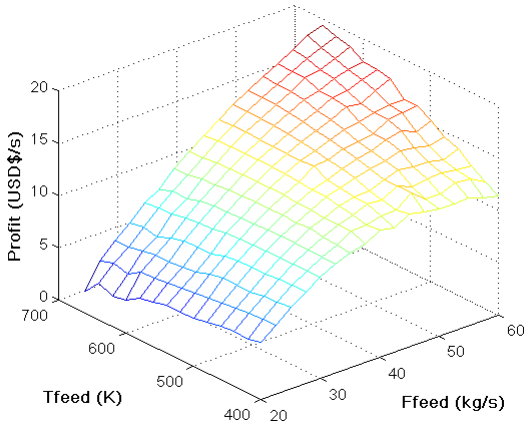

Figure 5.18 *Effect on profit by changes in F_{feed} and T_{feed} at F_{cat}: 385kg/s F_{air}: 37.6kg/s and T_{air}: 360K.*

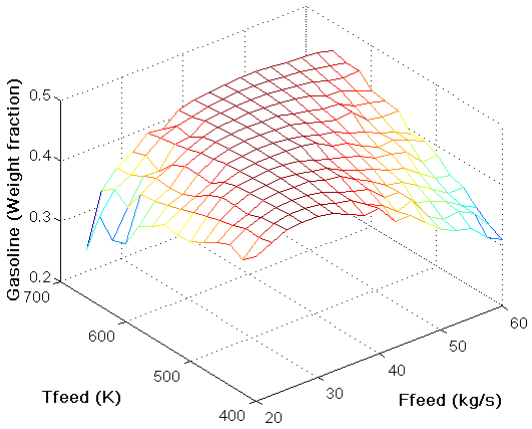

Figure 5.19 *Effect on gasoline weight fraction by changes in F_{feed} and T_{feed} at F_{cat}: 385kg/s F_{air}: 37.6kg/s and T_{air}: 360K.*

According to Figure 5.18, the highest profitability is obtained at high values of T_{feed} and F_{feed}. However, if FCC operates at high temperatures (700K) and feed flows around 20-30 kg/s, the process profitability decreases, as well as if it operates at high flows (60kg/s) and low temperatures (400K). These conditions of minimum profitability are due to the low gasoline weight fractions that are reached under these operating conditions. High feed temperatures benefit cracking reactions, and therefore the conversion to gasoline (Figure 5.19); however, as noted in the previous discussion, these high temperatures should be evaluated with other operating conditions, such as the F_{cat}/F_{eed} ratio, the air flow, and the feed temperature, to get the best operations conditions.

Finally, the effect of F_{air} and T_{air} on profit function and in the T_{ris} at F_{cat}, F_{feed} and T_{air} constant is depicted in Figure 5.20.

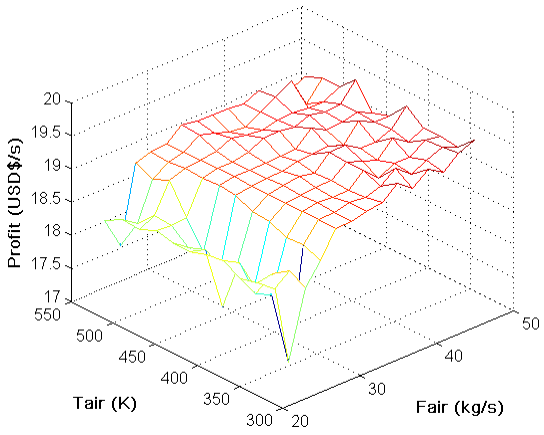

Figure 5.20 *Effect on profit by changes in F_{air} and T_{air} at F_{cat}: 385kg/s F_{feed}: 60 kg/s and T_{feed}: 650K.*

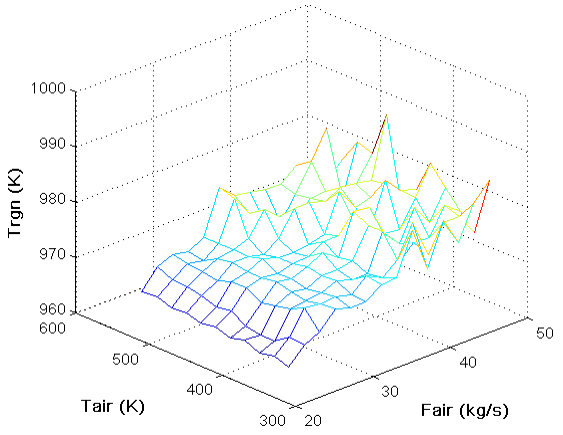

Figure 5.21 *Effect on T_{rgn} by changes in F_{air} and T_{air} at F_{cat}: 385kg/s F_{feed}: 60 kg/s and T_{feed}: 650K.*

In accordance with Figure 5.20, low air flows can reduce the profitability of the process, regardless of the temperature at which the air is. This is becausethe oxygen content in the regenerator, at low air flows, will not be enough to regenerate the catalyst that comes from the riser. Then, under these conditions, it will be preferred to operate at flows greater than 30kg/s to improve the catalyst regeneration. This can be contrasted with the regenerator temperature increasing reported in Figure 5.21, as a consequence of the regenerator combustion reactions with a greater amount of available air.

Sensitivity analysis allows identifying the conditions to which the highest profit is obtained (approximately 19.6 USD/s). This value will be an evaluation criterion of the optimization algorithms to determine if the algorithm is able to find the global optimum. In addition, it shows that at low F_{cat}/F_{feed} ratios, the model does not converge easily, so it is preferred to operate at values greater than 4. On the other hand, relationships between 6 to 7 are the preferred values as operating conditions to obtain the best profit.

5.4.2 Selection of optimization method

Initially, the evaluation of the objective function defined in section 2.1 was carried out using deterministic methods (Interior Point and SQP). Optimization was first developed for the process variables that can be manipulated in order to define the initial parameters of plant operation.

Since the objective function did not reach the maximum profit obtained in the sensitivity analysis the optimization process was also developed with a metaheuristic method (Genetic Algorithm).

Table 5.4 *Performance of three algorithms for FCCU optimization.*

	Lower bound	Upper bound	Initial Point	Method		
				Interior Point	SQP	Genetic Algorithm
$F_{cat}(kg/s)$	115	390	294.00	290.69	294.01	385.3
$F_{feed}(kg/s)$	20	60	40.63	58.75	40.63	59.58
$F_{air}(kg/s)$	20	46	25.38	45.95	25.38	37.6
$T_{feed}(K)$	400	670	434.63	448.51	434.69	656.80
$T_{air}\ (K)$	310	525	360.00	373.84	360.00	360
$T_{ris}\ (K)$	755	840	779.23	753.76	779.23	833.46
$T_{rgn}\ (K)$	810	1090	972.00	1006.64	972.00	1001.30
ON	85	100	91.71	89.00	91.67	97.30
$Profit\ (USD\$/s)$	-	-	9.69	12.09	9.89	19.87
$Run\ time\ (s)$	-	-	-	148	185	13932

Table 5.4 shows a value of profitability obtained by GA, which is better than the obtained by the IP and SQP algorithms, and the IP better than SQP. Although a better profit is obtained with the interior point than with the SQP, this value does not turn out to be the one expected according to the sensitivity analysis. On the other hand, the genetic algorithm is capable of reaching a value close to that expected; even those optimality conditions coincide with the $F_{cat}\ /F_{feed}$ ratio of higher profitability (6.46).

Results in Table 5.4 can be explained by the fact that deterministic methods can be trapped in a local optimum and then never converge on the global one. On the other hand, stochastic algorithms such as the GA can explore the entire optimality region and find better conditions into the study region. However, the problem here is that the run time turns out to be much longer for the GA than for deterministic methods, which could be a drawback in an RTO implementation. For this reason, it was decided to analyze the speed of the GA according to the number of generations needed to find a convergence, as they represent the iterations number of the algorithm to find the solution. The results obtained for four runs of GA are depicted in Figure 5.22. To analyze the performance and the confidence of the GA, Figure 5.22 shows the evolution of best and average fitness (the inverse of the objective function), as well as the stopping criterion and the generation for each run. The best and average fitness refers to the best fitness value among all members of the

population, while mean fitness refers to the average of all members of the current population.

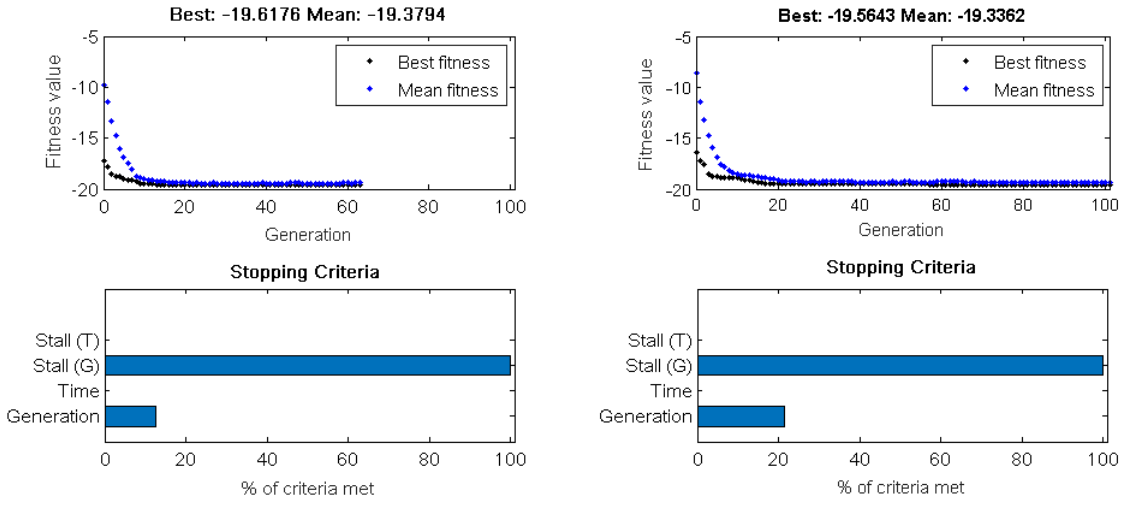

a) Run 1 *b) Run 2*

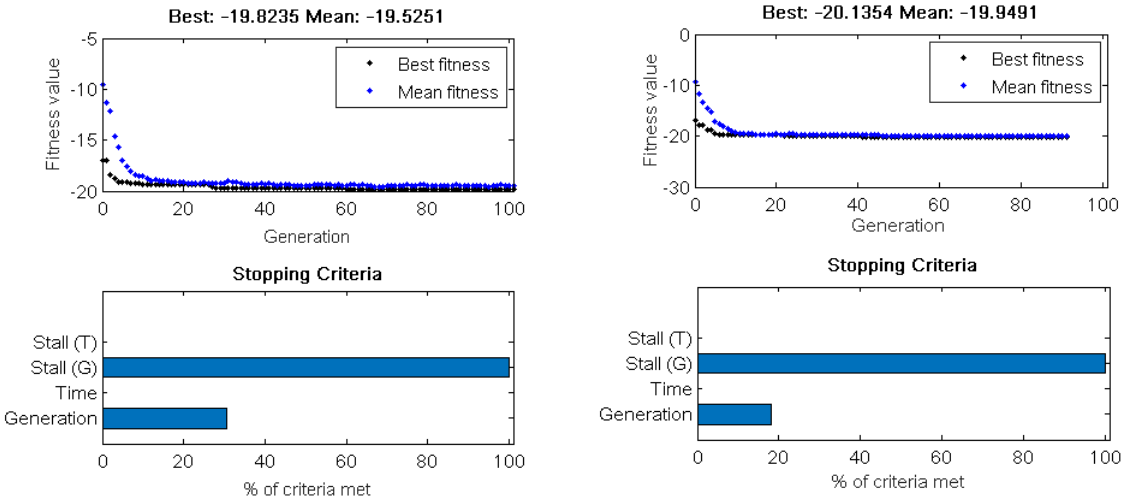

c) Run 3 *d) Run 4*

Figure 5.22 *Different runs for criteria selection in GA.*

The stopping criterion shows in what percentage the "Stall generation" (or minimum generations before stopping the GA) and the number of maximum of "Generations" have been used after the algorithm stops. For example, in Figure 5.22a the stall parameter is set to 50 while the maximum number of iterations is set to 500. The algorithm stops at iteration 101, which means the number of stall generations is completed and reaches 100% (101>50), and that the final generation in which GA stops is approximately 15% of the

maximum criterion of generations (500*15%=75 generations). Then, for this case the algorithm stopped in the 75th generation.

The diversity of the population refers to the average distance between the individuals of the population. In the initial stages of the search, a genetic algorithm shows a large diversity, while at the end the diversity decreases in order to achieve the solution. According to Figure 5.22, in all runs the diversity of the GA begins to decrease approximately in the 10th generation, and the difference between the best value and the average significantly decreases in generation 20 or even earlier.

In accordance to [134], "The algorithm stops if the average relative change in the best fitness function value over StallGenLimit generations is less than or equal to TolFun". As the "% of criteria" is completely fulfilled and the maximum of generations is not reached, the algorithm stops because the tolerance value (1.0×10^{-6}) is achieved. Such as in the 20th generation, no significant changes in the profit function value are observed, it does not make sense to continue iterating until reaching the 100 generations. Consequently, the number of Stall Generations is adjusted to 10 and the Maximum of Generations in 20 with a reduction in the computation time from 1.39×10^4 to 1.8×10^3 seconds (from 3.9 to 0.5 hours).

Considering that for metaheuristic algorithms the best parameter values depend on the problem, different values were tested for the GA. The best ones are depicted in Table 5.5.

Table 5.5 *Genetic Algorithm parameters for FCCU Optimization.*

Parameter	**Value**
Population Size	50
Tolerance	1.0 e-6
Crossover Fraction	0.8
Elite Count	2.5
Fitness Limit	-Inf.
Max Stall Time	Inf.
Max Time	Inf.
Population Type	Double Vector
Max. Stall Generations	10
Max. Generations	20

The optimal results for GA using the parameters mentioned in Table 5.5 are depicted in Figure 5.23. These results are not very different from those found by the GA in Table 5.4, but the computation time is significantly reduced.

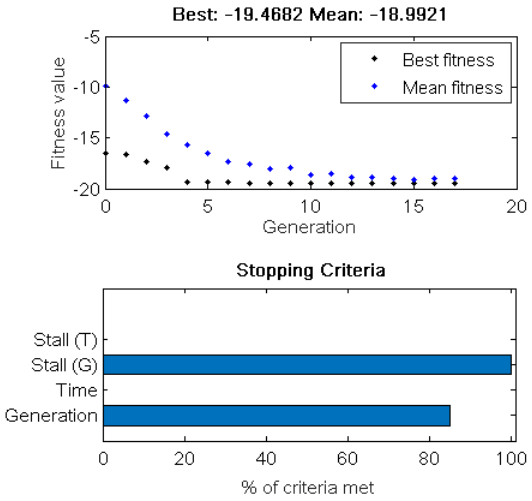

Optimum Values	
$F_{cat}(kg/s)$	388
$F_{feed}(kg/s)$	60
$F_{air}(kg/s)$	43
$T_{feed}(K)$	651
$T_{air}\ (K)$	360
$T_{ris}\ (K)$	829
$T_{rgn}\ (K)$	996
ON	97
$Profit\ (USD\$/s)$	19.78
$Run\ time\ (s)$	1800

Figure 5.23 *GA optimization results reducing the maximum numbers of generations and Stall Generations.*

It should be clarified that although the best profit results were obtained with the stochastic optimization, the deterministic methods are significantly faster than the stochastic. Therefore, the choice of the optimization method for an RTO strongly depends on the system response and its settling time.

Here, the IP algorithm presented an improvement for the profit value respect to the initial condition in a time of 148s (2.5min), whereas the GA yielded the value closest to the maximum possible profit value in a time of 1800s (30min). In the case of the FCCU, the stabilization times are around 4-6 hours, so the execution time of the GA results satisfactory for this application.

5.5 Conclusions

The FCCU was optimized using a cost function defined from the costs of production, the cost of raw materials, and the value of the products. For the main product (gasoline) a function for its value depending on its quality is proposed. A sensitivity analysis of the operating variables on the profit function was analyzed, and deterministic and metaheuristic methods were compared in order to find the best tool for the optimization of the unit. The sensitivity analysis indicated that the energy balance between the riser and the regenerator

is of great importance in the unit, as it ensures the energy for the cracking of the GO, as well as an adequate reactivation of the catalyst in the regenerator.

Certain FCC operating conditions can benefit some aspects of the system, but they also negatively affect others due to the strong interaction between the riser and the regenerator. Therefore, the optimal conditions must be determined through optimization methods that guarantee the best system operating values.

Besides providing an overview of the behavior of the system, the sensitivity analysis also allowed evaluating the performance of the optimization algorithm through the maximum possible value reached for the profit function, and using it as an additional criterion for the choice of the optimization algorithm in RTO.

The deterministic methods evaluated here (SQP and IP) are not able to find the global optimum, as they were easily trapped in local optima. For the FCCU optimization problem, metaheuristic algorithms work better in the search for global optima, but consume more computation time. Nevertheless, time can be significantly reduced if the stopping criteria are analyzed; in GA the key criteria are stall generation and a maximum of generations. Results indicate that GA is a good optimization algorithm for RTO on a FCCU virtual plant.

Chapter 6. PID Control

Abstract

Process control systems ensure that processes are executed efficiently, consistently, and with the least possible variation. In addition, they help maintain performance, quality, energy efficiency, and safety. All of these aspects are essential in a refinery process due to the process characteristics and the volumes handled. One of the most important processes in this industry is the FCCU where daily millions of oil barrels are converted to more valuable products. In this unit, the increase in profitability is directly related to the control of the process through the hierarchies of control. FCCU is known to be very difficult to model and control because of the presence of nonlinearities and riser-regenerator coupling. This chapter presents a brief review of the control strategies used in a FCCU and in the design of a PID controller that will be used in the implementation of RTO. The multivariable feedback PID controller design is based on an analysis by RGA and the NI index. The results disclose the effectiveness of a decentralized PID control scheme.

Keywords: FCCU, RTO, process control, PID, tuning.

6.1 Introduction

Several chemical products as oil derivates are produced from a series of operations that involve complex processes. In most of these stages, process control plays a fundamental role in maintaining safe operations, quality products, and business profitability. Control in this industry has been extended, and it is no longer just basic or regulatory control of direct actions on the instrumentation, but a much more elaborate structure of control hierarchies and decision making that involves different areas of the companies Figure 6.1

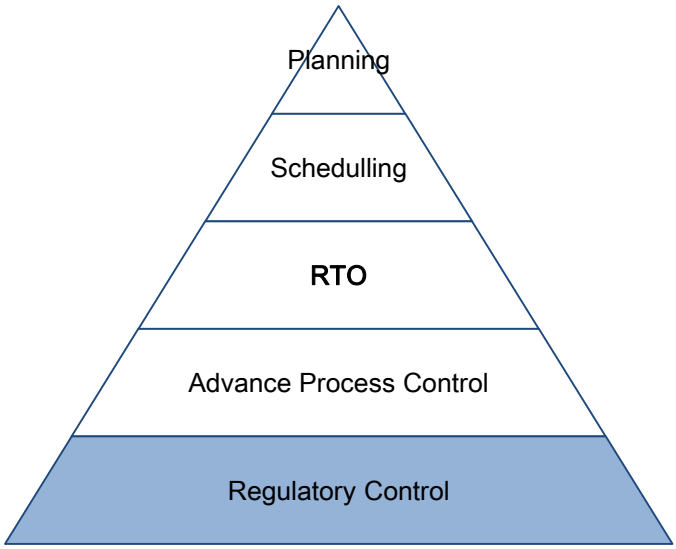

Figure 6.1 *The control and decision-making hierarchy of chemical plants. Adapted from [1].*

At the top level is the planning stage in which aspects such as what raw materials to buy, what products to manufacture, and the number of products to manufacture are defined. One level below is the programming stage which deals with when those actions established in the planning stage will be carried out, referring to times and events to execute the chosen plan. These first two levels are not executed all the time but intermittently according to the needs of the plant, e.g. weeks, days.

From the next layer (RTO), the lower levels are executed in real time, although at different intervals [4]. RTO is the connection between the regulatory control and the economic optimization of the unit, and it is mainly used when frequent changes occur in the variables of the process [135]. An RTO is a system based on a model that is responsible for calculating setpoints that maximizes the profit of the plant and sending them to the control systems, so that the desired optima are achieved through changes in the manipulated variables.

In an RTO system, the data are analyzed once it reaches a steady state through a reconciliation that seeks to compensate for systematic measurement errors [135], [136]. These data, generated in reconciliation, are used to calculate a new set of model parameters so that the plant is represented as accurately as possible at the current operating point. Once this is done, the current plant data are sent to a restricted economic optimization system for the calculation of the new set points of the plant. The optimal setpoints are then fed into a supervisory control system (where operators verify

verisimilitude, assign ramp changes, or execute actions that, according to their criteria, improve the implementation of SP. In the advanced control layer or supervisory control, there are control algorithms that are used to take into account process constraints, the coupling of process variables and processing units, and operational performance. In this layer, model predictive control (MPC) is usually used, it is a strategy based on optimal control concepts that determine an optimal trajectory of the input variable with respect to a performance index [3]. Control by MPC has two important advantages over other control strategies: the handling of process constraints and the multivariable interactions of non-linear MIMO systems [3].

Finally, the optimal values are sent to the regulatory control layer to implement the appropriate movements in the manipulated variables. The basic or regulatory control maintains the specified conditions for the process according to the operator's decision or by choices in the highest layers of the hierarchy. This means that this control is responsible for adjusting the signal to the final control element according to the setpoint. In this layer no decision is made as to whether the value of the setpoint is the most appropriate, it simply follows orders from the upper layers of the hierarchy. Typically, decentralized controllers (single loop) are used.

In the following sections, the two most common strategies and configurations used for the FCCU control will be discussed, and the methodology to evaluate the control strategy in this unit is presented. Finally, results, analysis, and conclusions are discussed in order to establish the configuration of the controller that will be used in the RTO.

6.2 FCC Control

FCC is one of the most important units in a refinery as it is responsible for about 40% of the gasoline pool [137]. The high non-linearity of the process and the strong interaction between the individual control loops make it difficult to design and implement an efficient control system. As a consequence, different traditional and advanced FCC control strategies have been tested, and their performance still remains as a research issue. Actually, supervisory control strategies such as advanced control and real-time optimization have been employed in order to improve the operational conditions and the process profit.

The most important controlled variables in an FCCU are the stripper catalyst level for the catalyst level stabilization; the riser temperature (T_{ris}) which is directly related to the conversion; the oxygen concentration in the flue gas (xO_2) that, indirectly, allows to check the coke combustion; the regenerator temperature (T_{rgn}) to recover the catalyst without excessive deactivation; and the cyclone temperature (T_{cy}) to avoid afterburning. On the other hand, the main manipulated variables comprise the spent and regenerated catalyst flow rates, the flue gas flow rate, and the blower air flow rate [137].

For the regulatory layer, different control structures have been proposed. [137] presents typical FCCU decentralized control structures for partial and complete combustion mode. Some control structures for partial combustion are presented in Table 6.1.

Table 6.1 *FCC Decentralized Control Structures* [137].

Control Structure	**Manipulated variables** $(\boldsymbol{u})$	**Controlled variables** $(\boldsymbol{y})$
Conventional	F_{cat} F_{air}	T_{ris} ΔT_{rgn}
Kurihara	F_{cat} F_{air}	ΔT_{rgn} T_{rgn}
Alternative Kurihara	F_{cat} F_{air}	T_{cy} T_{rgn}
Hicks	F_{cat} F_{air}	T_{ris} T_{cy}
Riser-Regenerator	F_{cat} F_{air}	T_{ris} T_{rgn}

Among the analyzed structures, the one that seems to perform better for partial combustion mode is the Riser-Regenerator control structure [137].

In terms of advanced control strategies, the MPC has been widely used, thanks to its multivariable characteristics, its anticipatory nature, and its ability to handle restrictions in both controlled and manipulated variables.

A comparison between decentralized and advanced control strategies was developed by [138]–[140]. These works demonstrate that advanced control strategies have better behavior than PID with respect to overshoot and response time. A more detailed control strategies analysis applied for FCCU is presented in [137].

6.2.1 PID control

PID controllers are the most common control used on chemical and petrochemical plants due to easy implementation and robustness [136]. A PID controller is a device that allows controlling a closed-loop system to reach the desired output state (set point). This type of controller is composed of three elements that are in charge of implementing actions that lead the variable to the desired point. These elements are known as proportional action, integral action and derivative action as presented in Figure 6.2.

The setpoint or reference value $r(t)$ indicates the desired value at the output of the process $y(t)$. The difference between $r(t)$ and the actual state of the system $y(t)$ is the error $e(t)$. The error signal is used by the PID controller to take corrective action through the proportional, integral and derivative action. The output of the PID controller is sent to the actuator to adjust the manipulated variable until the process variable reaches the desired value or SP.

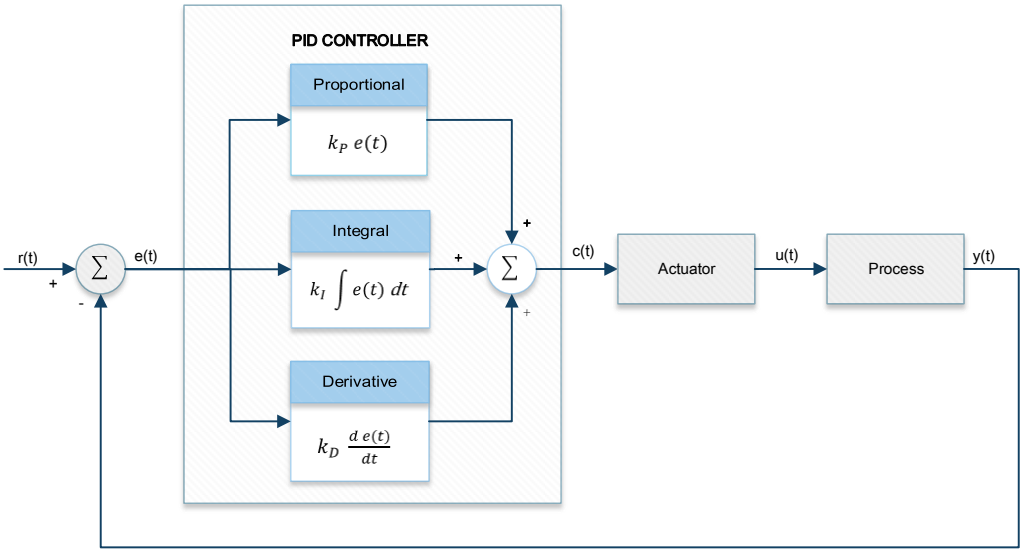

Figure 6.2 *Schematic of a PID controller.*

A discrete time PID controller is described by control algorithm [141]:

$$u(t) = k_P e(t) + k_I \sum_{i=0}^{t} e(i) + k_D[e(t) - e(t-1)] \qquad \textit{Equation 6.1}$$

where k_P, k_I and k_D are the controller parameters. The PID controller action depends on the proportional, integral, and differential control values.

Proportional action

This action is proportional to the error signal and attempts to minimize the system error by multiplying the error signal by a constant called k_P. When the error is large, the proportional control action is large and tends to minimize this error. A k_P increment accelerates the controller action and decreases the error, but also increases the instability of the system.

Derivative action

The derivative action k_D is proportional to the derivative of the error signal $e(t)$ and measures the "error rate". Thanks to the measure of this rate, the oscillations in the controller are avoided. This is because as the system gets closer to the reference point, the controller decreases the speed and prevents that the system overtakes the desired point. Increases in the k_D augment the stability of the system and slightly decreases its speed. This type of controller action is especially useful when it is desired to stabilize a response that oscillates too much.

Integral action

The integral action calculates the integral of the error signal $e(t)$ as the sum or accumulation of the error signal, and this value is multiplied by the integral factor k_I. As time passes, errors are added and the integral action goes increasing, which reduces the system error to reach the target value. The increase in the integral action k_I slightly increases the speed of the system but also its instability.

PID Tuning

The methods used for the parameters k_P, k_I and k_D tuning can be classified into two categories [136]: classical and artificial intelligence methods. Among the classical methods are Ziegler and Nichols[142], and Cohen and Coon [143] methods. Ziegler and Nichols are suitable for level controls but not for flow, that requires a rapid response. In these cases, Cohen and Coon's method is used [144].

On the other hand, artificial intelligence methods include Genetic and Differential Evolution Algorithms, Simulated Annealing (SA), fuzzy system, Artificial Bee Colony (ABC), Particle Swarm Optimization (PSO), etc.

Genetic algorithms have been widely used for this purpose [145]–[149]. In GA the tuning starts with a random population of chromosomes, each of which represents a solution to the problem. These values are evaluated in a fitness function that defines how good the solution to the problem is. The best individuals are selected to create a new generation from selection, crossover, and mutation stages. This process is repeated until a set of good individuals are found. Here, each chromosome corresponds to the parameters k_P, k_I and k_D; and each of these parameters is evaluated with a performance function (MSE Mean Square Error, IAE Integral absolute error, ISE Integral Squared Error, etc).

6.3 Methodology

The methodology followed for this chapter is presented in Figure 6.3. Each of the mentioned stages is explained below.

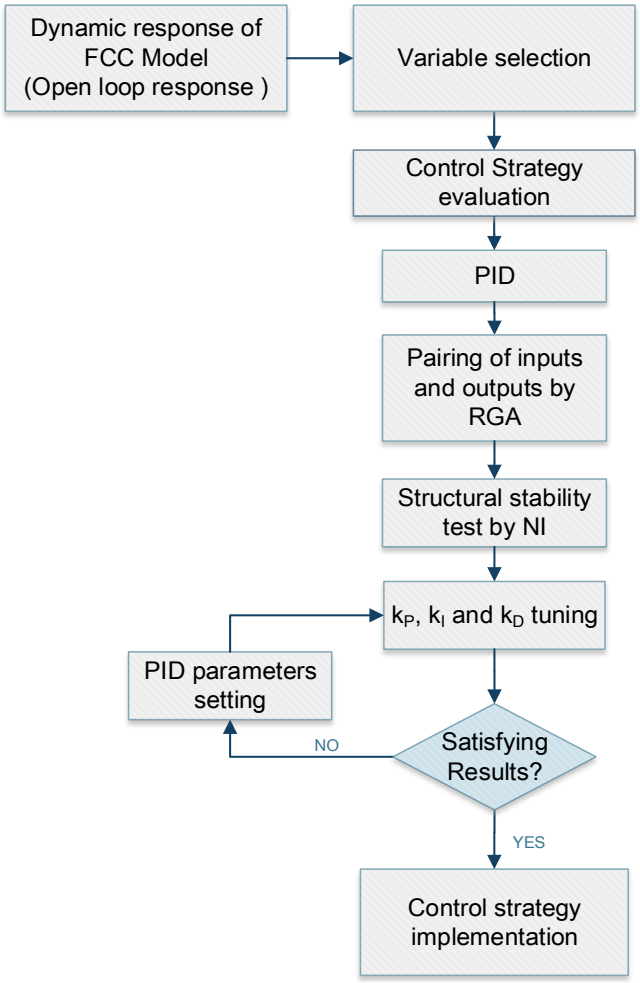

Figure 6.3 *Methodology followed for FCC control design.*

6.3.1 Variable classification

To implement the control system to be used in the FCC virtual plant, it is important to define the control variables, the manipulated variables, and the disturbances from the inputs and outputs of the system.

- *Outputs:* the outputs of the unit can be used as the controlled variables or control objectives of the system. Since the product distribution is defined by the reaction conditions within the riser, T_{ris} and T_{rgn} are important parameters for the control in the unit. These variables are directly related to the outlet temperature of the riser and the intake temperature of the riser, respectively. Moreover, T_{ris} has a very close relationship with the conversion in the riser.

  Another important aspect in the FCCU regarding partial combustion is the need to control the afterburning to avoid combustion in the flue gas leaving the dense bed; whereby, it is reasonable to control T_{cy}, T_{rgn} or ΔT_{rgn} at the level of regulatory control as it is presented in [65].

- *Inputs:* the independent variables of the unit are flow rate of regenerated catalyst entering the riser (F_{cat}), flow rate of air to the regenerator (F_{air}), feed oil composition (k_c), feed oil temperature (T_{feed}), feed oil flow rate (F_{feed}), and air temperature (T_{air}). From these, F_{cat} and F_{air} are normally used as manipulated variables. The remaining independent variables may be regarded as disturbances in the regulatory control system [65].

Table 6.2 *FCCU variable classificatio*n.

Manipulated Variables	Controlled Variables	Disturbances
F_{cat} F_{air}	T_{ris} T_{rgn} T_{cy} ΔT_{rgn}	F_{feed} T_{feed} T_{air}

6.3.2 Open loop responses

Open-loop responses to step-type disturbances (5%) of both the manipulated variables and those variables defined as system disturbances (Table 6.2) were obtained starting from a steady state. These disturbances are carried out in order to determine how each variable of interest is affected and determine the stabilization time of the open-loop system.

6.3.3 PID implementation

For the FCCU the basic control aim is to maintain the operating variables in the desired operating point or in that established by the optimization stage. PID control is among the most used strategies in the industry for this purpose. The implementation of a PID control system for a decentralized multivariable system consists mainly of [141]:

a) choice of the appropriate pairing of inputs and outputs

b) structural stability test respective to the chosen pairing

c) robust and decentralized controller design (PID tuning)

Pairing

One of the problems that arise in the implementation of a multivariable decentralized control is the choice of the input and the output variables that will be part of each control loop. The pairing is very important because some change in the manipulated variable can not only affect the controlled variable with which it was related but also other controlled variables that were not intended to be modified. To avoid these drawbacks, the control loops (pairs of inputs and outputs) must have the least possible interaction. One of the most used tools for this purpose and for the selection of the best decentralized or multilayered control structure is the relative gains matrix (RGA) proposed by [150]. The RGA matrix can be calculated from the expression:

$$\mathrm{RGA} = \Lambda = \begin{bmatrix} \lambda_{11} & \lambda_{12} & \cdots & \lambda_{1j} \\ \lambda_{21} & \lambda_{22} & \cdots & \lambda_{2j} \\ \vdots & \vdots & \ddots & \vdots \\ \lambda_{i1} & \lambda_{i2} & \cdots & \lambda_{ij} \end{bmatrix} \qquad \textit{Equation 6.2}$$

where

$$\lambda_{ij} = \frac{open\ loop\ gain\ between\ y_i\ and\ u_j}{closed\ loop\ gain\ between\ y_i and\ u_j}$$

In steady state, the RGA can be defined as:

$$RGA = G.(G^{-1})^T \qquad \textit{Equation 6.3}$$

where G is the steady state gain matrix, and $(G^{-1})^T$ its inverse transpose where the sign indicates the element-by-element multiplication. The RGA matrix is independent of the scale and the sum of the elements of each row or column must be equal to 1.

The resulting values of the RGA can be interpreted according to the pairing rules presented in [151], where if:

$\lambda_{ij} = 0$: the manipulated variable does not affect the controlled variable. Input u and output y should not be paired.

$\lambda_{ij} = 1$: there is no interaction with other loops. This is the most desirable pairing, u and y should be paired.

$\lambda_{ij} < 0$: unstable states for the controller, u and y should not be paired.

$0 < \lambda_{ij} < 1$: there is an interaction between the loops, pair that u and y if λ_{ij} is "close" to 1.

$\lambda_{ij} > 1$: greater gains are preferred in the controller, that u and y if λ_{ij} is "close" to 1.

$\lambda_{ij} > 10$: undesirable. It can refer to a system sensitive to small variations in the gain and therefore difficult to control.

The RGA values to the manipulated variables with the controlled variables presented in Table 6.2 were calculated from a step type disturbance (5%) in order to determine the best match between them.

Structural stability test

The RGA matrix is considered a good tool for loop pairing in a decentralized controller. However, this tool does not guarantee that the recommended pairings are adequately stable. So as an auxiliary tool, the Niederlinski theorem is frequently used to measure the integrity in closed loop (the ability of the system in closed loop to stay stable in front of changes in the actuator).

The Niederlinski Index (*NI*) determines the best control configuration for a system based on stability analysis and it is defined by:

$$NI = \frac{\det[G]}{\det[\check{G}]} \qquad \textit{Equation 6.4}$$

where $det(G)$ denotes the determinant of matrix G in steady state, and $\check{G}$ denotes the subsystem of G with all the off-diagonal elements ignored. Then,

$$\check{G} = diag\,[G] \qquad \textit{Equation 6.5}$$

[152] establishes a pairing criterion as “The input/output variables in a decentralized control system should be paired such that the corresponding *NI* is positive and closest to unity. In addition, in order to guarantee integrity, the corresponding RGA elements should also be positive”. Then, the *NI* is calculated for all possible pairings between the manipulated and controlled variables of the system as an auxiliary decision of the RGA matrix.

PID tuning

PID tuning is developed through genetic algorithms. Because the system consists of two PID controllers, a multiobjective genetic algorithm is used. Each chromosome is defined as the gains K_p, K_i, and K_d for each controller. The objective function for each controller is defined as the error minimization between the setpoint and the actual output, through MSE (mean squared error) as:

$$Fitness_x = \frac{\sum_{i=1}^{n}[SP_x - actual\ output_x]^2}{n} \quad \textit{Equation 6.6}$$

Therefore, the minimization of the fitness function to find the best tuning parameters for the PID controllers is defined as:

$$\begin{aligned} \min \quad & f_1(k_{P_1}, k_{I_1}, k_{D_1}) = Fitness_{T_{ris}} \\ & f_2(k_{P_2}, k_{I_2}, k_{D_2}) = Fitness_{T_{rgn}} \\ s.t. \quad & k_P, k_I, k_D \in \mathbb{R} \end{aligned} \quad \textit{Equation 6.7}$$

6.4 Results and discussion

6.4.1 Open loop responses

The open-loop performance of a FCCU when manipulated variables are subjected to different step is shown in Figure 6.4. On the left side of this figure, it is observed how the changes in the catalyst flow generate a proportional effect on the riser temperature. Thus, an increase in catalyst flow generates significant increases in the temperature of the riser, with the presence of some transition states. These transition states are a consequence of the direct influence that the catalyst flow has on the riser temperature when delivering more energy per unit of mass for cracking. On the other hand, variables such as T_{rgn}, T_{cy} and ΔT_{rgn} seem to have an inverse relationship with the catalyst flow. In these three cases, an increase in catalyst flow represents a decrease in these values, some with a greater

proportion than others. For example, the change in temperature in the regenerator T_{rgn} turns out to be milder than the change that occurs in the regenerator cyclone T_{cy}.

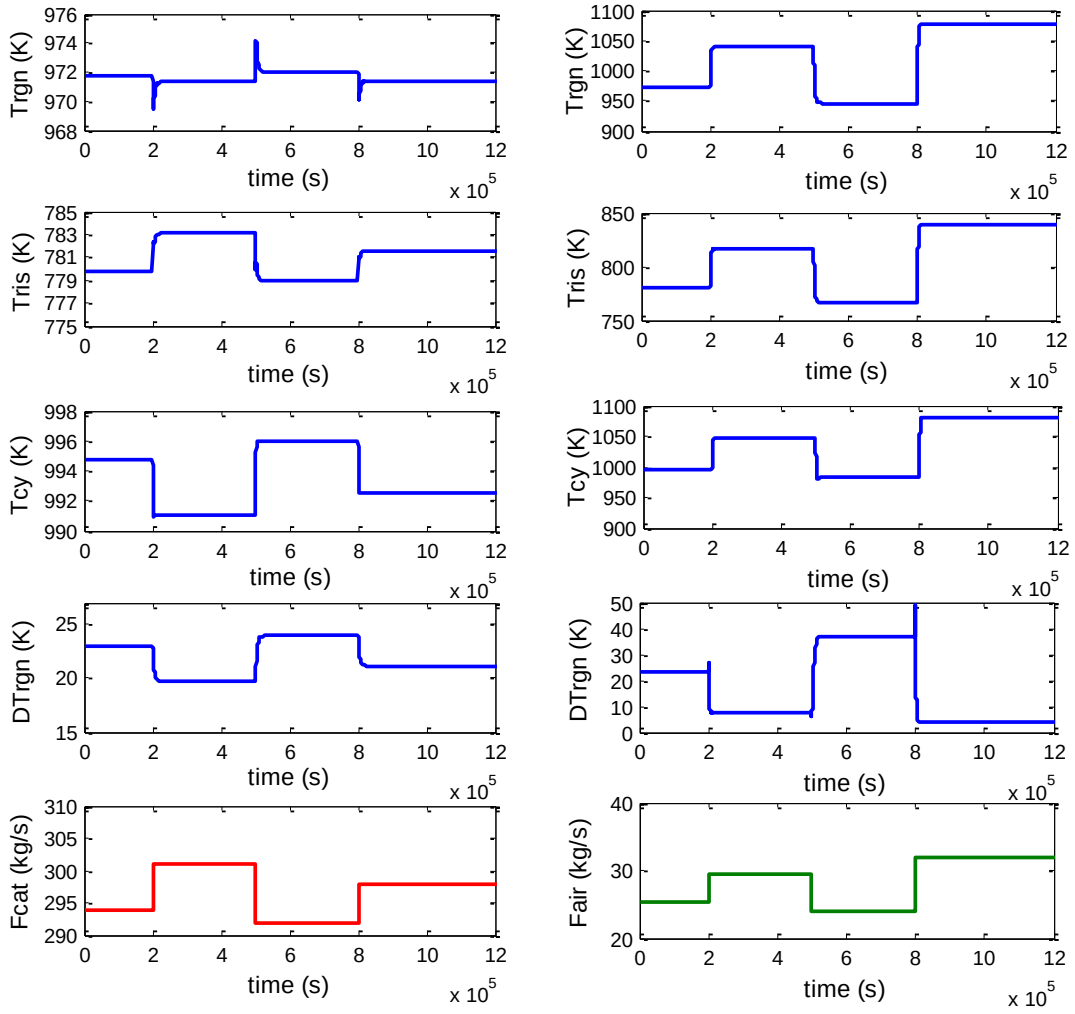

Figure 6.4 *Simulation of FCCU dynamic behavior in the presence of F_{cat} and F_{air} steps in open loop.*

The right side of Figure 6.4 depicts the variables response T_{ris} T_{rgn}, T_{cy} and ΔT_{rgn} respect to changes in air flow. In this case, the response of the air flow results proportional to T_{ris}, T_{rgn}, and T_{cy} and inversely proportional to ΔT_{rgn}.

This analysis is particularly important in the implementation of a decentralized control strategy since both the catalyst flow and air flow affect in some way all the possible control variables (T_{ris} T_{rgn}, T_{cy} and ΔT_{rgn}). As a consequence, a match between them does not turn out to be an obvious task, and tools that allow defining the best pairing as the RGA matrix must be evaluated.

6.4.2 PID Controller

In order to determine the better pairing variables, the *RGA* matrix is calculated. The results for the three possible options for pairing according to Table 6.2. are presented as follows:

$$\mathrm{RGA}_{(1)} = \begin{bmatrix} & \mathrm{T_{ris}} & \mathrm{T_{rgn}} \\ \mathrm{F_{cat}} & 1.1100 & -0.1100 \\ \mathrm{F_{air}} & -0.1100 & 1.1100 \end{bmatrix}$$

$$\mathrm{RGA}_{(2)} = \begin{bmatrix} & \mathrm{T_{ris}} & \mathrm{T_{cy}} \\ \mathrm{F_{cat}} & 0.5355 & -0.4645 \\ \mathrm{F_{air}} & -0.4645 & 0.5355 \end{bmatrix}$$

$$\mathrm{RGA}_{(3)} = \begin{bmatrix} & \mathrm{T_{ris}} & \Delta\mathrm{T_{rgn}} \\ \mathrm{F_{cat}} & 6.8129 & -5.8129 \\ \mathrm{F_{air}} & -5.8129 & 6.8129 \end{bmatrix}$$

From the *RGA* matrices, the better pairing corresponds to $F_{cat} - T_{ris}$ and $F_{air} - T_{rgn}$ obtained from the $RGA_{(1)}$ as they have the positive values closest to 1. In the other matrices F_{cat} is always the best pairing for T_{ris}, while F_{air} also be paired to T_{cy} and ΔT_{rgn}. However, the pairing with T_{rgn} is preferred to T_{cy} and ΔT_{rgn} because of the interaction with T_{rgn} is greater than the others.

To evaluate the stability for those possible configurations Niederlinski Index (*NI*) is calculated according to Equation 6.4, and the results are presented in Table 6.3.

Table 6.3 *NI index for the possible pairings.*

Pairing	NI
$T_{ris} \rightarrow F_{cat}$ $T_{rgn} \rightarrow F_{air}$	0.30
$T_{ris} \rightarrow F_{cat}$ $T_{cy} \rightarrow F_{air}$	1.73
$T_{ris} \rightarrow F_{cat}$ $\Delta T_{rgn} \rightarrow F_{air}$	1.71

Again, the most accurate pairing is the pair $T_{ris} \rightarrow F_{cat}$ and $T_{rgn} \rightarrow F_{air}$ as they present the closest value to 1. A representation of the decentralized PID controller for the FCCU after *RGA* and NI analysis is depicted in Figure 6.5.

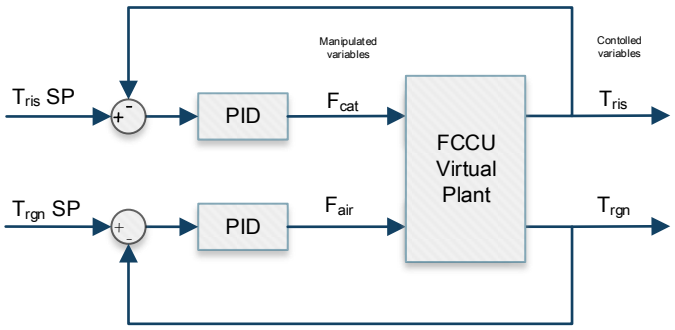

Figure 6.5 *Decentralized PID controller in the FCCU.*

PID tuning

For PID parameters tuning, f_1 and f_2 functions (Equation 6.7) are minimized using multiobjective GA algorithm. The best values for k_P, k_I, and k_D found by the optimization algorithm are presented in Table 6.4.

Table 6.4 *PID parameters tuning from GA optimization.*

	Controller T_{ris}	**Controller T_{rgn}**
$\boldsymbol{k_P}$	2.0526	0.9785
$\boldsymbol{k_I}$	0.577	1.8973
$\boldsymbol{k_D}$	1.1237	6.555
Fitness	2.6498	2.4978

The PID performance with these parameters is evaluated based upon setpoint tracking and regulatory control. Setpoint tracking describes how well a controller can react to the change of the desired setpoint of a process variable, whereas regulatory control assesses the ability of the controller to nullify the effect of any disturbance that appears in the system [153]. To perform this evaluation the system was disturbed four times from the base case. In each of the disturbances, the reference value was changed as well (Table 6.5).

Table 6.5 *Disturbances and set-point values*

Disturbance		**Set point value**	
Disturbance	**Value**	$\boldsymbol{T_{ris}\ (K)}$	$\boldsymbol{T_{rgn}(K)}$
$F_{feed}\ (kg/s)$	43	803	971
$F_{feed}\ (kg/s)$	45	796	975
$T_{air}\ (K)$	370	785	973
$T_{feed}\ (K)$	500	809	980

Disturbances were made in feed flow, air temperature, and feed temperature. Likewise, the setpoints of both the riser temperature and the regenerator temperature were modified in

each case. The response of the measured variables and the actuator due to the control action are shown below.

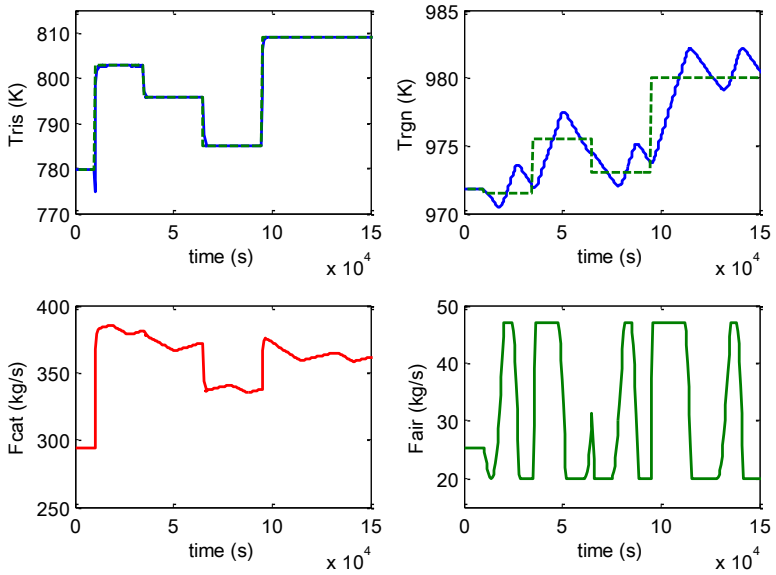

Figure 6.6 *Setpoint tracking performance for closed-loop PID controllers with the* $F_{cat} - T_{ris}$ *and* $F_{air} - T_{rgn}$ *pairing using the parameters found by GA.*

From Figure 6.6 a proper set point tracking of the tuning parameters for the setpoint tracking in the riser temperature is evidenced. However, in the regenerator temperature, continuous oscillations are presented which make convergence difficult at the desired operating point. Since the values obtained by the optimization are not good mainly for regenerator temperature, the parameters k_P, k_I and k_D are adjusted by trial and error using the GA values as starting points. The better-found values are presented in Table 6.6.

Table 6.6 *PID parameters tuning by trial and error after GA optimization.*

	Controller T_{ris}	**Controller T_{rgn}**
k_P	1.025	9.778
k_I	0.677	1.8973
k_D	1.923	3.555
Fitness	3.2401	1.7714

The response of the measured variables and the actuator due to the control action with the adjusted parameters are shown below:

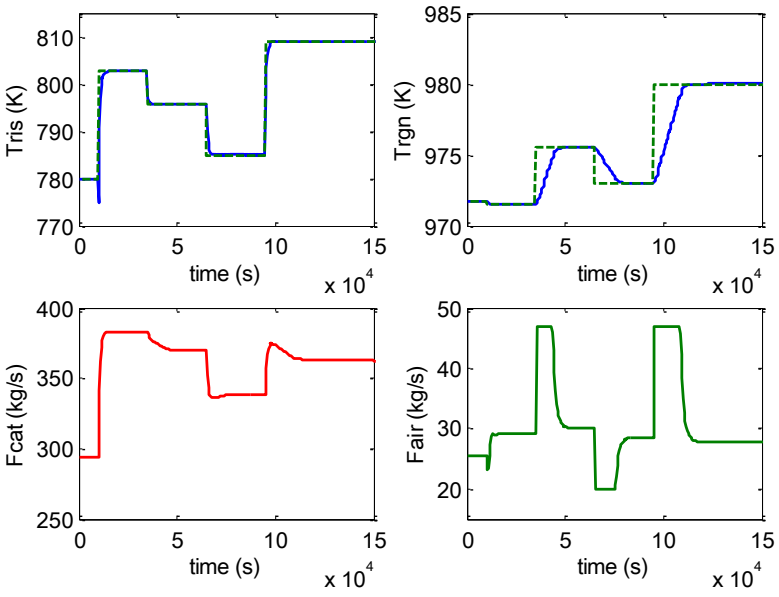

Figure 6.7 *Closed-loop PID controllers for the $F_{cat} - T_{ris}$ and $F_{air} - T_{rgn}$ pairing by trial and error.*

In this case, the reduction of oscillations in the system is achieved by adjustments in all the tuning parameters of the two controllers, mainly in the derivative action of the controller for the regenerator temperature. If the value of the derivative action is increased, it is possible to decrease the oscillations to the point that they disappear but the response becomes a little slower.

From Figure 6.7, it is evident that PID controller 1 can quickly react to a change of setpoint in the riser temperature and has proportional movements in the actuators. On the other hand, PID controller 2 has a much slower response than Controller 1 although it follows the desired trajectory; this is mainly a characteristic of the system since a change in the temperature of the regenerator is inherently slower than a change in the temperature of the riser. It is also important to note that given the interconnection between riser and regenerator, changes in the catalyst flow and air flow may simultaneously modify both riser and regenerator temperature.

Regulatory control assesses a controller's ability to nullify a disturbance when it enters the system. According to Figure 6.7, the PID controller has good behavior taking into account that the effect of the disturbance seems not to affect the set point tracking and it reaches the desired operation point.

6.5 Conclusions

A decentralized PID control was implemented in order to control the FCC model presented in Appendix B. For this, the typical controlled and manipulated variables for this unit were defined. The choice of the appropriate pairing of inputs and outputs was made through the RGA matrix. A structural stability test to chosen pairing using the Niederlinski index was calculated, and the respective robust and decentralized controller design (PID tuning) was developed by trial and error. Initial values for the PID tuning were obtained from the minimization of the error between the setpoint and the value of the variable using a Genetic Algorithm.

The results indicated that the presence of nonlinearities and coupling makes FCCU a challenge to control. The complexity of the FCC process comes from strong interactions between the reactor and the regenerator, nonlinearities in the models and catalyst deactivation by coke deposition, and coke burning. In an FCCU, a single manipulated variable can strongly affect several controlled variables due to the interactions among process variables. Although different pairings exist between the manipulated and controlled variables, the RGA matrix and the *NI* (as stability test) yielded the best values for the pair $F_{cat} - T_{ris}$ and $F_{air} - T_{rgn}$ showing the strong interaction between them. On the other hand, decentralized PID controller parameters can be tuned using a genetic algorithm that minimized the error between setpoint and the controlled variable value. This method does not yield the best tuning values, but allows finding k_P, k_i, and k_d parameters values close to the desired ones. Later, these values can be adjusted so that both the response time and the overshoot of the system are reduced. The final tuning parameters found by trial and error, from the ones obtained with the GA, presented a good response time and allow the process variables to be brought to their desired operating point.

Chapter 7. RTO Implementation and Assessment

Abstract

A study of each of the stages of real-time optimization (RTO) and a diagnosis that presents its behavior and performance evaluation is poorly discussed in the literature. Normally, each of the stages is separately studied and a complete analysis of all the stages implemented as a whole is not presented. This chapter evaluates and analyzes the performance of an RTO applied to a virtual plant of a fluid bed catalytic cracking unit (FCCU) making an analysis of the behavior and performance of the selected strategies for each RTO stage, according to studies applied in previous chapters.

The results show that the chosen methods have a successful performance, and they lead to improve the plant profit even when contaminated data and typical disturbances in the system are present. Besides, the performance assessment in scenarios with and without RTO are compared demonstrating an important increase in the FCCU profit when RTO is used.

Keywords: RTO, FCCU virtual plant, Implementation, assessment.

7.1 Introduction

RTO (real-time optimization) is part of the so-called control hierarchy, a traditional way for decision making in industries. Many industries follow this hierarchy in which the levels of decision making are represented in a pyramidal form. Thus, the frequency of decision making increases from top to bottom, while the impact and importance of decision making increases from the bottom up [154]. The layers that make up this pyramid are planning, scheduling, real-time optimization, supervision, and control as shown in Figure 7.1.

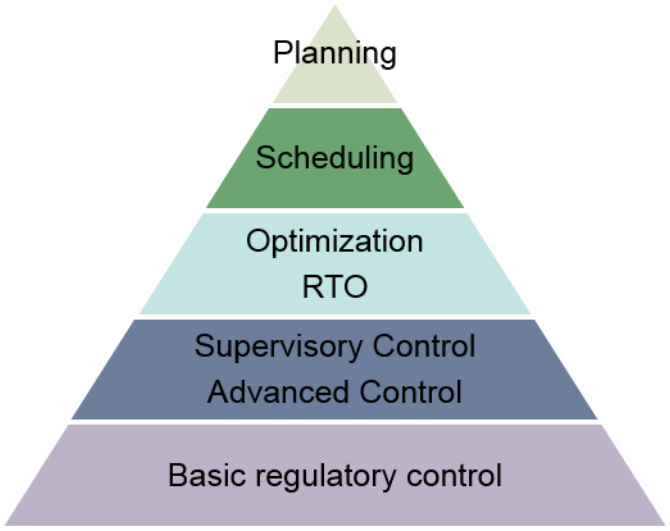

Figure 7.1 *Process automation hierarchy. Adapted from* [5]

At the top, the resource allocation, supply and demand forecasting, and pricing schedule forecasting are determined in the planning layer; while production capacity targets, raw material availability, and production schedule are calculated in the scheduling layer [155]. Planning and scheduling usually use linear models, and their decisions are made over a longer period for supplying the entire plant instead of a single process.

In the next level, RTO is in charge of improving the performance of industrial processes through an optimization function that calculates new stable operating conditions while the process constraints are met. RTO is used mainly due to real-time changes and process disturbances that make the optimal conditions not to be the same, and therefore they must be recalculated. The implementation of these solutions is done autonomously and can take from minutes to several hours. At this level first principle, detailed, and non-linear models, normally in steady state are used.

Multivariable or advanced control ensures that the process remains as stable as possible from the process variability reduction. It executes all tasks close to the plant constraints, which ultimately results in greater efficiency [156]. At this level, Predictive Model Control (MPC) is often used, which uses a dynamic internal model of the process, an optimization cost function, and a history of past control movements to determine the optimal control required.

Finally, in the regulatory control layer, the control variables are kept close to the set point in spite of local disturbances. Furthermore, this layer allows the operator to take control of

the plant if necessary. The PID controller is widely used to implement the local single input single output (SISO) control loops [155].

The advanced process control seeks to determine the optimal process conditions; it does not take into account the nonlinearities of the model due to changes in economic, environmental, and/or operational conditions. It may make the process work in suboptimal conditions. In these cases, the use of more rigorous models to determine the new optimal operating conditions after any disturbance is required. In this sense, the use of a tool that provides better estimates of operating conditions during the process can result in improved performance, lower operating costs, better product quality, and greater operational flexibility. In fact, today, real-time control and optimization have become a necessity for process companies to compete in the market and maintain the profitability of their operations [157]. RTO is especially useful when there are frequent changes in the variables that generate non-linear behavior in the process. Some large applications systems include petroleum refineries, well networks, combustion, and membrane filtration. These and other RTO applications can be consulted in Chapter 2.

RTO applications are very useful in refineries because the operation must be flexible to be able to respond to changes in demand, and in the price of crude, distillates, and other products. Then, a refinery must have the capacity to deal with processes variability to avoid the loss of millions of dollars per day. As FCCU is one of the most important and profitable conversion processes of refining, an RTO implementation is of the great interest in this industry.

In general, an RTO uses a non-linear steady-state model and process measurements to calculate the optimal operating values. The calculation of the new setpoints involves two models: an economic model and an operational model. The economic model arises from the maximization or minimization of an objective function, while the operation model is a steady-state process model, which considers all the process constraints.

A typical RTO implementation involves the execution of an algorithm that collects data, reconciles them, adapts the model parameters to be consistent with the reconciled data, calculates the optimal conditions of the process, and modifies the setpoints to be reached through a control system [135].

The most used approach and possibly the only static real-time optimization strategy available in commercial RTO systems is the two-step approach [5], [112], [158]. More about RTO can be consulted in Chapter 2.

7.2 RTO system description

A traditional RTO system based on the two-step approach involves many stages as depicts Figure 7.2. The cycle begins with the data collection of the process, and it is followed by noise elimination, steady-state detection, reconciliation of data, and estimation of parameters, and optimization of the operating conditions. The optimal points are sent to the control system to finally adjust the process variables. Each of these stages is detailed below.

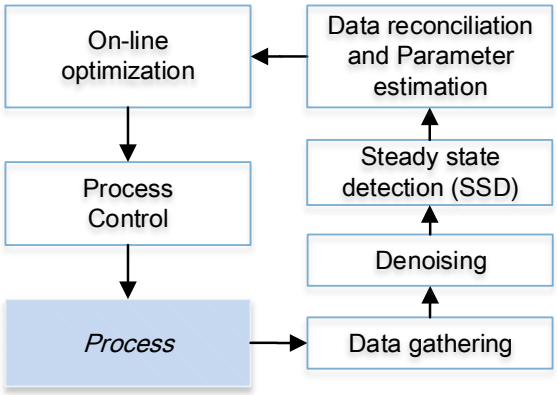

Figure 7.2 *RTO general structure.*

Data gathering: It is done in real time in a time interval determined by the process or by the conditions of the instrumentation used for this purpose.

Denoising: As a result of the unavoidable noise of the signals generated in data collection, a noise elimination stage is included here in order to get more reliable process data and to make the execution of the later stages of the RTO easier.

Steady-state detection (SSD): The RTO loop execution begins with the detection of a steady state. Once data are collected, measurements are checked for steady-state operation. It has some implementation issues, due to signal noise and outliers. These problems can be reduced by smoothing the plant data using smoothing and denoising [158].

Data Reconciliation and Parameter estimation: If the plant is in steady state, data reconciliation is executed to eliminate random errors from measured variables following the

balance equations that result from conservation laws of mass, energy, etc. This adjustment uses optimization techniques to update the plant process model.

Optimization: After the data are consistent, the updated data along with the economic data are fed to the rigorous model in steady state to find the new optimal process conditions.

Optimal set points implementation: The new setpoints are now passed to the control system to be implemented on the plant [159], so that from adjustments in the manipulated variables the desired setpoints are reached.

7.3 Methodology

The methodology followed for this chapter is divided into two stages. The first corresponds to the implementation of the strategies that presented the best results in each of the RTO stages evaluated in the previous chapters (a), and the second corresponds to the evaluation of the performance of each of them after being fully integrated into the RTO (b). They are presented in Figure 7.3. Each of those stages is detailed below.

7.3.1 RTO Implementation

In order to implement the RTO on the virtual plant, each of the stages described in previous chapters is incorporated as shown in Figure 7.3.

FCC model and Virtual Plant

FCCU virtual plant is developed in Matlab using the model presented by [66], [160]. This is derived from the model proposed by [161] for partial combustion, explained in Chapter 3. In order to simulate real plant measurements, output data from the FCCU model are contaminated using a Gaussian error with a signal-noise ratio 50 (SNR 50), gross error of the overall random data, and errors from 0 to 5% of the maximum values. Measured variables were also contaminated with random bias errors as it is described in Chapter 4.

Denoising

With the purpose of cleaning the data coming from the virtual plant, eliminating the noise, the gros error and the bias, signal Wavelet shrinkage threshold (WST) was used. Symlets basis function combined with the sqtwolog and heursure threshold algorithms are employed to the variables denoising. More details about this procedure are detailed in Chapter 4.

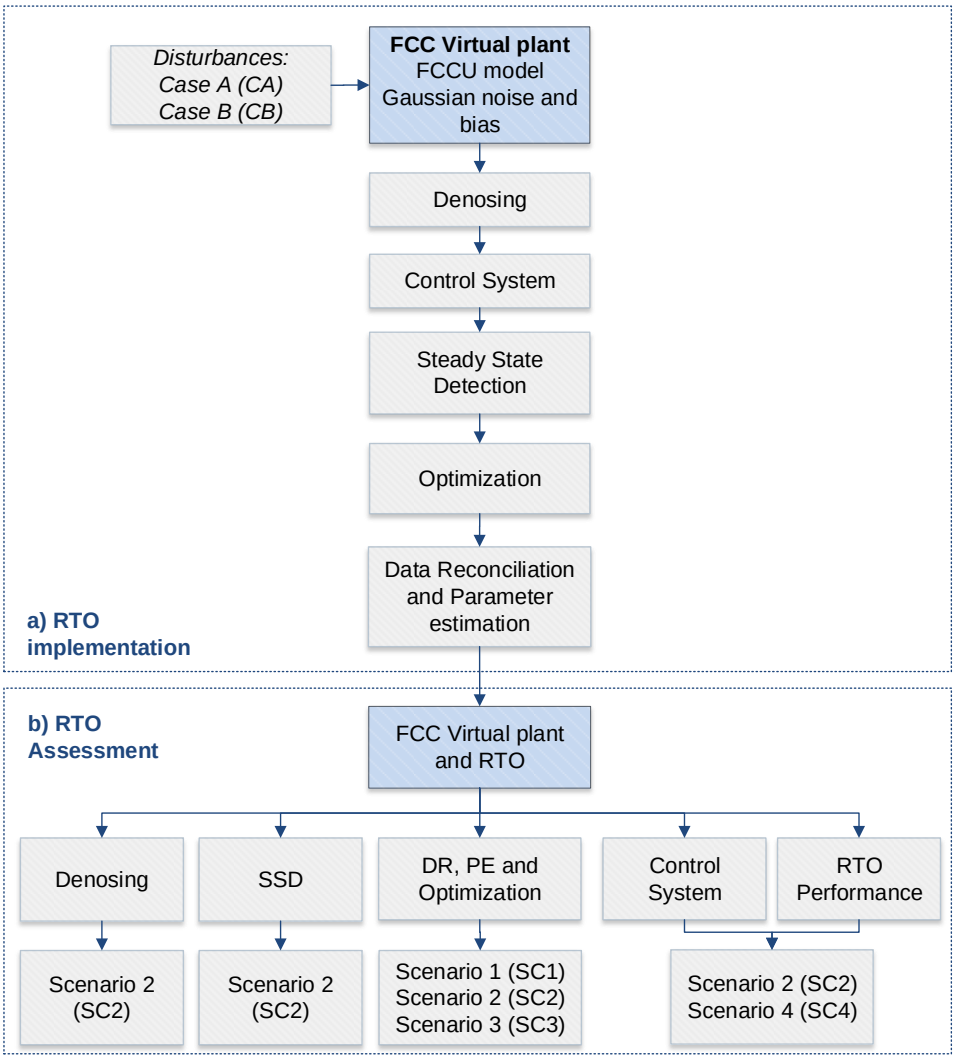

Figure 7.3 *Methodology followed for implementation and assessment of a RTO in a FCCU virtual plant.*

Control

PID controller is implemented in RTO according to the procedure presented in Chapter 6. Each of the tuning parameters is again adjusted by trial and error due to changes in the signals when noise is incorporated into the signal.

Steady-state detection

For steady-state detection, the standard deviation method is used and S1 and S2 parameters are tuned according to the methodology presented in Chapter 4.

Optimization

For steady-state optimization, genetic algorithm with a reduction of the maximum number of generations and stall generations to decrease the running time is employed. Additional to this, a penalty function is included in the optimization objective function to guarantee a stationary steady state as reported in Chapter 5.

Data Validation and parameter estimation

Data reconciliation and parameter estimation are incorporated in the RTO using the Hampel estimator in agreement with the procedure presented in [105]. It can be consulted in Chapter 4.

7.3.2 RTO assessment

Each of the mentioned stages is incorporated into the virtual plant to evaluate and compare it with the plant in absence of RTO. This assessment is done in terms of the algorithm execution time and the economic benefits when different disturbances are applied to the system. In order to evaluate the global RTO and each stage performance, four scenarios were compared. Scenario 1 (SC1) employs data from the model without noise, online optimization, and the PID control. This scenario is considered the ideal situation since there are no noise, gross error or bias in the data. Scenario 2 (SC2) considers the full RTO assessment in a simulated real situation, with noisy data. Scenario 3 (SC3) tries to analyze the effect of turning off the data reconciliation and parameter estimation algorithm in an RTO system, and Scenario 4 (SC4) simulates the performances of a control system without any optimization on a plant with noisy data. A brief representation of all of them is summarized in Figure 7.4.

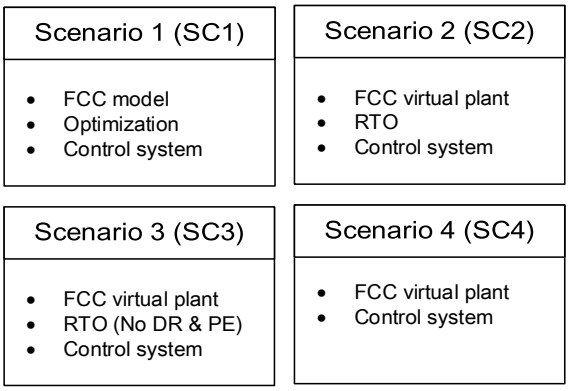

Figure 7.4 *Scenarios used for RTO assessment.*

The performance of the system in each scenario was analyzed under disturbances presented in Table 7.1. These disturbances were selected considering they could happen in the normal operation of the FCCU.

Table 7.1 *Disturbances for Scenarios 1-4*.*

	Case A (CA)		Case B (CB)	
1	↑ F_{feed}	42.59 kg/s	↓ F_{feed}	35kg/s
2	↑ F_{feed}	45 kg/s	↑ T_{air}	370 K
3	↑ T_{air}	370 K	↓ T_{feed}	420 K
4	↑ T_{feed}	500 K	↑ F_{feed}	47 kg/s

*Base case: F_{feed}:40.63 kg/s, T_{air}:360 K, T_{feed}: 434 K. The other base case conditions can be found in Appendix B.

7.4 Results and discussion

The final algorithm implemented for an RTO over an FCCU virtual plant is presented in Figure 7.5. It includes the sequence of the steps the unit follows when it enters an RTO cycle and when it does not. The results for each stage are given below.

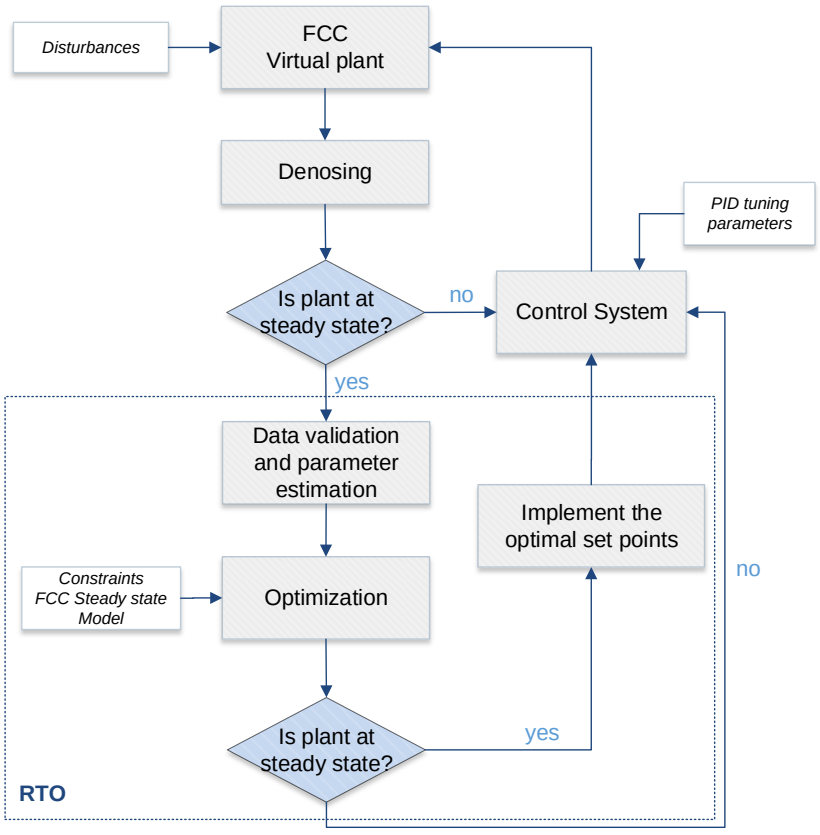

Figure 7.5 *FCC Virtual plant RTO scheme implemented.*

7.4.1 Denoising

For denoising wavelet shrinkage threshold (WST), symlets basis function combined with the sqtwolog algorithms, were used. Figure 7.6 shows the riser temperature signal in SC2 -CA where the signal is shown without Gaussian noise (clean signal), with noise (noisy signal), and after the noise elimination using the wavelet transforms (denoised signal). The setpoint established by the RTO and its tracking for the riser temperature is also displayed.

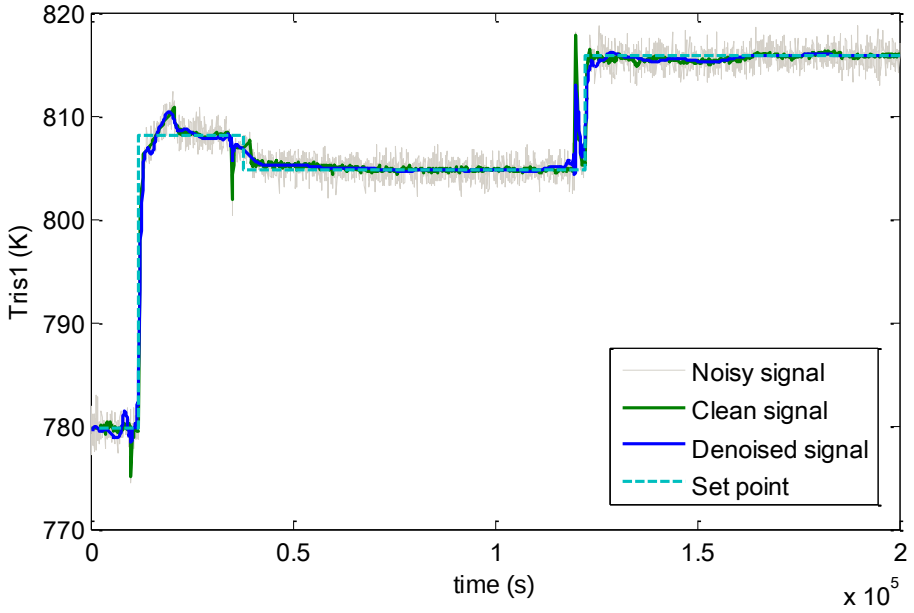

Figure 7.6 *Riser temperature denoised signal in RTO system (SC2-CA).*

Figure 7.6 presents a satisfactory noise elimination by using wavelet transforms (WT) since the denoised signal is quite close to the clean signal. This indicates that denoising based on WT is able to generate appropiated data for the next RTO steps. Furthermore, the denoised signal follows the trend even when set points are changed which results of great asistance for all the RTO stages. This behavior was not only observed for the SC2-CA, but also for scenarios 2, 3, and 4, and the corresponding cases A and B. A more detailed discussion on the different strategies evaluated for denoising using the wavelet transforms is presented in Chapter 4.

7.4.2 Steady-state detection

For steady-state detection, the standard deviation method was used. The achieved results are summarized in Figure 7.7 where the riser and the regenerator temperature profile

(Figure 7.7a and Figure 7.7c) are presented, along with the steady-state detection for each of these temperatures (Figure 7.7b and Figure 7.7d) and for the unit as a whole, after disturbing the system (Figure 7.7e).

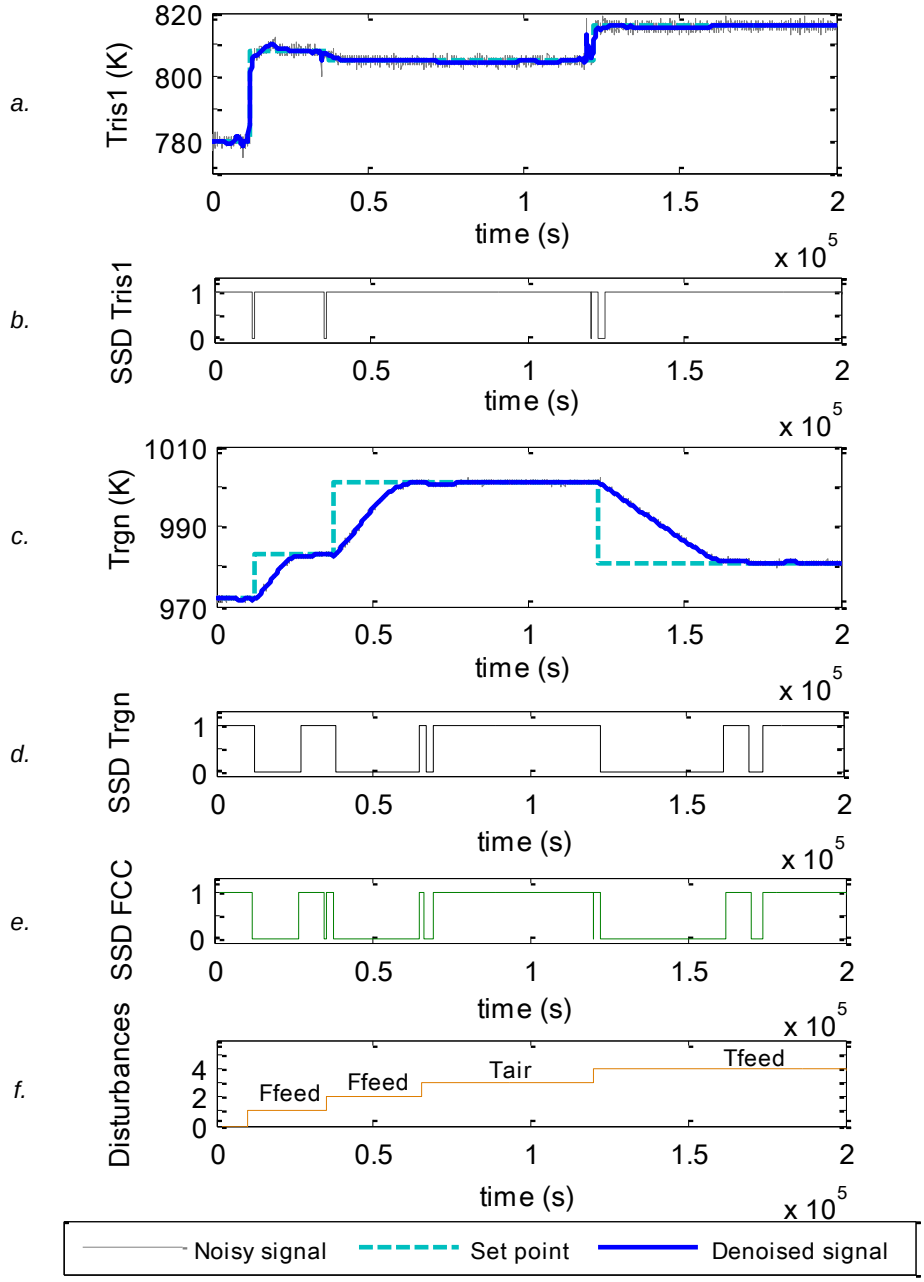

Figure 7.7 *SSD for FCCU in a virtual plant after 5% disturbances in Ffeed, Ffeed, Tair and Tfeed.*

The purpose of the steady-state detection is to identify those time intervals where the analyzed variable are in a relatively steady state, and the others in which the value of the variable changes significantly. In this way, a state change is detected when there are variations in the variable; if it is in a steady state, the value of SSD is one; otherwise, the

value of SSD will be zero. In the standard deviation method, the suitable detection of each state depends on an appropriate S1 and S2 parameters tuning (Chapter 4).

In Figure 7.7, it is observed that when either the system is disturbed or there is a setpoint change, the standard deviation method reacts and marks these states as unstable (SSD=0), just at the time period in which those changes take place. A good performance of the method is observed for the riser temperature, that has a fast response to the disturbances, as well as for the regenerator temperature, that requires relatively long time to react. According to Figure 7.7e, the steady state of the process (SSD FCC) is mainly dependent on the regenerator stability (SSD Trgn) and influenced by the riser steady state (SSD Tris). This is because the dynamics in the regenerator is much slower (hours) than that of the riser (seconds), so the process variables associated with these sections have similar behavior. Thus, the oxygen concentration and the coke in the regenerator stabilize when the regenerator temperature reaches the steady state. In the same way, the gasoline concentration, the gas oil concentration, and the coke produced in the riser stabilize when the riser temperature is in steady state.

7.4.3 Data reconciliation, parameter estimation and optimization

After the system reaches a stationary state, it is possible to start with data reconciliation and parameter estimation. To this stage, Hampel maximum likelihood estimator was used. Some of the reconciled values and estimated parameters for the first RTO cycle (after the first disturbance) are presented in Table 7.2.

Table 7.2 *Comparison of actual, noisy, and reconcilied variables values.*

Variable	Measured value	Real value	Estimated value	%Error
$F_{air}\ (kg/s)$	22.10	28.29	26.06	7.87
$xO_{2(in)}{}^{*}$	0.2136	0.2136	0.2136	0.00
$xN_{2(in)}{}^{*}$	0.7864	0.7864	0.7864	0.00
$F_{fg}(kg/s)$	25.40	30.34	27.81	8.34
$xCO_{(out)}{}^{*}$	unknown	0.0591	0.0585	1.02
$xCO_{2(out)}{}^{*}$	unknown	0.1005	0.0991	1.38
$xO_{2(out)}{}^{*}$	0.0043	0.0043	0.0042	1.70
$xN_{2(out)}{}^{*}$	unknown	0.6765	0.6806	0.60
$xH_2O_{(out)}{}^{*}$	unknown	0.1596	0.1576	1.24

Table 7.2 *Comparison of actual, noisy, and reconcilied variables values.*

Variable	Measured value	Real value	Estimated value	%Error
σ	1.6928	1.7023	1.6961	0.36
$T_{cy}\ (K)$	997.69	995.62	995.91	0.03
$T_{rgn}\ (K)$	973.70	971.74	972.44	0.07
$F_{feed}(kg/s)$	40.63	42.59	42.39	0.47
$F_{prod}(kg/s)$	40.49	40.53	40.64	0.25
${go_{(out)}}^*$	0.3466	0.3585	0.3459	3.52
${g_{(out)}}^*$	0.5168	0.4982	0.5181	4.00
${lg_{(out)}}^*$	0.1365	0.1433	0.1361	5.08
$T_{ris(1)}(K)$	776.4	779.8	775.6	0.53
$C_{coke,prod}$	unknown	0.0067	0.0066	1.70
$C_{coke,ris}$	unknown	0.0110	0.0109	1.10
$C_{coke,sep}$	unknown	0.0110	0.0109	1.10
$C_{coke,rgn}$	unknown	0.0043	0.0043	0.19
ΔH_{cb}	unknown	-523942.9	-523673.8	0.05
$r_{cb}(kg/s)$	unknown	2.0342	1.9614	3.58

*weight fraction

According to Table 7.2, the relative error is low and oscillates between 0 and 8% showing a suitable performance with respect to the real values, as it was obtained in Chapter 4. Figure 7.8 shows how optimization works when data are reconciled and when they are not, according to the profit scenarios 1, 2, and 3 before and after the execution of the first RTO cycle (tRTO1).

Before the first RTO execution, in the interval (0- tRTO1), the initial point of profit for SC1, SC2, and SC3 is not the same because data in SC2 and SC3 are contaminated and data reconciliation has not been executed yet. When the first RTO is executed, the profit reached by SC1 increases from 9-12.9 USD/s (33%), while for SC2 and SC3 it changes 8.9-12.1 (35%) with respect to the initial value as a result of optimization. On the other hand, the profit improvements between the other optimization cycles (tRTO2, tRTO3 and tRTO4) are between 2-7% for the disturbances corresponding to case CA.

From all the RTO cycles execution, the insertion of data reconciliation (SC2) let to find values closer to real profit (SC1) than those determined by an optimization system without data reconciliation (SC3). The real values estimation for these cycles improved between 5-50%, but the DR was not enough to reach the real value of the variables for the case

evaluated. This indicates that although the relative error is low for the parameters and process variables (Table 7.2), this deviation from real values generates underestimated or overestimated profits, according to the bias of the variables. This is the reason why a good data reconciliation is a fundamental step for the knowledge of the real plant state and the optimization of its operating conditions.

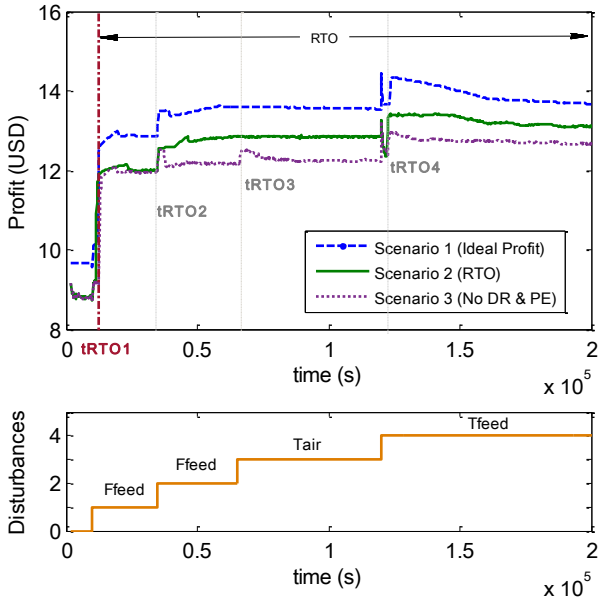

Figure 7.8 *Profit comparison in Scenarios 1, 2 and 3 for CA.*

Figure 7.8 also shows that the time instants in which each RTO cycle is executed are not the same in which the disturbances occur. This is a consequence of the steady state-RTO since once the system is disturbed, the RTO will only run when the system returns to a steady state. Once the stability of the system is ensured (SSDFCC=0), the RTO performs data reconciliation, parameter estimation, and optimization; and then it sends the values of the new setpoints to the control system. The stabilization time of the FCCU system is mainly dependent on the stabilization of the regenerator variables (as mentioned in the previous section), and it can take between 3e4 - 5e4s (8-13h) depending on the disturbance. The RTO execution after the system stabilization for the 4 cycles of RTO ranged between 2700-4500s (0.75-1.25h), which is short compared to the time frame of the system (several hours) [6].

7.4.4 Control performance

In addition to data reconciliation, parameter estimation, and optimization, other aspects must be taken into account during the execution of the RTO; for example, the behavior of the controlled and manipulated variables of the control system against set points with and without RTO. This lets to evaluate how the control system reacts from changes in the setpoint, and if the system is able to reach the conditions provided by the optimizer. Figure 7.9 shows the riser and regenerator temperature behavior (controlled variables) with respect to the catalyst flow and air flow to the regenerator, after disturbing the system with RTO (SC2) and without RTO (SC4).

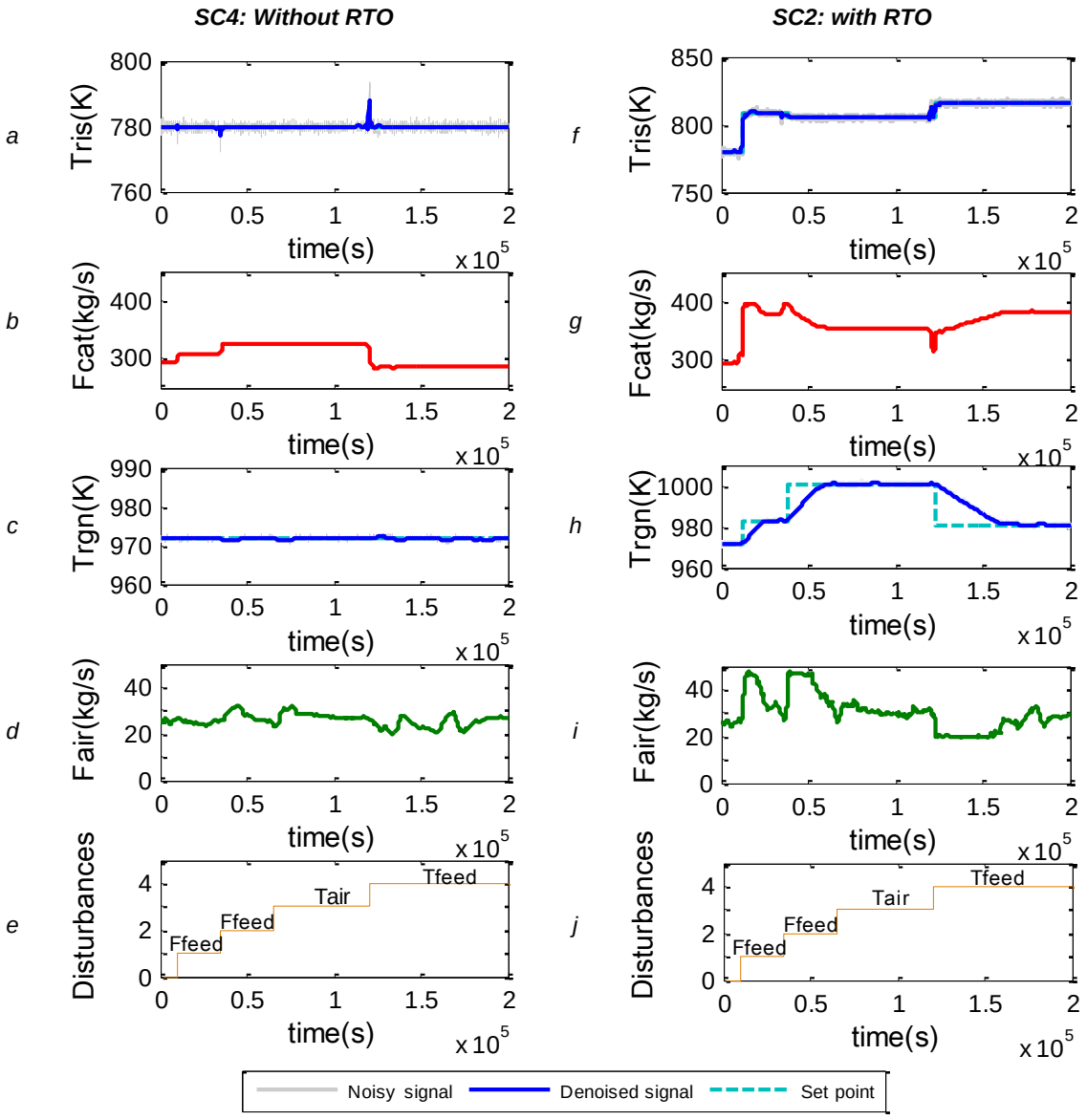

Figure 7.9 *Manipulated and controlled variables behavior with and without RTO (SC2 and SC4) in CA.*

On the left side (Figure 7.9a, Figure 7.9b Figure 7.9c, Figure 7.9d), the response of the controlled variables T_{rgn} and T_{ris} and manipulated F_{cat} and F_{air} for SC4 (without RTO) are presented. Peaks in the riser temperature profile appear when disturbances are applied (mainly for temperature and feed flow) at those moments when the response of the manipulated variable (F_{cat}) try to compensate the system to return it to the setpoint.

Disturbances in the air fed temperature do not seem to have a significant effect on the riser temperature, but a slight effect on the regenerator temperature. So, a 5% disturbance in air temperature is relatively small to cause a significant change in the process variables.
In the regenerator temperature, the immediate effect of the disturbances is less than in the riser, as there are no peaks. However, this does not mean that this variable is not affected by these changes, which is reflected in the continuous variations in the manipulated variable (F_{air}) to maintain the setpoint in the system.

On the right side (Figure 7.9g, Figure 7.9h Figure 7.9i, Figure 7.9j), the manipulated and controlled variable behavior by setpoint changes, as a result of the optimization (scenario with RTO) is observed. Here, the manipulated variables movements turn out to be stronger than in SC4 (without RTO), so the valve opening must be subjected to strong and continuous movements to reach the desired setpoint.

The regenerator temperature in SC2 (with RTO) changes much more between optimization cycles than without RTO. This, in turn, makes the manipulated variable (F_{air}), also oscillate more than in the SC4 (without RTO). In both scenarios, PID control is efficient to bring the system to the desired conditions.

Although PID has a good performance, the constant oscillations and the abrupt changes (high changes in SP) can be harmful for the instrumentation. For this reason, it is recommended to use an MPC control, which in addition to making gradual adjustments of the process variables avoids the oscillation of the variable during the operation.

7.4.5 RTO implementation

Figure 7.10 shows the comparison between the profit evaluated for the virtual plant in SC4 (without RTO) and SC2 (with RTO) for cases A and B, in a run time of $2x10^5$ s.

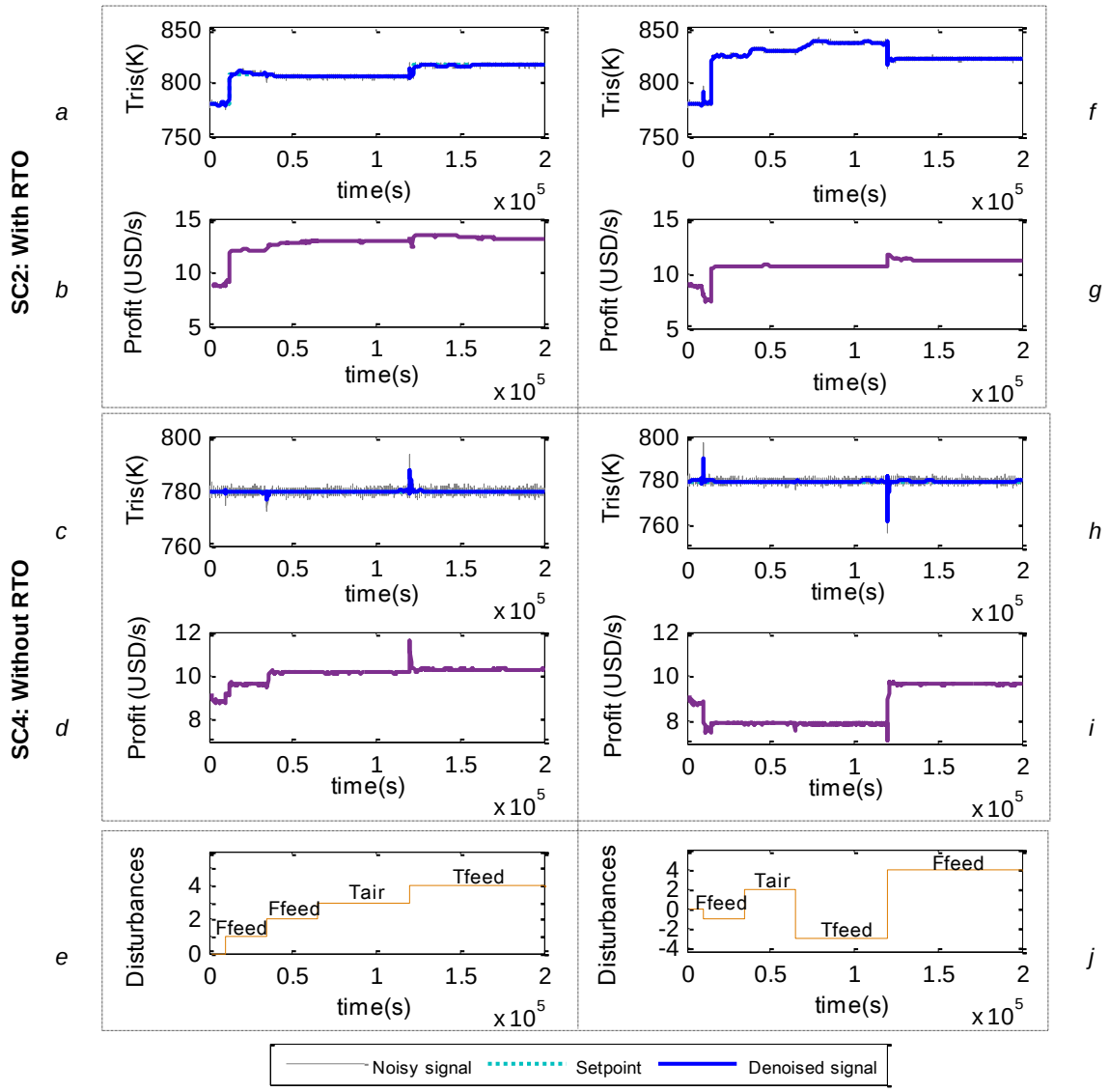

Figure 7.10 *Performance of the virtual plant with RTO and without RTO comparison (Case A).*

In this simulation, a series of disturbances of 5% is performed for each variable indicated in Figure 7.10e (Case A) and Figure 7.10j (Case B). For both cases, the increase in profit when the RTO cycles are executed is observed. In case A (figures on the left side), it is observed that when the first disturbance takes place, the profit in SC2 and SC4 raises due to the increase in F_{feed}, and therefore, the gasoline fraction that is produced.

However, after optimization, in the scenario with RTO (SC2), the increase in profit is higher than in SC4. So, in SC2 the profit is increased to approximately 12.5 USD/s (33%), while in SC4 it does not exceed 10 USD/s (10%). This is detailed in Figure 7.11 (the first RTO cycle for CA), where the first disturbance occurs at t1, and the first RTO cycle at tRTO1.

The profit increase as a consequence of an increase in the feed flow is evident in both scenarios (with RTO and without RTO), but a substantial difference is observed after riser and regenerator temperature setpoints are modified due to optimization.

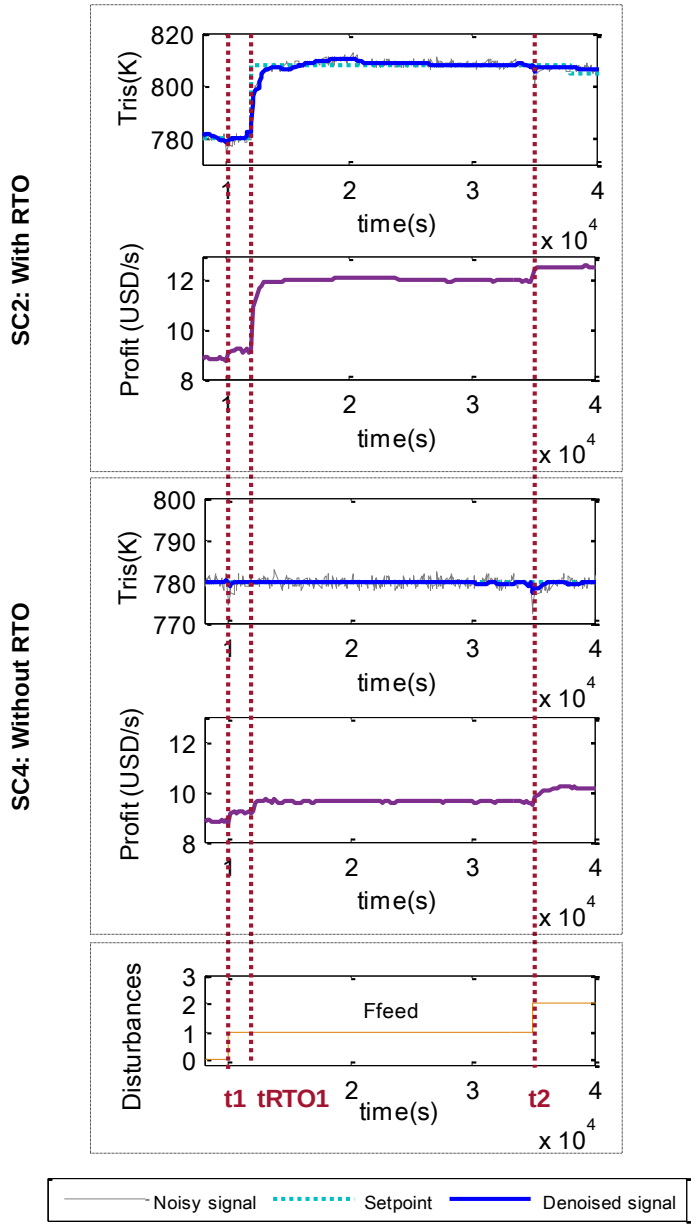

Figure 7.11 *Profit comparison of in SC2 and SC4 for case A.*

In the second system disturbance (Figure 7.10-Case A), when the feed flow is increased again, a similar behavior to the first disturbance is observed. However, in this case, the profit increase is relatively lower than in the first disturbance (4USD/s). In both disturbances, SC2 presents better profits than those reached by SC4 as a result of the RTO.

The increase in feed temperature (T_{feed}) in Case A also improves the profit of the system since it promotes the cracking reactions. In SC2 (with RTO) for this disturbance, the profit reaches approximately 14 USD / s, while in SC4 (without RTO), this generates a peak in the profit and T_{ris}, but they are counteracted by the control system that must keep the two variables controlled at their setpoint. So far, only increases in the process variables chosen as disturbances were analyzed. So, in order to see how the RTO and profit behave respect to negative changes, Case B is presented (right side of Figure 7.10).

From the same initial condition of Case A, the feed flow is reduced by 5%. In this case, there is a clear decrease in profit (16%) both in SC2 and SC4 due to lower gasoline production. However, when the RTO (SC2) is executed, the setpoint of the controlled variables is adjusted to bring the system to better operating conditions. Then after optimization (SC2), the profit increases from 7 to 11 USD/s as a result of setpoint adjustments, and better performance of SC2 than in the SC4 is reached.

Next, there is an increase in T_{air} as a second disturbance, which does not seem to significantly affect the riser operating conditions, since unlike in the previous disturbances no peaks are generated. However, this disturbance does change the new optimal operating conditions, as reflected by the variation in the riser setpoint (Figure 7.10) at 4e4s, at which time the second RTO cycle is executed. The profit value for these new operating conditions does not change significantly. The third disturbance (a F_{feed} decrease) causes a change in the process operating conditions (Figure 7.10f, T_{ris} setpoint increase). The profit reached in this case for SC2 is very similar to that attained before the F_{feed} decrease, whereas in SC4 (without RTO), this disturbance does not affect the profit as setpoints are not optimized. Finally, for a F_{feed} increment, the profit increase in SC2 is greater than SC4 profit by the reasons discussed in case A.

From all the typical disturbances, F_{feed} has the greatest impact on profitability. Every time this variable is modified, the change of the setpoints of the controlled variables turns out to be stronger than those necessary to reach the optimal conditions when other disturbances are made. In the analyzed cases, the profit is also affected, since the greater the flow of gas oil, the more gasoline will be produced (as long as an adequate F_{cat} / F_{feed} relationship is maintained).

According to the results presented above, an RTO implementation (SC2) is very convenient to get higher profits than in a plant with a traditional control system (SC4). The continuous update of the setpoints gives flexibility to the operation and improves its performance, still in the presence of system disturbances.

7.5 Conclusions

Each of the stages of the classic RTO was implemented on a virtual FCCU plant to see its behavior as a whole. The use of RTO in a FCCU (for the analyzed cases) proved to be a valuable alternative to increase the unit's profitability up to 35% compared to a scenario without RTO, and between 2-7% from cycles after RTO is implemented.

It was found that the noise reduction based on WT allows obtaining an improved value of the signal. This results in a clearer signal than that presented with noise and, therefore, in better-estimated values for later stages in the RTO. The proposed standard deviation method for steady-state detection was able to detect those states in which the variables are in a continuous change and those in which the variable reached a stable state. To make these appropriate adjustments, parameters S1 and S2 must be adjusted.

Although it was not possible to attain a complete cleaning of the data and exactly obtain the real value of the signal, data reconciliation using Hampel estimators allows having a better estimate of the system's real conditions; and therefore, a better approximation of the profit real value. Even though error in data reconciliation is low, this can affect the determination of the profit that the plant could reach if its real values were known.

The optimization performed by genetic algorithms showed a good performance both in the search for better operating conditions for the process and in the computation time required. Nevertheless, its performances is highly dependent on the values delivered by data reconciliation and parameter estimation.

The presence of noise in a signal affects the tuning of the parameters of the PID controller, so this type of deviations must be taken into account in its implementation. The manipulated variables behavior using a PID controller in the RTO implementation undergoes more drastic changes than when it operates without RTO. This is mainly due to the changes of setpoints of the process as a consequence of the online optimization stage.

Typical and sometimes undesirable disturbances could have a negative effect on system profitability. However, it was shown that when leading the system to a new state by a change in the setpoint of the controlled variables, by using a RTO, such disturbances can be treated so that high rentability of the process at those conditions is reached.

Conclusions and recommendations

It was demonstrated that the integration of the RTO with PID control improved the profitability of the FCCU in 35% in comparison with a scenario without RTO, and it was observed a profit variation no greater than 7% after each RTO execution cycle. One of the most relevant aspects found in this thesis is that each of the RTO stages must be evaluated as a whole since sometimes studying them separately does not guarantee a successful RTO implementation.

The noise in a real plant is a very important aspect to consider when performing simulations since these deviations seriously affect the performance of each RTO stage. This noise can trigger the values of the actual process conditions to be underestimated or overestimated.

It was not possible to clean up completely the contaminated signal and obtain exactly the value of the real signal. However, tools such as wavelets transform (for denoising) and Hampel estimators (for data reconciliation and parameter estimation), significantly improve the data analysis performance, making easier to get reliable information not only for the optimization but also for the process control.

The error percentage between real and reconciled values in the process variables after data reconciliation stage was about 8%. However, the estimate of the profit after this reconciliation was strongly affected by these deviations and its value was only corrected by 50%. For this reason, it would be interesting to explore other methodologies for data reconciliation in RTO.

Steady-state detection is an essential stage to perform data reconciliation and optimization. An early detection generates wrong values in reconciliation and optimization, while a late detection generates economic losses since the plant operates under suboptimal conditions. The method proposed in this work, based on the process standard deviation, was able to detect those states in which the variables are in a continuous change and those in which

the variable reaches a steady state. To get suitable results S_1 and S_2 parameters of the standard deviation method must be adjusted.

Optimization in steady state is one of the most delayed steps in the execution of an RTO, which is a disadvantage in the traditional RTO because, in that time period, the process is operated in sub-optimal conditions. The methodology proposed for this stage allowed to reduce the computation timethrough a sensitivity analysis within the region of operation to determine the highest possible profitability, and the parameters adjustment of the genetic algorithm (mainly stall generations and maximum of generations). This criterion can be applied to more complex models to reduce computation time.

Due to the multiplicity of states in the FCCU, the inclusion of a stability criterion (such as the Lyapunov criterion) before implementing the optimum conditions, allows the system to reach a stable optimum. This criterion included in the RTO guarantees that the optimal conditions can be really reached by the system.

The presence of nonlinearities and FCCU coupling make the unit difficult to control due to the strong interactions between the reactor and the regenerator. In this thesis, a decentralized PID controller was implemented; the pairing of variables was made from an analysis by RGA and Niederlinski Index. Tuning parameters were found using a multiobjective genetic algorithm and a later trial and error procedure. The PID controller allowed to obtain a suitable response time and allow the process variables reaching their desired operating point. Although the PID control has a good performance, an implementation of an Advanced Control System (as MPC) would improve the speed of the response, reduce drastic changes, and find a suitable trajectory for the operation variables, in presence of disturbances.

The implementation of RTO systems in process units that are subject to continuous changes during their operation is an effective tool to increase the productivity and competitiveness of companies. However, the inclusion of the RTO layer increases the complexity of the control system.

The analysis on the virtual plant behavior allowed to establish that certain FCCU operating conditions can positively affect some system variables and negatively others due to the strong interaction between the riser and the regenerator. Therefore, the optimal conditions

must be determined through optimization methods that include all these possible effects in the system and allow guarantee the best-operating values.

An aspect of great importance in a FCCU is the change of composition in the feed stream to the unit. Thus, that it would be interesting to implement the strategies evaluated here with a more rigorous and detailed FCC model. It could include the change in the feed composition and the monitoring of the conversion along the riser based on models with more lumps.

In the literature it is difficult to find documentation that presents a study of all the stages of a traditional RTO and its behavior as a whole. It is expected that this work be of great help for those who wish to deepen the subject and improve the performance of process units through RTO technology.

Appendix A: Research Products

- "*Data Analysis and Modelling of a Fluid Catalytic Cracking Unit (FCCU) for an Implementation of Real Time Optimization*"
  Juan D.Reyes, Adriana L.Rodríguez, Carlos A.M.Riascos.
  12th International Symposium on Process Systems Engineering and 25th European Symposium on Computer Aided Process Engineering. Computer Aided Chemical Engineering. Volume 37, 2015, Pages 611-616.
  https://doi.org/10.1016/B978-0-444-63578-5.50097-9

- "*Data reconciliation and control analysis on a Fluid Catalytic Cracking (FCCU) for an implementation of Real Time Optimization*".
  Oral presentation in the 10th European Congress of Chemical Engineering/ 3rd European Congress of applied biotechnology/ 5th European process intensification conference. (Niza, France). September 27th - October 1st, 2015.

- Research work on nonlinear real time process optimization of a Fluid Catalytic Cracking Unit in Pyomo. Participation in the Process System Engineering group in Carnegie Mellon University PA from October 5th , 2015 to December 22nd, 2015.

Appendix B: FCC Model

The FCCU model used in this work is the model followed by [66], [160]. This is derived from the model proposed by [161] for partial combustion mode. This model augments the regenerator model [162] with the riser model of [163].

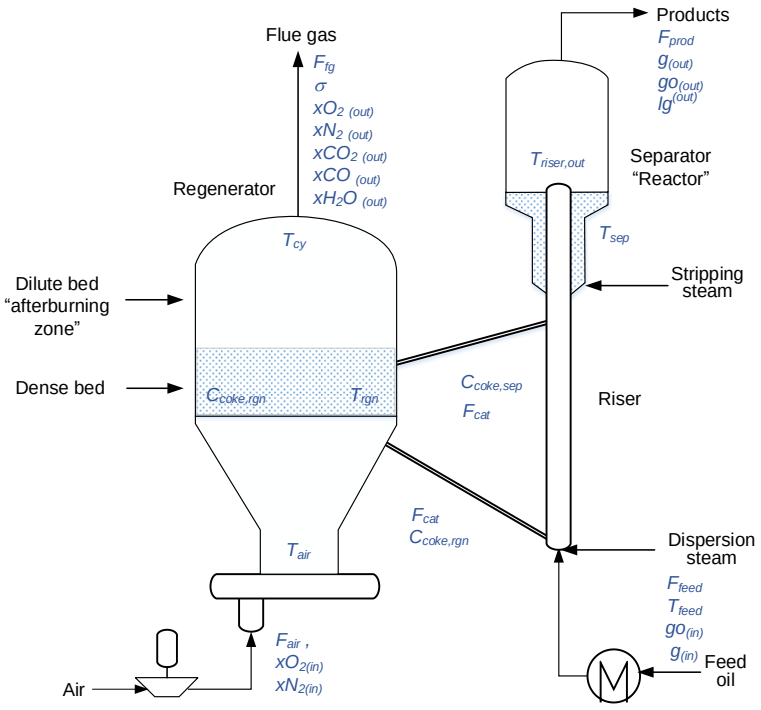

Figure B1. *FCC plant scheme* [160]

Riser model

The residence time in the riser is only a few seconds, so a static model is used. The model uses an ideal plug-flow model and the three lump kinetic scheme of [164], where the feed is gas oil, which can crack to gasoline or light gases/coke, but it does not consider the change in feed composition as an input variable.

The static riser model is used to compute:

$T_{ris(1)}$= temperature at the riser outlet

$C_{coke\,ris(1)}$ = mass fraction of coke on catalyst at riser outlet

The feed temperature $T_{ris}(z=0)$ at the riser inlet is derived from an energy balance at the inlet:

$$F_{cat}Cp_{cat}(T_{rgn}-T_{ris}(0)=F_{feed}[Cp_{ol}\left(T_{boil}-T_{feed}\right)+\Delta H_{vap}+Cp_{og}(T_{ris}(0)-T_{boil})]$$

Resulting in:

$$T_{ris}(0)=\frac{F_{cat}Cp_{cat}T_{rgn}-F_{feed}(Cp_{ol}\left(T_{boil}-T_{feed}\right)+\Delta H_{vap}-Cp_{og}T_{boil})}{F_{cat}Cp_{cat}+F_{feed}Cp_{og}}$$

In the riser, only two components are considered: gas oil and gasoline. The kinetic constants follow Arrhenius law. Then, for gas oil consumption:

$$k_1=k_{10}\exp(-E_{af}/(RT_{ris}))$$

and for gasoline production:

$$k_3=k_{30}\exp(-E_{ag}/(RT_{ris}))$$

The catalyst deactivation along the riser caused by coke deposition is given by:

$$\phi=\phi_0\exp(-\alpha t_c z C_{owr})$$

where ϕ_0 represents the reduction in catalyst activity caused by the coke remaining in the catalyst after regeneration

$$\phi_0=\left(1-m\,C_{coke,rgn}\right)$$

and C_{owr}, is the catalyst to oil ratio

$$C_{owr}=\frac{F_{cat}}{F_{feed}}$$

Then, material balance for gas oil is given by

$$\frac{dy_{go}}{dz}=-k_1y_{go}^2C_{owr}\phi t_c$$

and a material balance for gasoline

$$\frac{dy_g}{dz} = (\alpha_2 k_1 y_{go}^2 - k_3 y_g) C_{owr} \phi t_c$$

A correlation taken from [165] is used to estimate the amount of coke produced

$$C_{cokeprod} = k_c \sqrt{\frac{t_c}{C_{coke,rgn}^{n_{prod}}} \exp\left(-\frac{E_{acf}}{RT_{ris}(1)}\right)}$$

The amount of coke on the catalyst leaving the riser is thus

$$C_{coke,ris} = C_{coke,rgn} + C_{coke,prod}$$

The energy balance yields:

$$\frac{dT_{ris}}{dz} = \frac{\Delta H_{r,crack} F_{feed}}{F_{cat} C_{p,cat} + F_{feed} C_{p,ol} + \lambda F_{feed} C_{p,steam}} \frac{dy_{go}}{dz}$$

and for the initial condition

$$T_{ris}(0) = \frac{F_{cat} C_{p,cat} T_{reg} - F_{feed}\left(C_{p,ol}\left(T_{boil} - T_{feed}\right) + \Delta H_{vap} - C_{p.og} T_{boil}\right)}{F_{cat} C_{p,cat} + F_{feed} C_{p,og}}$$

A material balance gives the amount of coke produced during the cracking reactions.

$$F_{coke} = F_{cat} * (C_{cokesep} - C_{cokergn})$$

The product flows (kg/s) of unconverted gas oil, gasoline, and light gases are given by the material balances for gas oil and gasoline in the products stream.

$$F_{go} = go_{(1)} * F_{feed}$$

$$F_g = g_{(1)} * F_{feed}$$

$$F_{lg} = \left(1 - go_{(1)} - g_{(1)}\right) * F_{feed} - F_{coke}$$

$$F_{prod} = F_{go} + F_g + F_{lg}$$

Stripper model

No reactions occur in the reactor as it is used as a stripping vessel where volatile hydrocarbons are stripped from the catalyst using steam. The flow rate of stripping steam is small compared to the flow rates of catalyst and feed oil and the effect of the steam on the balance of the reactor is ignored.

Assuming the stripping is effective, the only effect on the reactor will be to introduce a lag between the riser exit and the catalyst return to the regenerator. This lag is modeled using an ideal mixing tank.

A separator follows the riser with a mass balance for the coke on the catalyst:

$$\frac{\mathrm{d}C_{cokesep}}{dt} = \frac{F_{cat}(C_{cokeris_{(1)}} - C_{coke,sep})}{m_{cat\ sep}}$$

And an energy balance giving the temperature variation

$$\frac{dT_{sep}}{dt} = \frac{F_{cat}C_{p,cat}\left(T_{ris_{(1)}} - T_{sep}\right)}{m_{cat,sep}C_{pcat}}$$

The catalyst holdup in the reactor is assumed to be kept constant by perfect control. Therefore, the flow rate of spent catalyst from the reactor to the regenerator equals the flow rate of regenerated catalyst.

Regenerator model

The regenerator follows the model described by [65]. In this, the catalyst residence time is about 10 min. When modeling the regenerator is a common assumption that the temperature and the amount of coke on the catalyst is uniform through the regenerator dense bed. Oxygen is also assumed to be uniformly distributed. This assumption allows operational data to be described well [162].

This gives a third order model for regenerator, with the following states:

- $C_{coke,reg}$: mass fraction of coke on the regenerated catalyst
- xO_2: mole fraction of oxygen in the gas leaving the dense bed
- T_{rgn}: regenerator dense bed temperature

Balance for coke on the regenerated catalyst

$$\frac{dC_{coke,reg}}{dt} = \frac{F_{cat}\left(C_{cokesep} - C_{coke,reg}\right) - \gamma_{cb}}{m_{cat,\ reg}}$$

where the rate of coke combustion of coke γ_{cb} in kg/s is equal to:

$$\gamma_{cb} = k_{cb} \exp\left(-\frac{E_{acb}}{RT_{reg}}\right) x_{O_2} C_{coke,reg} m_{cat,reg}$$

The concentration of oxygen in the regenerator dense bed is given by a material balance:

$$\frac{dxO_2}{dt} = \frac{1}{m_{air,rgn}}\left[\frac{F_{air}}{M_{w_{air}}}\left(xO_{2_{in}} - xO_2\right) - \frac{(1+\sigma)n_{CH} + 2 + 4\sigma}{4(1+\sigma)}\frac{\gamma_{cb}}{M_{w_{coke}}}\right]$$

where CO_2/CO ratio (σ), is defined as

$$\begin{aligned} \sigma &= 0.000953\ exp(5585/T_{reg}) && if\ T_{reg} < 803 \\ \sigma &= 1 + \left(T_{reg} - 803\right)0.00142 && if\ 803 < T_{reg} < 873 \\ \sigma &= 1.1 + \left(T_{reg} - 873\right)0.0061 && if\ 873 < T_{reg} \end{aligned}$$

Energy balance

$$\frac{dT_{reg}}{dt} = \frac{1}{m_{cat,reg}C_{p,cat}}\left(F_{cat}C_{p,cat}T_{sep} + F_{air}C_{p,air}T_{air} - \left(F_{cat}C_{p,cat} + F_{air}C_{p,air}\right)T_{rgn} - \Delta H_{cb}\frac{\gamma_{cb}}{M_{w,coke}}\right)$$

where the heat of coke combustion ΔH_{cb} is given by:

$$\Delta H_{cb} = -\Delta H_1 - \Delta H_2\left(T_{rgn} - 960\right) + 0.6\left(T_{rgn} - 960\right)^2$$

In order to compute the regenerator cyclone temperature T_{cy}, the afterburning of CO to CO_2 in the dilute phase in the regenerator is represented using a simple equation taken from [165].

$$T_{cy} = T_{rgn} + c_t xO_2$$

To this equation be reasonable, there must be an excess of CO over O_2 in the gas leaving the regenerator dense bed, which means this is only valid in the partial combustion mode.

Flows in the output of the regenerator can be calculated from the stoichiometry of combustion reactions for the dense phase. So combustion kinetics is ruled by [133]:

$$CH_{n_{(s)}} + \frac{n_{CH}}{4} + \frac{\beta + 2}{2\beta + 2}\, O_{2(g)} \rightarrow \frac{\beta}{1+\beta}\, CO_{(g)} + \frac{1}{1+\beta} CO_{2(g)} + \frac{n_{CH}}{2} H_2O_{(g)}$$

Where β represents the molar ratio CO/CO_2 in the catalyst.

Gasoline octane model

The octane number (ON) is a measure of the ignition quality of gasoline to describe the behavior of the fuel in the engine during combustion. The higher the number, the better the fuel burns within the engine of a vehicle. Its value ranges from 0 to 100. In determining the octane number, two concepts are considered: research octane number (RON) and the motor octane number (MON).

The research octane number (RON) describes the behavior of the fuel in the engine at lower temperatures and speeds, that simulate acceleration behavior. Gasoline must be at least 95.0 and at least 98.0 for a Super Plus gasoline.

The motor octane number (MON) describes the behavior of the fuel in the engine at high temperatures and speeds – a full-throttle range, comparable to driving fast on a highway [166].

MON for Super gasoline must be at least 85.0 and at least 88.0 for a Super Plus gasoline.

The motor octane number (MON) and the research octane number (RON) are estimated using the empirical correlations reported by [167], [168].

$$MON = 72.5 + 0.05(T_{ris} - 900\text{°F}) + 0.17(X_{wt.} - 0.55)$$

$$RON = 1.2931MON + 12.06897$$

where

MON is the motor octane number.

RON research octane number

T_{ris} temperature at the outlet of the riser, °F

T_r, avg =average temperature in riser used in yield optimization model, °F

$X_{wt.}$ weight fraction conversion

The gas oil conversion $X_{wt.}$ is estimated using the expression developed by[169]

$$X_{wt.} = 1 - \frac{k_2 t_c}{k_2 t_c - k_1 t_c COR(e^{-k_2 t_c} - 1)e^{-Ef/T_{r,avg}}}$$

$$T_{r,avg} = 0.3T_0 + 0.7T_{ris}$$

$$T_0 = \frac{F_{cat,rgn} C_{p,c} T_{rgn} + F_{feed} C_{p,oil} T_{feed}}{F_{cat,rgn} C_{p,c} + F_{feed} C_{p,oil}}$$

where

COR: catalyst to oil ratio

t_c: catalyst residence time in riser [s]

T_{ris}: riser outlet temperature, °F

k_1: empirical constant, s^{-1}

k_2: empirical constant, s^{-1}

E_f: activation energy of gas oil cracking reaction

T_{feed}: temperature of fresh feed entering

Polytrophic compressor equation

A polytrophic compressor head is given by :

$$H_{poly} = \frac{1}{g_c} \cdot \frac{zRT_1}{M} \cdot \frac{1}{\widetilde{m}} \cdot \left[\left(\frac{P_2}{P_1} \right)^{\widetilde{m}} - 1 \right] \cdot \frac{1}{F_0}$$

where:

H_{poly}: polytrophic compressor head (m)

g_c: unit conversion factor ($9.80665\ kg\ m/\ kgf\ s^2$)

z: Compressibility factor (Table A1)

R: Gas constant ($8314.34 J/mol\ K\ kg$)

T_1: inlet temperature (K)

M: molecular weight ($kg\ /\ kmol$)

P_2: discharge pressure (kPa)

P_1: inlet pressure (kPa)

F_0: Conversion Factor (9.806)

g: gravitational acceleration ($9.80665\ m/s^2$)

$\widetilde{m}$: Average polytrophic exponent of temperature increase

$\widetilde{m}$ is calculated from an average of the polytropic exponent of temperature increase between inlet and outlet from the compressor, as follows:

$$\widetilde{m} = \frac{m_1 + m_2}{2}$$

$$m_1 = \frac{\left(\frac{k_{(T_1,P_1)} - 1}{k_{(T_1,P_1)}}\right)}{\eta_p} \quad , \qquad m_2 = \frac{\left(\frac{k_{(T_2,P_2)} - 1}{k_{(T_2,P_2)}}\right)}{\eta_p}$$

Where

k: Specific heat ratio, Cp/Cv (Table B2)

η_p: polytrophic efficiency (Figure B1)

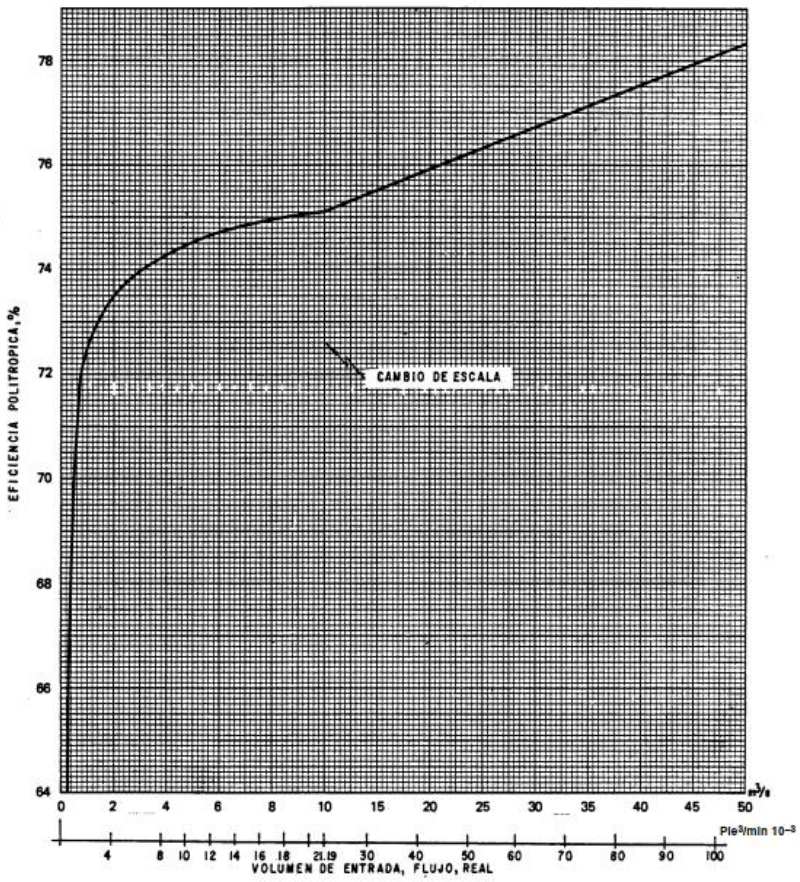

***Figure B2**. Polytrophic efficiency of centrifugal compressors without cooling*

Table B1 *Compressibility factor*

Z	Pressure (kPa)				
T(°C)	**50**	**100**	**1000**	**4000**	**10000**
-100	0.999	0.996	0.959	0.843	0.701
-50	1.000	0.999	0.985	0.941	0.881
0	1.000	1.000	0.995	0.983	0.971
50	1.000	1.000	0.999	0.998	1.01
100	1.000	1.000	1.000	1.005	1.023
150	1.000	1.000	1.003	1.011	1.031

Table B2 *Specific heat ratio Cp/Cv*

Cp/Cv	Pressure (kPa)				
T(°C)	**50**	**100**	**1000**	**4000**	**10000**
-100	1.386	1.408	1.47	1.84	2.517
-50	1.402	1.405	1.438	1.572	1.899
0	1.402	1.403	1.422	1.484	1.62
50	1.400	1.401	1.414	1.458	1.523
100	1.396	1.398	1.408	1.445	1.497
150	1.394	1.394	1.401	1.423	1.475

The model presented here has some advantages and disadvantages that must be taken into account for its implementation. Some of these are mentioned in Table B3. A more detailed discussion is presented in [170]

Table B3 *Advantages and disadvantages from the FCCU model*

Advantages	Disadvantages
• Rigorous model that allows estimating values of the main variables of the FCCU. • Description of mass and energy balances from a series of ordinary differential equations and non-linear algebraic equations that can be easily solved by different numerical methods. • Description of the gasoline quality from its octane number. • Low computing requirements and faster convergence, which is favorable for RTO implementations.	• Kinetics based only on three lumps which limit the analysis of other products that may be of interest in the FCCU. • Lack of detailed kinetics for the combustion of CO and CO_2. It uses a CO_2/CO ratio which does not allow modeling of the impact of catalytic combustion promoters. • It neglects the impact of coke on catalyst on the relative kinetics.

Notation

Symbol	Significance	Value
F_{cat}	Mass flow rate of catalyst (kg/s)	294
F_{feed}	Mass flow rate of oil in the feed (kg/s)	40.63
F_{air}	Mass flow rate of air to regenerator (kg/s)	25.378
T_{air}	Temperature of air to regenerator (K)	360
T_{feed}	Temperature of feed (K)	434.63
C_{owr}	catalyst to oil ratio on a mass basis	7.2360
T_{boil}	Boiling temperature of feed (K)	700
ΔH_{vap}	Heat of vaporization of oil (J/kg)	$1.56*10^5$
Cp_{ol}	Heat capacity of oil as a liquid (J/kgK)	2671
Cp_{og}	Heat capacity of oil as a gas (J/kgK)	3299
Ea_{cf}	Activation energy for coke formation (J/mol)	$41.79*10^3$
n_{prod}	Exponent in expression of coke produced	0.4
tc	Catalyst time residence in riser (s)	9.6
kc	Rate constant for catalytic coke formation $(s^{0.5})$	0.0176
Cp_{air}	Heat capacity of air (J/kgK)	1074
Cp_{cat}	Heat capacity of catalyst (J/kgK)	1005
Cp_{steam}	Heat capacity of dispersing steam (J/kgK)	1900
λ	Weight fraction of steam in feed stream to riser	0.035
k_{10}	Reaction rate constant for cracking of gas oil	$9.65*10^5$
k_{30}	Reaction rate constant for cracking of gasoline	$4.22*10^5$
Ea_f	Activation energy for gas oil cracking (J/mol)	$101.5*10^3$
Ea_g	Activation energy for gasoline cracking (J/mol)	$112.6*10^3$
m	Empirical Deactivation factor	80
α	Catalyst decay rate constant (s^{-1})	0.12
α_2	Fraction of the gas oil that cracks to gasoline	0.75
$\Delta H_{r,crack}$	Heat of reaction for gas oil cracking (J/kg)	$506.2*10^3$
k_{cb}	Reaction rate constant for coke combustion	$2.077*10^8$
Ea_{cb}	Activation energy for coke combustion (J/mol)	$158.59*10^3$
R	Gas constant $(J/molK)$	8.31434
$m_{cat,reg}$	Holdup of solid in regenerator (kg)	175738
$m_{cat,sep}$	Holdup of solid in separator (kg)	17500
$m_{air,reg}$	Holdup of air in regenerator (mol)	20000
nCH	Number of hydrogen in coke of formula CHn	2
Mw_{coke}	Molecular weight of coke (kg/mol)	0.014
ΔH_1	Parameter in heat of reaction for coke combustion	$521.15*10^3$
ΔH_2	Parameter in heat of reaction for coke combustion	245
Mw_{air}	Air molecular weight (kg/mol)	0.028854
$xO_{2(in)}$	Concentration of oxygen in air to regenerator $(molefraction)$	0.2136
N	Exponent for the dependence of $C_{cokeris}$	0.4125
Ct	Factor to calculate T_{cy}	5555

Steady State values

$T_{ris(0)}$	temperature at the riser at $z = 0\ (K)$	805.141
$T_{ris(1)}$	temperature at the riser at $z = 1\ (K)$	779.762
T_{rgn}	Temperature in the dense bed of the regenerator (K)	971.757
$C_{coke,rgn}$	Coke concentration in the regenerator (kg/kg)	0.004
$C_{cokeris(1)}$	Coke concentration in the riser at $z = 1\ (kg/kg)$	0.011
$xO_{2(\mathrm{out})}$	Oxygen mole fraction in the regenerator	0.004
$go_{(out)}$	Weight fraction of gas oil in the riser at $z = 1$	0.498
$g_{(out)}$	Weight fraction of gasoline in the riser at $z = 1$	0.359
T_{cy}	regenerator cyclone temperature	994.774
σ	molar ratio of CO_2 to CO in the regenerator dense bed	1.702
β	molar ratio CO/CO_2 in the regenerator dense bed	0.702

Appendix C: Wavelet Denoising

The discrete WT noise eliminations can be implemented in three steps [93]:

1. Signal decomposition: Wavelet transforms the noisy signal. In this step, a wavelet is chosen at level N and wavelet decomposition of the signal s at level N is computed.
2. Determination of threshold contraction coefficients. For each from level 1 to N, a threshold is selected, and a soft threshold to the detailed coefficients is applied.
3. Signal reconstruction: a wavelet reconstruction is calculated applying the inverse wavelet transformation to modified wavelet coefficients. This is done based on the original coefficients approximation of level N and modified detailed coefficients of levels from 1 to N.

As a first step, WT transforms digital signals to discrete coefficients in the wavelet domain. The idea of discrete WT is a multilevel decomposition of the signal into approximated and detailed coefficients for each level. Then, the wavelet coefficient can be computed by a pyramid algorithm using low pass filter(h), high pass filter (g) and down-sampling by a two factor at each stage of the filter (Figure C1).

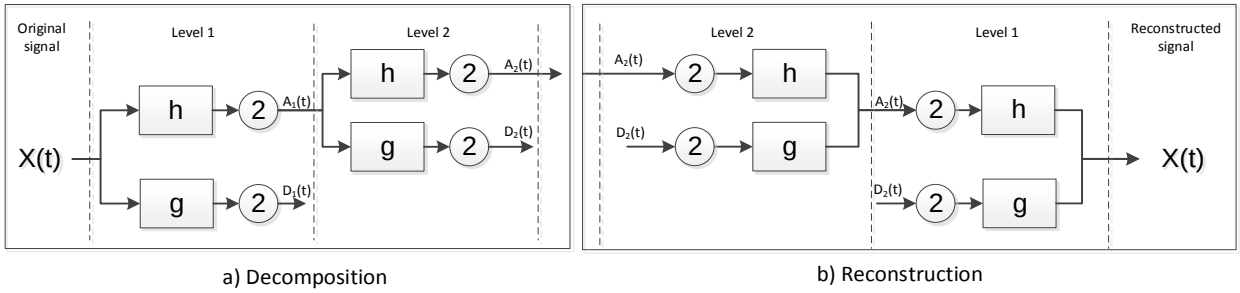

Figure C1 *The discrete WT decomposition and reconstruction steps of a 1D signal for level 2* [79]

The low pass (LP) and high-pass (HP) filters used in the algorithm are determined according to the mother wavelet in use [83]. The outputs of LP filters are called

approximation coefficients and the outputs of the HP filters are named detailed coefficients. Wavelet coefficients of the signal can be considered as a noisy version of the original signal.

In a second step, each coefficient is compared with a threshold level (λ) in order to decide if it is a desired part of the signal or not. This technique is named thresholding and was established in 1993 by [83]. One of the main advantages is that this method does not require any particular assumption about the nature of the signal and, permits discontinuities and space variations in the signal.

The threshold coefficients are applied to detailed coefficients and usually not to approximation coefficients. It is because of the last one refers to the low frequency, they usually contain important components of the signal and then, are less affected by noise.

The threshold can hard or soft. In hard thresholding, the wavelet coefficient below a given value is settled to zero while in soft thresholding the wavelet coefficient is reduced to a thresh value [79]. This threshold value is usually calculated from the standard deviation of the detail coefficient [171]. Hard and soft thresholding are represented in Figure C2.

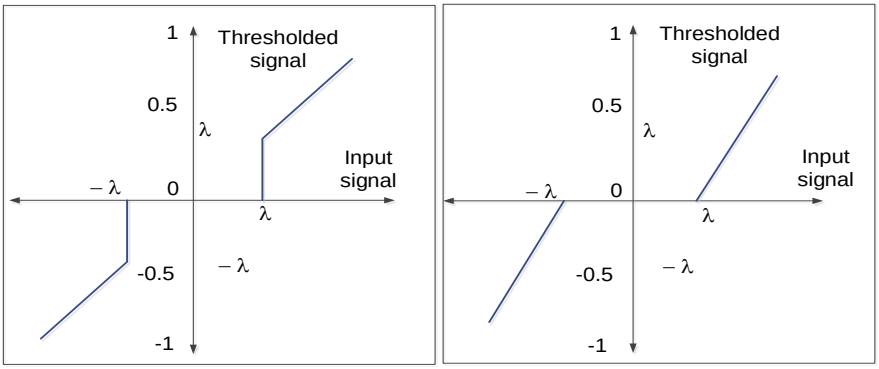

a) Hard thresholding b) Soft thresholding

Figure C2. *Hard and soft thresholding.* $\lambda = 3$

The most known threshold selection algorithms are universal threshold (sqtwlog), minimax thresholding, sure shrink (rigrsure) and, heursure methods [86], [94], [171].

Finally, the third step (reconstruction) consists of how those components can be assembled back into the original signal with no loss of information. The process of reconstruction comprises upsampling and filtering which is made through inverse discrete wavelet transform. In this way, upsampling is the process of lengthening a signal through the

insertion of zeros between samples [172]. A representation of discrete WT analysis is shown in Figure C3

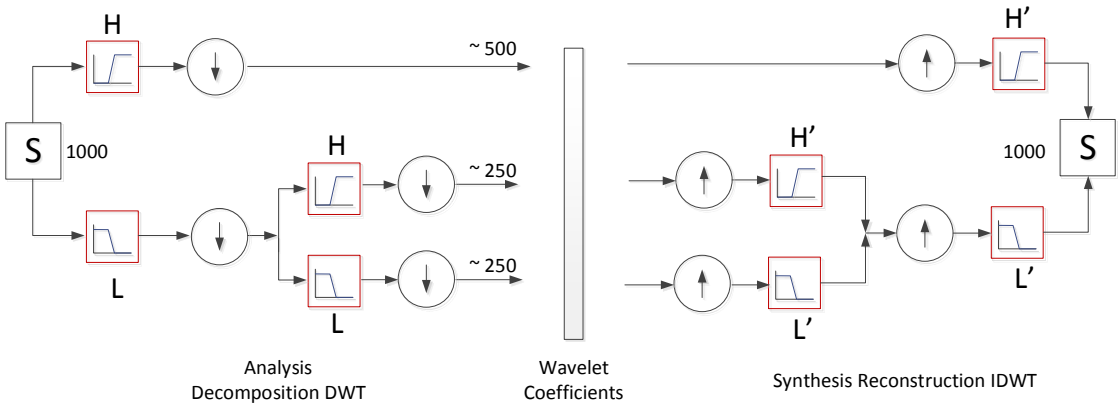

Figure C3 *A multistep analysis-synthesis process with DWT* [173]

Appendix D: Lyapunov Stability

The stability of a linear or non-linear dynamic denotes to how close the system will remain around a point of equilibrium after it is disturbed. The stability concept depends on the initial conditions and the equilibrium point. A non-linear system can have one or several points of equilibrium. These points can refer to local stability or global stability. In local stability, the system returns to the point of equilibrium after being slightly disturbed; while in global stability the system returns from any point to the same equilibrium point after performing any disturbance.
Many stability analyzes that are carried out on local stability equilibrium points. One of the best known are the methods of Lyapunov.

- *The First method of Lyapunov (Indirect method):* local stability of a non-linear system from its linear approximation. Usually, the first step for the analysis of a non-linear system is to perform a linearization around a point of equilibrium x = 0.
- *The Second method of Lyapunov (Direct method)* Stability is determined from the concept of energy and is not restricted to a local case.

The First method of Lyapunov or indirect method[174].

A solution is stable if every equilibrium point is stable if all solutions that start near that point remain close to it. To determine if the system will reach a point of equilibrium after a small disturbance, the indirect method of Lyapunov can be used. This consists of:

1. Calculate the Jacobian system J (matrix of partial derivatives) evaluated at the equilibrium point.

$$J(x_1, x_2, x_3, \dots, x_n) = \begin{bmatrix} \frac{\partial f_1}{\partial x_1} & \frac{\partial f_1}{\partial x_2} & \frac{\partial f_1}{\partial x_3} & \cdots & \frac{\partial f_1}{\partial x_n} \\ \frac{\partial f_2}{\partial x_1} & \frac{\partial f_2}{\partial x_2} & \frac{\partial f_2}{\partial x_3} & \cdots & \frac{\partial f_2}{\partial x_n} \\ \frac{\partial f_3}{\partial x_1} & \frac{\partial f_3}{\partial x_2} & \frac{\partial f_3}{\partial x_3} & \cdots & \frac{\partial f_3}{\partial x_n} \\ \vdots & \vdots & \vdots & \ddots & \vdots \\ \frac{\partial f_m}{\partial x_1} & \frac{\partial f_m}{\partial x_2} & \frac{\partial f_m}{\partial x_3} & \cdots & \frac{\partial f_m}{\partial x_n} \end{bmatrix}$$

2. Calculate as eigenvalues of J $(i = 1, \dots, n)$ defined as λ_i
3. Determine stability from the eigenvalues of J using linearization theorem of Lyapunov and Poincaré, which defines that:
    - The origin is asymptotically stable if $\lambda_i < 0$ for all eigenvalues of J
    - The origin is unstable if $\lambda_i > 0$ for one or more eigenvalues of J
    - If $\lambda_i = 0$, nothing is known.

The eigenvalues of the Jacobian matrix can also be complex numbers. In this case, the imaginary part of the eigenvalues represents undamped oscillation that neither expands or contracts. If this part is negative the oscillation contracts, and it expands if it is positive.
If any eigenvalue has a real positive part, the deviation from the stable point increases and the system moves away from the equilibrium point. If all the real parts and the eigenvalues are exactly zero, there is neutral stability, where after a small disturbance the system will oscillate around the equilibrium point, but it will not return, nor move away from it.

References

[1] S. Skogestad, “Real Time Optimization,” in *Chemical and Energy Process Engineering*, vol. 1, CRC Press, Ed. Elsevier Ltd, 2009, pp. 395–413.

[2] J. K. Bailey, A. N. Hrymak, S. S. Treiber, and R. B. Hawkins, “Nonlinear optimization of a hydrocracker fractionation plant,” *Comput. Chem. Eng.*, vol. 17, no. 2, pp. 123–138, 1993.

[3] A. A. Koutinas and I. K. Kookos, “Process Optimization,” in *Modeling, Control, and Optimization of Natural Gas Processing Plant*, vol. 2, Inc., Elseiver, 2017, pp. 173–213.

[4] M. L. Darby, M. Nikolaou, J. Jones, and D. Nicholson, “RTO: An overview and assessment of current practice,” *J. Process Control*, vol. 21, no. 6, pp. 874–884, Jul. 2011.

[5] D. Bonvin and G. Bunin, “Real-Time Optimization of Chemical Processes,” 2013.

[6] D. Muller, B. Dercks, E. Nabati, M. Blazek, and T. Eifert, “Real-Time Optimization in the Chemical Processing Industry,” *Chemie Ing. Tech.*, no. 11, pp. 1464–1470, 2017.

[7] M. Mansour and J. E. Ellis, “Methodology of on-line optimisation applied to a chemical reactor,” *Appl. Math. Model.*, vol. 32, no. 2, pp. 170–184, Feb. 2008.

[8] A. J. E. Graciano, “Real Time Optimization in chemical processes : evaluation of strategies , improvements and industrial application Real Time Optimization in chemical processes : evaluation of strategies , improvements and industrial application,” Universidade de São Paulo, 2016.

[9] S. Engell, “Online Optimizing Control : The Link Between Plant Economics and Process Control,” *10th Int. Symp. Process Syst. Eng. PSE 2009*, pp. 79–86, 2009.

[10] A. J. E. Graciano, J. Jäschke, G. A. C. Le Roux, and L. T. Biegler, “Integrating self-optimizing control and real-time optimization using zone control MPC,” *J. Process Control*, vol. 34, pp. 35–48, 2015.

[11] R. Huang, “Nonlinear Model Predictive Control and Dynamic Real Time Optimization for Large-scale Processes,” Carnegie Mellon University, 2010.

[12] D. F. Mendoza, A. J. E. Graciano, S. Liporace, and G. A. Carrillo, “Assessing the Reliability of Different Real-Time Optimization Methodologies †,” *Can. J. Chem. Eng.*, no. June, pp. 1–63, 2015.

[13] S. Shokri, R. Hayati, M. Marvast, M. Ayazi, and H. Ganji, “Real Time Optimization As a Tool for Increasing Petroleum Refineries Profits,” *Pet. Coal*, vol. 51, no. 2, pp. 110–114, 2009.

[14] O. & G. Journal, “Real-time optimization for refining,” *Oil Gas J.*, Apr. 2003.

[15] M. Campo, H. Teixeria, F. Liporace, and M. Gomes, “Challenges and problems with advanced control and optimization technologies,” 2007.

[16] X. Chen, “The Optimal Implementation of on-Line Optimization for Chemical and Refinery Processes,” University of Mississippi, 1993.

[17] F. S. Liporace, M. V. C. Gomes, A. C. Katata, A. C. Zanin, L. F. L. Moro, and C. R. Porfirio, “PETROBRAS Experience Implementing Real Time Optimization,” *10th Int. Symp. Process Syst. Eng. PSE2009*, pp. 1245–1250, 2009.

[18] J. O. Trierweiler, “Real-Time Optimization of Industrial Process,” *Encyclopedia of Systems and Control*. Springer- Verlag, pp. 1–11, 2014.

[19] S. Skogestad, *Economic Plantwide Control*. 2012.

[20] C. A. I. Hinojosa, “Integration of real time optimization (rto) and model predictive control (mpc) of an industrial propylene/propane splitter,” (Schiavon Júnior & Corrêa, 2000), 2015.

[21] N. Yusoff and M. Ramasamy, “Integrated scheduling and RTO of RGP with MPC and PI controllers Integrated Scheduling and RTO of RGP with MPC and PI Controllers,” *J. Appl. Sci.*, no. December, pp. 482–487, 2009.

[22] A. L. Schiavon Júnior and R. G. Corrêa, “Applications of an alternative formulation for one-layer real time optimization ,” *Brazilian Journal of Chemical Engineering* , vol. 17. scielo , pp. 685–694, 2000.

[23] T. Tran, K.-V. Ling, and J. M. Maciejowski, “Economic Model Predictive Control - A Review,” *31st Int. Symp. Autom. Robot. Constr. Min. (ISARC 2014)*, no. Isarc, 2014.

[24] M. Ellis and P. D. Christofides, “Integrating dynamic economic optimization and model predictive control for optimal operation of nonlinear process systems,” *Control Eng. Pract.*, vol. 22, pp. 242–251, Jan. 2014.

[25] A. Gopalakrishnan and L. T. Biegler, “Economic Nonlinear Model Predictive Control for periodic optimal operation of gas pipeline networks,” *Comput. Chem. Eng.*, vol. 52, pp. 90–99, May 2013.

[26] J. B. Jørgensen, L. N. Petersen, and J. B. Rawlings, “Economic Optimization of Spray Dryer Operation using Nonlinear Model Predictive Control with State Estimation,” *IFAC Proc. Vol.*, vol. 48, pp. 507–513, 2015.

[27] E. Almeida Nt and a. R. Secchi, “Dynamic optimization of a fcc converter unit: Numerical analysis,” *Brazilian J. Chem. Eng.*, vol. 28, no. 1, pp. 117–136, 2011.

[28] M. T. Gouvêa and D. Odloak, “One-layer real time optimization of LPG production in the FCC unit: procedure, advantages and disadvantages,” *Comput. Chem. Eng.*, vol. 22, Supple, pp. S191–S198, Mar. 1998.

[29] K. V Pontes, I. J. Wolf, M. Embiruçu, and W. Marquardt, “Dynamic Real-Time Optimization of Industrial Polymerization Processes with Fast Dynamics,” *Ind. Eng. Chem. Res.*, vol. 54, no. 47, pp. 11881–11893, Dec. 2015.

[30] P. A. Rolandi and J. A. Romagnoli, “A Performance Study of Dynamic RTO Applied to a Large-Scale Industrial Continuous Pulping Process,” in *10th International Symposium on Process Systems Engineering: Part A*, vol. Volume 27, C. A. O. do N. and E. C. B. B. T.-C. A. C. E. Rita Maria de Brito Alves, Ed. Elsevier, 2009, pp. 1341–1346.

[31] M. Ellis, H. Durand, and P. D. Christofides, “A tutorial review of economic model predictive control methods,” *J. Process Control*, vol. 24, no. 8, pp. 1156–1178, Aug. 2014.

[32] R. Huang, V. M. Zavala, and L. T. Biegler, “Advanced step nonlinear model predictive control for air separation units,” *J. Process Control*, vol. 19, no. 4, pp. 678–685, Apr. 2009.

[33] L. T. Biegler, *Nonlinear Programming: Concepts, Algorithms, and Applications to Chemical Processes*. 2010.

[34] A. J. E. Graciano, J. Jaschke, G. A. C. Le Roux, and L. T. Biegler, “Integrating self-optimizig control and real-time optimization using zone control MPC,” *J. Process Control*, 2015.

[35] I. P. Miletic and T. E. Marlin, “On-line Statistical Results Analysis in Real-Time Operations Optimization,” *Ind. Eng. Chem. Res.*, vol. 37, no. 9, pp. 3670–3684, 1998.

[36] N. Zhang, “Optimisation is key to high-performing refineries,” *Bus. Brief. Oil Gas Process. Rev.*, pp. 33–35, 2006.

[37] L. F. L. Moro, “Process technology in the petroleum refining industry – Current situation and future trends.,” *Comput. Chem. Eng.*, vol. 27, pp. 1303–1305, 2003.

[38] L. F. L. Moro, “Optimization in the petroleum refining industry – the virtual refinery,” *10th Int. Symp. Process Syst. Eng.*, p. Salvador, Brazil, 2009.

[39] “Real-time optimization for refining,” *Oil Gas J.*, 2003.

[40] M. L. Darby and D. C. White, “On-line Optimization of Complex Process Units,” *Chem. Engr. Prog*, vol. 84, no. 10, pp. 51–59, 1998.

[41] D. M. Starks and E. Arrieta, “Maintaining AC & O Applications, Sustaining the Gain.,” in *AIChE Spring Meeting*, 2007.

[42] M. Piccolo and S. Shyr, “Repsol Cartagena Utilities Real Time Optimization - A Success Story,” in *Proceedings from the Twenty-first National Industrial Energy Technology Conference*, 1999, p. 115.

[43] J. D. Terry, J. M. Righi, J. W. Moore, and M. . Shah, “Baytown Refinery Pipestill 3 RTO,” in *IPS North American Client Conference,* 2008.

[44] J. Greuel, “Refinery-Wide ARPM at Sarnia Refinery,” in *IPS North American Client Conference*, 2008.

[45] Evonik, “Intelligent production with real-time optimization,” *Corporate Press*, 2015. [Online]. Available: https://corporate.evonik.com/en/media/press_releases/Pages/article.aspx?articleId=106439. [Accessed: 08-Jul-2017].

[46] Schneider-Electric, “Unit Performance Suite Real-Time Optimization System for Refineries Unit Performance Suite,” 2017.

[47] Grand View Research, “Fluid Catalytic Cracking (FCC) Market Analysis, Market Size, Application Analysis, Regional Outlook, Competitive Strategies, and Forecasts, 2015 To 2022,” *Report Summary*, 2014. [Online]. Available: https://www.grandviewresearch.com/industry-analysis/fluid-catalytic-cracking-fcc-market. [Accessed: 29-May-2018].

[48] E. T. C. Vogt and B. M. Weckhuysen, “Fluid catalytic cracking: recent developments on the grand old lady of zeolite catalysis,” *Chem. Soc. Rev.*, vol. 44, no. 20, pp. 7342–7370, 2015.

[49] R. Sadeghbeigi, *Fluid Catalytic Cracking Handbook*, 3rd ed. Houston, TX., 2012.

[50] International Council on Clean Transportation, “An Introduction to Petroleum Refining and the Production of Ultra Low Sulfur Gasoline,” Bethesda, Maryland, 2011.

[51] J. Arandes, M. J. Azkoite, J. Bilbao, and H. De la Casa, “Modelling FCC Units under Steady and Unsteady state conditions,” *Can. J. Chem. Eng.*, vol. 78, 2000.

[52] J. Jechura, “Chapter 6. Fluidized Catalytic Cracking.” School of mines Colorado, pp. 1–38, 2018.

[53] M. A. Fahim, T. A. Alsahhaf, and A. Elkilani, “Fluidised Catalytic Cracking,” in *Fundamentals of Petroleum Refining*, First., vol. 54, Oxford, UK: Elseiver, 2010, pp. 1–9.

[54] Koch-Glitsch, “Severe Services ®Intalox Packed Tower Systems, Sever Services,” *Bull. KGSP-2. Rev. 4-*, 2015.

[55] J. H. Gary and G. E. Handwerk, *Petroleum Refining. Technology and Economics*, 4th ed. Marcel Dekker, 2001.

[56] J. Fu, S. Kim, R. P. Rodgers, C. L. Hendrickson, and A. G. Marshall, “.,” *Energy fuel*, vol. 20, pp. 661–667, 2006.

[57] X. Ma, K. Sakanishi, T. Isoda, and I. Mochida, “.,” *Fuel*, vol. 76, pp. 329–339, 1997.

[58] D. Odloak, L. F. L. Moro, and R. Spandri, “Constrained Multivariable Control Of Fluid Catalytic Cracking Converters, A Practical Application.,” *AIChE Spring Meet.*, vol. II, pp. 84–90, 1995.

[59] U. K. Chitnis and A. B. Corropio, “On-line optimization of a Model IV catalytic cracking unit.,” *ISA Trans.*, vol. 37, pp. 215–226, 1998.

[60] A. C. Zanin, M. T. Gouvêa, and D. Odloak, “Industrial implementation of a real-time optimization strategy for maximizing production of LPG in a FCC unit.,” *Comp. Chem. Engng.*, vol. 24, pp. 525–531, 2000.

[61] E. E. Ali and S. S. E. H. Elnashaie, “Nonlinear Model Predictive Control of Industrial Type IV Fluid Catalytic Cracking (FCC) Units for Maximum Gasoline Yield,” *Ind. Eng. Chem. Res.*, vol. 36, no. 2, pp. 389–398, Feb. 1997.

[62] P. E. Perry Nordh, “Maximize Control & Optimization ROI,” 2017.

[63] G. Sivasubramanian, “Plant optimisation: leveraging data analytics and modelling,” *Digital Refining. Processing , Operations and Maintenance*, Jan-2018.

[64] T. Lid and S. Strand, “Real-Time Optimization of a Cat Cracker Unit,” *Comput. chem. Eng.*, vol. 21, pp. 887–892, 1997.

[65] M. Hovd and S. Skogestad, “Procedure for Regulatory Control Structure Selection with Application to the FCC Process,” *AIChE J.*, vol. 39, no. 12, pp. 1938–1953, 1993.

[66] J. P. Corriou, *Process Control.Theory and applications*. Springer Berlin Heidelberg, 2004.

[67] R. Maya-Yescas, D. Bogle, and F. Lo Isunza, “Approach to the analysis of the dynamics of industrial FCC units,” *J. Proc*, vol. 8, no. 2, pp. 89–100, 1998.

[68] F. Serralunga, M. C. Mussati, and P. Aguirre, “An alternative real-time optimization algorithm with modifier adaptation: Application to heat and power systems,” *Comput. Aided Chem. Eng. (22nd Eur. Symp. Comput. Aided Process Eng.*, vol. 30, pp. 367–371, 2012.

[69] Z. Zhang, Y.-Y. Chuang, and J. Chen, “Methodology of data reconciliation and parameter estimation for process systems with multi-operating conditions,” *Chemom. Intell. Lab. Syst.*, vol. 137, pp. 110–119, 2014.

[70] B. Baloochy, S. Shokri, and M. A. Marvast, “A Fast Method for Data Validation in RTO Technology,” *Chem. Eng.*, vol. 1, no. 3, pp. 230–233, 2010.

[71] M. Korbel, S. Bellec, T. Jiang, and P. Stuart, “Steady state identification for on-line data reconciliation based on wavelet transform and filtering,” *Comput. Chem. Eng.*, vol. 63, pp. 206–218, Apr. 2014.

[72] J. L. Thompson, “An Empirical Evaluation of Denoising Techniques for Streaming Data,” 2014.

[73] D. M. Prata, J. C. Pinto, and E. L. Lima, “Comparative Analysis of Robust Estimators on Nonlinear Dynamic Data Reconciliation,” pp. 501–506, 2008.

[74] D. Gidaspow and M. Driscoll, “Porosity and Pressure Waves in a Fluidized Bed of FCC Particles,” *Ind. Eng. Chem. Res.*, vol. 48, no. 5, pp. 2422–2429, Mar. 2009.

[75] T. Köhler and D. Lorenz, “A comparison of denoising methods for one dimensional time series,” 2005.

[76] L. Levy Vehel, Jacques and B. Guilheneuf, “Multifractal image denoising,” in *SCIA’97: 10th Scandinavian conference on image analysis*, 1997.

[77] G. Chen and T. Bui, “Denoising of three dimensional data cube using bivariate wavelet shrinking.,” *Image Anal. Recognit.*, pp. 45–51, 2010.

[78] M. Ustundag, A. Sengur, M. Gokbulut, and F. Ata, “Performance comparison of wavelet thresholding techniques on weak ECG signal denoising,” *Prz. Elektrotechniczny*, no. 5, pp. 63–66, 2013.

[79] B. Ergen, “Signal and Image Denoising Using Wavelet Transform,” in *Advances in Wavelet Theory and Their Applications in Engineering, Physics and Technology*, D. D. Baleanu, Ed. Turkey: InTech, 2012, p. 495-.

[80] A. Nieslony, “Wavelet-Based Methods for Denoising,” 2005.

[81] S. Dangeti, “Denoising techniques - A comparison,” Andhra University College of Engineering, 2003.

[82] S. A. Mallat, *A Wavelet Tour of Signal Processing*, Second. Elseiver, 1998.

[83] R. Cohen, “Signal Denoising Using Wavelets,” 2012.

[84] M. Misiti, Y. Misiti, G. Oppenheim, and J.-M. Poggi, “Wavelet Toolbox User’s Guide,” *MathWorks, Inc*, p. 698, 2015.

[85] K. Budu, “Comparison of Wavelet-Based ANN and Regression Models for Reservoir Inflow Forecasting,” *J. Hydrol. Eng.*, vol. 19, no. 7, pp. 1385–1400, 2014.

[86] J. Jeena, P. Salice, and J. Neetha, “Denoising Using Soft Thresholding,” *Int. J. Adv. Res. Electr. Electron. Instrum. Eng.*, vol. 2, no. 3, pp. 1027–1032, 2013.

[87] A. Graps, “An introduction to wavelets,” *IEEE Computational Science and Engineering*, vol. 2, no. 2. pp. 50–61, 1995.

[88] S. Mallat and W. L. Hwang, “Singularity detection and processing with wavelets,” *IEE Trans. Inf. theory*, vol. 38, pp. 617–643, 1992.

[89] F. Flehmig, R. Watzdorf, and W. Marquardt, “Identification of Trends in Process Measurements using the Wavelet Transform,” *Comput. chem. Eng.*, vol. 22, pp. 491–496, 1998.

[90] T. Jiang, B. Chen, and X. He, “Industrial application of Wavelet Transform to the on-line prediction of side draw qualities of crude unit,” *Comput. Chem. Eng.*, vol. 24, no. 2–7, pp. 507–512, 2000.

[91] A. K. Verma and N. Verma, “Performance analysis of wavelet thresholding methods in denoising of audio signals of some Indian Musical Instruments,” *Int. J.*

Eng. Sci. Technol., vol. 4, no. 5, pp. 0975–5462, 2012.

[92] S. A. Mallat, *A Wavelet Tour of Signal Processing*, Second. Elseiver, 1998.

[93] P. Klapetek, D. Nečas, and C. Anderson, “Chapter 4: Data Processing and Analysis Basic Operations. Wavelet Transform,” *Gwyddion user guide*, 2018. [Online]. Available: http://gwyddion.net/documentation/user-guide-en/wavelet-transform.html. [Accessed: 27-Apr-2018].

[94] D. L. Donoho and I. M. Johnstone, “Minimax estimation via wavelet shrinkage,” *Ann. Stat.*, vol. 26, no. 3, pp. 879–921, 1998.

[95] D. Valencia, D. Orejuela, J. Salazar, and J. Valencia, “Comparison analysis between rigrsure, sqtwolog, heursure and minimaxi techniques using hard and soft thresholding methods,” *2016 21st Symp. Signal Process. Images Artif. Vision, STSIVA 2016*, pp. 1–5, 2016.

[96] K. Sreedevi, “Wavelet Transform based Atmospheric Radar Signal Processing. Chapter 3 Wavelet Designing and Denoising,” University of Hyderabad, 2009.

[97] S. Cao and R. R. Rhinehart, “An efficient method for on-line identification of steady state,” *J. Proc. cont*, vol. 5, pp. 363–374, 1995.

[98] S. Narasimhan, R. S. H. Mah, A. C. Tamhane, J. W. Woodward, and J. C. Hale, “A composite statistical test for detecting changes of steady states,” *AIChE J.*, vol. 32, no. 9, pp. 1409–1418, 1986.

[99] S. Narasimhan, C. S. Kao, and R. S. H. Mah, “Detecting changes of steady states using the mathematical theory of evidence,” *AIChE J.*, 1987.

[100] J. Siyi, Z. Chuanguang, Z. Wen, and Y. Chaohe, “Detecting changes of process steady states using the period extending strategy,” *Comput. Aided Chem. Eng.*, pp. 858–863, 2003.

[101] A. Savitzky and M. J. E. Golay, “Smoothing and Differentiation of Data by Simplified Least Squares Procedures.,” *Anal. Chem.*, vol. 36, no. 8, pp. 1627–1639, 1964.

[102] T. Jiang, B. Chen, X. He, and P. Stuart, “Application of steady-state detection method based on wavelet transform,” *Comput. Chem. Eng.*, vol. 27, pp. 569–578, 2003.

[103] S. A. Bhat and D. N. Saraf, “Steady-State Identification, Gross Error Detection, and Data Reconciliation for Industrial Process Units,” *Ind. Eng. Chem. Res.*, vol. 43, no. 15, pp. 4323–4336, Jul. 2004.

[104] S. Narasimhan and C. Jordache, *Data reconciliation and gross error detection. An intelligent use of process data*. Houston, Texas: Gulf Publishing Company, 2000.

[105] N. Arora and L. T. Biegler, “Redescending estimators for data reconciliation and parameter estimation,” *Comput. Chem. Eng.*, vol. 25, no. 11–12, pp. 1585–1599, Nov. 2001.

[106] I. B. Tjoa and L. T. Biegler, “Simultaneous strategies for data reconciliation and

gross error detection of nonlinear systems," *Comput. Chem. Eng.*, vol. 15, no. 10, pp. 679–690, 1991.

[107] P. J. Huber, *Robust Statistics*. Springer Berlin Heidelberg, 2014.

[108] D. B. Özyurt and R. W. Pike, "Theory and practice of simultaneous data reconciliation and gross error detection for chemical processes," *Comput. Chem. Eng.*, vol. 28, no. 3, pp. 381–402, Mar. 2004.

[109] D. B. Özyurt and R. W. Pike, "Theory and practice of simultaneous data reconciliation and gross error detection for chemical processes," *Comput. Chem. Eng.*, vol. 28, pp. 381–402, 2004.

[110] L. T. Biegler and I. E. Grossmann, "Retrospective on optimization," *Comput. Chem. Eng.*, vol. 28, no. 8, pp. 1169–1192, 2004.

[111] Á. Marcelo and A. Peña, "La importancia de la optimización en la industria," *Revista Virtual Pro*, no. 159, 2015.

[112] M. R. Naysmith and P. L. Douglas, "Review of Real Time Optimization in the Chemical Process Industries," *Dev. Chem. Eng. Miner. Process.*, pp. 67–87, 1995.

[113] J. L. Fernandes, C. I. C. Pinheiro, N. Oliveira, and F. Ramôa, "Multiplicity of steady states in an UOP FCC unit with high efficiency regenerator," pp. 1575–1580, 2006.

[114] M. R. Naysmith and P. L. Douglas, "Review of Real Time Optimization in the Chemical Process Industries," *Dev. Chem. Eng. Miner. Process.*, vol. 3, no. 2, pp. 67–87, May 2008.

[115] M. Cavazzuti, *Optimization Methods : From Theory to Design*. Modena, 2013.

[116] F. Glover and G. A. Kochenberger, *Handbook of Metaheuristics*, Second Edi. London: Springer Science. International Series in Operations Research & Management Science, 2010.

[117] J. Nocedal and S. J. Wright, *Springer Series in Operations Research and Financial Engineering Springer Series in Operation Research and*, Second edi. Springer, 2006.

[118] S. S. Aji, Y. S. Kim, K. Y. Ahn, and Y. D. Lee, "Life-Cycle Cost Minimization of Gas Turbine Power Cycles for Distributed Power Generation Using Sequential Quadratic Programming Method †," *Energies*, pp. 1–21, 2018.

[119] MathWorks ®, "Constrained Nonlinear Optimization Algorithms," 2019. [Online]. Available: https://es.mathworks.com/help/optim/ug/constrained-nonlinear-optimization-algorithms.html. [Accessed: 09-Feb-2019].

[120] R. H. Byrd, J. C. Gilbert, and J. Nocedal, "A trust region method based on interior point techniques for nonlinear programming," *Math. Program.*, vol. 185, pp. 149–185, 2000.

[121] R. H. Byrd, M. E. Hribar, and J. Nocedal, "An interior point algorithm for large scale nonlinear programming," *SIAM J. Optim.*, vol. 9, no. 4, pp. 877–900, 1999.

[122] A. Waltz, L. Morales, J. Nocedal, and D. Orban, “An interior algorithm for nonlinear optimization that combines line search and trust region steps,” *Math. Program.*, vol. 408, pp. 391–408, 2006.

[123] S. Sinha and C. Praveen, “Optimization of Industrial Fluid Catalytic Cracking Unit having Five Lump Kinetic Scheme using Genetic Algorithm,” *C. - Comput. Model. Eng. Sci.*, vol. 32, pp. 85–101, 2008.

[124] D. C. Melo, R. M. Filho, and M. R. W. Maciel, “Fluid Catalytic Cracking Optimisation Using Factorial Design and Genetic Algorithm Techniques,” *Can. J. Chem. Eng.*, vol. 9999, pp. 1–12, 2012.

[125] K. Saleh, H. Ibrahim, M. Jayyousi, and A. Diabat, “A novel optimization formulation of Fluid Catalytic Cracking unit,” in *Proceedings of 2013 International Conference on Industrial Engineering and Systems Management (IESM)*, 2013, pp. 1–5.

[126] O. Y. Raji, U. A. El-Nafaty, M. Jibril, and B. Y. Danjuma, “Modelling and Optimization of Fluid Catalytic Cracking Unit (FCCU) Using Hysys,” *Int. J. Emerg. trends Eng. Dev.*, vol. 3, no. 2, 2012.

[127] MathWorks ®, “Find global minima for highly nonlinear problems (Genetic Algorithm),” 2019. [Online]. Available: https://www.mathworks.com/discovery/genetic-algorithm.html. [Accessed: 31-Jan-2019].

[128] V. Mallawaarachchi, “Introduction to Genetic Algorithms — Including Example Code,” *Towards Data Science*, 2017. [Online]. Available: https://towardsdatascience.com/introduction-to-genetic-algorithms-including-example-code-e396e98d8bf3. [Accessed: 21-Jan-2018].

[129] Zauba, “Detailed Export Data of vacuum gas oil,” 2018. [Online]. Available: https://www.zauba.com/export-VACUUM+GAS+OIL-hs-code.html. [Accessed: 10-Nov-2018].

[130] Alibaba, “FCC catalyst zeolite ZSM5,” 2018. [Online]. Available: https://www.alibaba.com/showroom/fcc-catalyst-price.html. [Accessed: 10-Nov-2018].

[131] U. S. D. of Energy, “Weekly Retail Gasoline and Diesel Prices,” 2018. [Online]. Available: https://www.eia.gov/dnav/pet/pet_pri_gnd_dcus_nus_a.htm.

[132] U. S. D. of Energy, “Selecting the Right Octane Fuel,” 2018. [Online]. Available: https://www.fueleconomy.gov/feg/octane.shtml. [Accessed: 10-Nov-2018].

[133] J. R. Hernandez Barajas, R. Vazquez Roman, and D. Salazar Sotelo, “Multiplicity of steady states in FCC units: effect of operating conditions,” *Fuel*, vol. 85, no. 5–6, pp. 849–859, Mar. 2006.

[134] MathWorks ®, “How the Genetic Algorithm Works,” *Genetic Algorithm*, 2018. [Online]. Available: https://www.mathworks.com/help/gads/how-the-genetic-algorithm-works.html. [Accessed: 29-Jan-2019].

[135] J. H. Lee and J. M. Lee, “Progress and challenges in control of chemical processes.,” *Annu. Rev. Chem. Biomol. Eng.*, vol. 5, no. March, pp. 383–404, 2014.

[136] O. & G. Portal, “Latest Advancements in Process Control in Refineries and Chemical Plants.” [Online]. Available: http://www.oil-gasportal.com/latest-advancements-in-process-control-in-refineries-and-chemical-plants/. [Accessed: 28-Feb-2019].

[137] C. Pinheiro and J. Fernandes, “Fluid catalytic cracking (FCC) process modeling, simulation, and control,” *Ind. …*, pp. 1–29, 2011.

[138] M. V Cristea and P. Ş. Agachi, “Comparison between Different Control Approaches of the UOP Fluid Catalytic Cracking Unit,” pp. 1–6, 2007.

[139] R. Roman, Z. K. Nagy, M. V. Cristea, and S. P. Agachi, “Dynamic modelling and nonlinear model predictive control of a Fluid Catalytic Cracking Unit,” *Comput. Chem. Eng.*, vol. 33, no. 3, pp. 605–617, Mar. 2009.

[140] M. V Cristea, “Simulation and model predictive control of a UOP fluid catalytic cracking unit,” *Chem. Eng. Process.*, vol. 42, pp. 67–91, 2003.

[141] D. Rosinová and A. Kozáková, “Robust Decentralized PID Controller Design,” in *PID Controller Design Approaches - Theory, Tuning and Application to Frontier Areas*, InTech, 2012, pp. 133–168.

[142] J. G. Ziegler and N. B. . Nichols, “Optimum Settings for Automatic Controllers,” *Trans. ASME*, pp. 759–765, 1942.

[143] G. H. Cohen and G. A. Coon, “Theoretical Consideration of Retarded Control.pdf,” *Trans. ASME*, vol. 75, pp. 827–834, 1953.

[144] L. Payne, “Tuning PID control loops for fast response,” *Control Engineering*.

[145] R. A. Krohling and J. P. Rey, “Design of Optimal Disturbance Rejection PID Controllers Using Genetic Algorithms,” *IEEE Trans. Evol. Comput.*, vol. 5, no. 1, pp. 78–82, 2001.

[146] J. F. M. Amaral, R. Tanscheit, and M. A. C. Pacheco, “Tuning PID Controllers through Genetic Algorithms,” pp. 2–5.

[147] B. Tandon and R. Kaur, “Genetic Algorith based parameter tuning of PID controller for composition control system,” *Int. J. Eng. Sci. Technol.*, vol. 3, no. 2011, 2015.

[148] D. C. Meena, “Genetic Algorith Tuned PID controller for process control,” *IEEE*, pp. 1–6, 2017.

[149] J. M. Herrero, M. Martinez, and J. V Salcedo, “Optimal PID tuning with Genetic Algorithms for non linear process models,” *Elseiver IFAC Publ.*, pp. 31–36, 2002.

[150] E. H. Bristol, “On a New Measure of Interaction for Multivariable Process,” *IEE Trans. Autom. Control*, pp. 133–134, 1966.

[151] P. Ş. Agachi, V. M. Cristea, A. A. Csavdári, and B. Szilágyi, *Advanced Process Engineering Control*. De Gruyter Graduate, 2017.

[152] P. Taylor, Z. Zhu, and A. Jutan, “A new variable pairing criterion based on the Niederlinski Index,” *Chem. Eng. Comm.*, vol. 121, pp. 235–250, 1993.

[153] M. Aminul, I. Khan, S. A. Imtiaz, F. Khan, and M. A. A. S. Choudhury, “Comparative Study of Different Supervisory Control Structures,” *Adconip 2014*, no. DMC, 2014.

[154] L. T. Biegler, “Efficient Nonlinear Programming Algorithms for Chemical Process Control and Operations,” in *System Modeling and Optimization*, 2009, pp. 21–35.

[155] B. Coleman and J. Babu, “Introduction,” in *Techniques of Model-Based Control*, Prentice Hall, 2002, pp. 1–12.

[156] A. Premier, “Real time optimization with Advanced Process Control,” *Innovative Thinking*, 2018. [Online]. Available: https://info.premierautomation.com/blog/real-time-optimization-with-advanced-process-control. [Accessed: 25-Mar-2019].

[157] Honeywell, “An overview of Honeywell’s layered optimisation solution,” *Digital Refining. Processing , Operations and Maintenance*, 2018.

[158] J. O. Trierweiler, “Real-Time Optimization of Industrial Processes Control Layers and the RTO Concept.” Springer- Verlag, pp. 1–11, 2014.

[159] O. Taha and M. R. Khan, *Advanced process control for clean fuel production: smart plant of the future*. Woodhead Publishing Limited, 2011.

[160] M. Hovd and S. Skogestad, “Controllability Analysis for the Fluid Catalytic Cracking Process.pdf,” *AIChE Annual Meeting*. pp. 1–30, 1991.

[161] E. Lee and F. R. Groves, “Mathematical Model of the Fluidized Bed Catalytic Cracking Plant,” *Trans. Soc. Comput. Simul. Int.*, vol. 2, no. 3, pp. 219–236, 1985.

[162] A. F. Errazu, H. I. D. Lasa, and F. Sarti, “A fluidized bed catalytic cracking regenerator model. Grid effects,” *Can. J. Chem. Eng.*, vol. 57, no. 2, pp. 191–197, 1979.

[163] Y. T. Shah, G. P. Hullng, J. A. Paraskos, and J. D. McKinney, “A Kinematic Model for an Adiabatic Transfer Line Catalytic Cracking Reactor,” *Ind. Eng. Chem. Process Des. Dev.*, vol. 16, no. 1, pp. 89–94, 1977.

[164] V. W. Weekman and D. M. Nace, “Kinetics of catalytic cracking selectivity in fixed, moving, and fluid bed reactors,” *AIChE J.*, vol. 16, no. 3, pp. 397–404, 1970.

[165] H. Kurihara, “Optimal control of fluid catalytic cracking processes,” Massachusetts Institute of Technology, 1967.

[166] M. & Bahls, “Octane Number,” 2018. [Online]. Available: https://www.marquard-bahls.com/en/news-info/glossary/detail/term/octane-number-ron-mon.html. [Accessed: 15-Dec-2018].

[167] R. C. Ellis, X. Li, and J. B. Riggs, “Modeling and optimization of a model IV fluidized catalytic cracking unit,” *AIChE J.*, vol. 44, no. 9, pp. 2068–2079, 1998.

[168] P. D. Khandalekar, “Control and optimization of fluidized catalytic cracking process,” Texas Tech University, 1993.

[169] R. C. Ellis, X. Li, and J. B. Riggs, “Modeling and optimization of a model IV fluidized catalytic cracking unit,” *AIChE J.*, vol. 44, no. 9, pp. 2068–2079, Sep. 1998.

[170] A. Arbel, Z. Huang, and I. H. Rinard, “Dynamic and Control of Fluidized Catalytic Crackers. 1. Modeling of the Current Generation of FCC’s,” pp. 1228–1243, 1996.

[171] D. L. Donoho, “De-noising by soft-thresholding,” *IEEE Trans. Inf. Theory*, vol. 41, no. 3, pp. 613–627, May 1995.

[172] M. Misiti and Y. Misiti, “Wavelet Toolbox,” in *Matlab User’s Guide*, Mathworks, 2014.

[173] M. Misiti, Y. Misiti, G. Oppenheim, and J.-M. Poggi, *Wavelet Toolbox For Use with Matlab*, Version 1. The MathWorks, Inc., 1996.

[174] U.- Ingeniería, “Análisis de la Estabilidad Interna de los Sistemas No Lineales,” 1996.